This is to certify that the

dissertation entitled

THE APPLICATION OF OPTICAL ABSORPTION AND RESONANCE RAMAN SPECTROSCOPY TO THE STUDY OF HEME PROTEINS AND MODEL COMPOUNDS

presented by

Robert T. Kean

has been accepted towards fulfillment
of the requirements for

Ph.D. degree in Chemistry

Gerald T. Babcock
Major professor

Date 3/4/87.

THE APPLICATION OF OPTICAL ABSORPTION AND RESONANCE RAMAN SPECTROSCOPY TO THE STUDY OF HEME PROTEINS AND MODEL COMPOUNDS

By

Robert T. Kean

A DISSERTATION

Submitted to

Michigan State University

in partial fulfillment of the requirements

for the degree of

DOCTOR OF PHILOSOPHY

Department of Chemistry

1987

ABSTRACT

THE APPLICATION OF OPTICAL ABSORPTION AND
RESONANCE RAMAN SPECTROSCOPY TO THE STUDY
OF HEME PROTEINS AND MODEL COMPOUNDS

By

Robert T. Kean

A variety of experiments have been performed with the goal of elucidating the reaction pathway for the reduction of oxygen by cytochrome oxidase. Because of the complexity of cytochrome oxidase, much of this work has involved studies of heme compounds in solution and species of simpler heme proteins as models for species in the cytochrome oxidase catalytic cycle. These studies have focused on ferrous oxy (Fe^{II}-O_2) and ferryl oxo (Fe^{IV}=O) hemes, which have been identified as key intermediates in other heme enzymes. Since ferrous oxy and ferryl oxo hemes are unstable at room temperature, low temperature optical absorption and resonance Raman spectroscopic techniques have been developed for characterization of these species. Low temperature studies of solution species have been used to interpret results from the corresponding protein species. Raman studies with cold trapped cytochrome oxidase species support the hypothesis that both ferrous oxy and ferryl oxo species are active in the catalytic cycle. These studies, in conjunction with studies of other ligand bound heme species, demonstrate that the peripheral porphyrin substituents have little or no affect on the bond strengths of the axial ligands as

monitored by their Fe-ligand vibrational frequencies. The chemistry of species such as the ferrous oxy (Fe^{II}-O_2), ferryl oxo (Fe^{IV}=O) and ferric cyanide (Fe^{III}-CN^-) seem to be controlled by out-of-plane effects such as trans ligand strength, steric constraints, and hydrogen bonding. However, comparison of the optical absorption spectra of protein and solution hemes suggests direct perturbation of the porphyin ring by specific amino acid residues in the protein species. Studies with a copper chelating heme model species indicate a structure analogous to that of the cytochrome oxidase oxygen reduction site. This model duplicates the six-coordinate high-spin heme geometry of cytochrome oxidase as detected by Raman spectroscopy. EPR studies indicate that the presence of an oxo (O^{-2}) bridge between the two metal centers can produce magnetic exchange coupling like that observed in the resting state of cytochrome oxidase. Optical absorption studies of various ligated states of this model suggest a possible identification of the 655 nm absorption band observed in resting cytochrome oxidase.

To my mother and in memory of my father.

ACKNOWLEDGMENTS

I would like to thank: Keki, Manfred, and Scott (the worlds finest glassblowers) for the fabrication of Dewars and glassware; Deak, Russ, and Dick for equipment fabrication; Marty for electronic design and assistance in electronic trouble-shooting; Ron and Scott for laser and equipment repair; and Tom for assistance with my computer work. Without their skills and expertise, I could not have completed this research. I would like to thank: Dr. Babcock, my graduate advisor, for his guidance and financial support; Dr. Chang for his cooperation and advice; and Dr. Schwendeman and Dr. Ferguson-Miller for being part of my committee. M. S. Koo and Asaad Salehi have graciously provided me with compounds for study; John Manthey and Stephan Witt (from the California Institute of Technology) have worked with me in the joint study of cytochrome oxidase intermediates. Tony and Dwight deserve a special thanks for their technical assistance with Raman spectroscopy and computers respectively. I am grateful to the other members of the Babcock group for their friendship, comradery, and comic relief. I am extremely indebted to Nirmala and Ravishankar, who helped me in my final months by giving me a place to live. Finally, I would like to thank Mary for her love, help, and constant encouragement through my last year of research and the entire preparation of this dissertation. This research was supported in part with a grant from the National Institute of Health.

TABLE OF CONTENTS

LIST OF TABLES vii

LIST OF FIGURES viii

CHAPTER 1 INTRODUCTION

A. Overview of Heme Proteins 1

B. Structure and Reactivity of Molecular Oxygen . . . 5

C. Physical Techniques for Heme Protein Research . . . 10

D. Peroxidases, Catalases, and Cytochromes P-450 . . . 23

E. Cytochrome c Oxidase 25

CHAPTER 2 EQUIPMENT AND TECHNIQUES

A. Resonance Raman Spectroscopy 36

B. Low Temperature Spectroscopy 41

C. Anaerobic Techniques 48

D. Electrochemistry 53

CHAPTER 3 RESONANCE RAMAN CHARACTERIZATION OF CYANIDE BOUND HEME PROTEINS AND MODEL COMPOUNDS

A. Introduction 57

B. Materials and Methods 59

C. Results 61

D. Discussion 66

CHAPTER 4 CHARACTERIZATION OF CYTOCHROME a_3 MODEL COMPOUNDS

A. Introduction 77

B. Materials and Methods 80

C. Meso-diphenylporphyrin Results 82

D. Cytochrome Oxidase Model Compound Results 91

E. Discussion 111

CHAPTER 5 CHARACTERIZATION OF "OXY" AND "OXO" HEMES AS MODELS OF HEME PROTEIN REACTION INTERMEDIATES

A. Introduction 124

B. Materials and Methods 128

C. Results 130

D. Discussion 146

CHAPTER 6 RESONANCE RAMAN SPECTROSCOPY OF CYTOCHROME OXIDASE "PSEUDO-INTERMEDIATES"

A. Introduction 167

B. Materials and Methods 169

C. Results 171

D. Discussion 188

CHAPTER 7 CONCLUSIONS AND FUTURE WORK

A. Conclusions 201

B. Future Work 204

APPENDIX 1 210

LIST OF REFERENCES 211

LIST OF TABLES

Table 4.1	Raman Peaks of Fe^{III} Meso-Diphenylporphyrins.	90
Table 4.2	Comparison of High-Spin Fe^{III} Meso-Diphenylporphyrin Concentrations as Determined by Optical Absorption and EPR Spectroscopy.	105
Table 4.3	Slope and Intercept Values for the Core Size Dependent High Frequency Raman Peaks of Fe^{III} Meso-Diphenylporphyrins.	105
Table 4.4	Comparison of the Vibratons of Three Different Porphyrin Types.	105
Table 5.1	Optical Absorption Peaks of Ferrous Oxy and Ferryl Oxo Heme Species.	132
Table 5.2	Raman Peaks of Iron Octaethylporphyrin Species.	137
Table 5.3	Raman Peaks of Iron PPIX Protein and Model Species.	142
Table 5.4	Raman Peaks of Various TPP Type Heme Species.	148
Table 5.5	Optical Absorption Peaks of Protoheme Containing Ferrous Oxy and Ferryl Oxo Species.	149
Table 5.6	Comparison of Iron-Oxygen Stretching Frequencies for Various Ferrous Oxy and Ferryl Oxo Species.	153
Table 5.7	Iron-Imidazole Stretching Frequencies of Five-Coordinate ferrous Hemes.	163
Table 6.1	Distinguishing Characteristics and Raman Peaks of Frozen Cytochrome Oxidase Species.	173
Table 6.2	Raman Peaks of Heme *a* Model Compounds.	174
Table 6.3	Assignment of the Mid- and Low-Frequency Raman Peaks of Resting and 580 nm Species of Cytochrome Oxidase.	189

LIST OF FIGURES

Figure 1.1 The structure of a heme (from Callahan, 1983). 2

Figure 1.2 The structure of protoheme: a) unmodified, b) thioether-linked to the protein. 4

Figure 1.3 The structure of heme a. 6

Figure 1.4 The molecular orbital description of dioxygen (O_2) (adapted from Jones et al., 1979). 7

Figure 1.5 The one electron reduction potentials of O_2 in solution at different pH values. Potentials are solution versus a normal hydrogen electrode (NHE) (from Sawyer and Nanni, 1981). 9

Figure 1.6 The interaction of iron out of plane orbitals with the π^* orbitals of O_2 in Fe^{II} "oxy" heme complexes (from Reed, 1978). 11

Figure 1.7 The optical absorption spectrum of Fe^{II} cytochrome C. 15

Figure 1.8 The 2 HOMO's and 2 LUMO's of porphyrins, within the 4 orbital model (from Longuet-Higgins, 1950). 16

Figure 1.9 Relative energy levels of porphyrin (-·-) and iron (——) orbitals for ferric porphyrin complexes (adapted from Zerner et al., 1966). 18

Figure 1.10 Raman (Stokes and anti-Stokes) and Rayleigh light scattering. 20

Figure 1.11 A comparison of normal and resonance Raman light scattering (from Ondrias, 1980). 22

Figure 1.12 Aerobic respiration (adapted from Lehninger, 1975). 27

Figure 1.13 The shape of cytochrome oxidase (adapted from Henderson, 1977). 28

Figure 1.14	The relative locations of the metal centers in cytochrome oxidase (from Blair, 1983).	30
Figure 1.15	a) The optical absorption spectrum of oxidized and reduced cytochrome oxidase, b) The approximation of the spectral contributions from the individual heme centers (from Vanneste, 1966).	32
Figure 1.16	Heme a models for the heme centers in cytochrome oxidase (Figure courtesy of G. T. Babcock).	34
Figure 1.17	A proposed catalytic cycle for oxygen reduction by cytochrome oxidase (Figure courtesy of G. T. Babcock).	35
Figure 2.1	Computer interfaced scanning Raman spectrometer system.	38
Figure 2.2	Low temperature Raman backscattering Dewar.	43
Figure 2.3	Liquid nitrogen temperature backscattering Dewar system.	45
Figure 2.4	Low temperature Dewar system for optical absorption spectroscopy.	47
Figure 2.5	Anaerobic/vacuum system.	49
Figure 2.6	Anaerobic glassware.	51
Figure 2.7	Electrochemistry cell for small volume anaerobic work.	54
Figure 2.8	A. Cyclic voltammagram of bis 1-methyl-imidazole heme a (Fe^{III}) in CH_2Cl_2 (electrolyte TBAP .1M) B. Optical absorption spectrum of bis 1-methylimidazole heme a in CH_2Cl_2, which was reduced at -0.2 V (vs. pesudo reterence).	55
Figure 3.1	The structures of iron deuteroporphyrin DME and iron deuterochlorin.	62
Figure 3.2	Optical absorption spectra of bis-NMI, CN^-/NMI, and bis-CN^- ligated Fe^{III} deuteroporphyrin.	63
Figure 3.3	The optical absorption spectra of bis-NMI, NMI/CN^-, and bis-CN^- ligated Fe^{III} deuterochlorin.	64

gure 3.4	Raman spectra of bis-NMI, NMI/CH^-, and bis-CN^- ligated Fe^{III} deuteroporphyrin.	65
gure 3.5	Raman spectra of bis-NMI, NMI/CN^-, and bis-CN^- ligated Fe^{III} deuterochlorin.	67
gure 3.6	Raman spectra of NMI, CN^- NMI/CN^- ligated Fe^{III} deuteroporphyrin and deuterochlorin with isotope labeled CN^-.	68
gure 3.7	The Raman spectra of bis-CN^- Fe^{III} deuteroporphyrin and deuterochlorin with isotope labeled CN^-.	69
gure 3.8	The optical absorption spectra of native and CN^- bound horseradish peroxidase.	70
gure 3.9	The Raman spectra of native and CN^- bound horseradish peroxidase.	71
gure 3.10	Raman spectra of CN^- bound horseradish peroxidase with isotope labeled CN^-.	72
igure 4.1	Structures of Fe^{III} meso-diphenylporphyrin species.	83
igure 4.2	Optical absorption spectra of Fe^{III} meso-diphenylporphyrin species.	84
gure 4.3	Comparison of the optical absorption spectra of six-coordinate high-spin Fe^{III} meso-diphenylporphyrin species.	86
gure 4.4	High frequency Raman spectra of Fe^{III} meso-diphenylporphyrin species.	88
gure 4.5	Low frequency Raman spectra of Fe^{III} meso-diphenylporphyrin species.	89
gure 4.6	Structures of meso-diphenylporphyrin cytochrome oxidase model compounds.	92
ure 4.7	Comparison of the optical absorption spectra of five-coordinate, Cl^- ligated Fe^{III} meso-diphenylporphyrin species.	94
ure 4.8	Comparison of the optical absorption spectra of five-coordinate, OH^- ligated/ O^{-2} bridged Fe^{III} meso-diphenylporphyrin species.	95
re 4.9	Comparison of the optical absorption spectra of six-coordinate, Cl^- ligated Fe^{III} meso-diphenylporphyrin species.	96

gure 4.10	Comparison of the optical absorption spectra of six-coordinate, OH^- ligated/ O^{-2} bridged Fe^{III} meso-diphenylporphyrin species.	97
gure 4.11	Comparison of the high frequency Raman spectra of five-coordinate, Cl^- ligated Fe^{III} meso-diphenylporphyrin species.	99
gure 4.12	Comparison of the high frequency Raman spectra of five-coordinate, OH^- ligated/ O^{-2} bridged Fe^{III} meso-diphenylporphyrin species.	100
gure 4.13	Comparison of the high frequency Raman spectra of six-coordinate, Cl^- ligated Fe^{III} meso-diphenylporphyrin species.	101
gure 4.14	Comparison of the high frequency Raman spectra of six-coordinate, OH^- ligated/ O^{-2} bridged Fe^{III} meso-diphenylporphyrin species.	102
gure 4.15	EPR spectra of Met Mb F^- and five-coordinate, Cl^- ligated Fe^{III} meso-diphenyl porphyrin species.	104
gure 4.16	EPR spectra of five-coordinate, OH^- ligated/ O^{-2} bridged Fe^{III} meso-diphenylporphyrin species.	107
gure 4.17	EPR spectra of six-coordinate Fe^{III} meso-diphenylporphyrin species.	108
gure 4.18	A plot of signal intensity versus 1/T (Curie Law) for Met Mb F^- and the five-coordinate O^{-2} bridged cytochrome oxidase model compound.	110
gure 4.19	The core size dependence of the high frequency Raman vibrations of Fe^{III} meso-diphenylporphyrin species.	113
gure 5.1	Optical absorption spectra of Bis-NMI and "oxy" ferrous octaethylheme.	131
ure 5.2	Identification of $\nu(Fe^{II}-O_2)$ for ferrous oxy octaethylheme, protoheme, and heme *a*.	133
ure 5.3	Raman spectra of Bis-NMI and "oxy" ferrous octaethylheme (low frequency region).	135
ure 5.4	Raman spectra of Bis-NMI and "oxy" ferrous octaethylheme (high frequency region).	136
ure 5.5	Optical absorption spectra of ferryl oxo protoheme, octaethylheme, and tetraphenylheme.	138

igure 4.10	Comparison of the optical absorption spectra of six-coordinate, OH^- ligated/ O^{-2} bridged Fe^{III} meso-diphenylporphyrin species.	97
igure 4.11	Comparison of the high frequency Raman spectra of five-coordinate, Cl^- ligated Fe^{III} meso-diphenylporphyrin species.	99
igure 4.12	Comparison of the high frequency Raman spectra of five-coordinate, OH^- ligated/ O^{-2} bridged Fe^{III} meso-diphenylporphyrin species.	100
igure 4.13	Comparison of the high frequency Raman spectra of six-coordinate, Cl^- ligated Fe^{III} meso-diphenylporphyrin species.	101
igure 4.14	Comparison of the high frequency Raman spectra of six-coordinate, OH^- ligated/ O^{-2} bridged Fe^{III} meso-diphenylporphyrin species.	102
igure 4.15	EPR spectra of Met Mb F^- and five-coordinate, Cl^- ligated Fe^{III} meso-diphenyl porphyrin species.	104
igure 4.16	EPR spectra of five-coordinate, OH^- ligated/ O^{-2} bridged Fe^{III} meso-diphenylporphyrin species.	107
igure 4.17	EPR spectra of six-coordinate Fe^{III} meso-diphenylporphyrin species.	108
igure 4.18	A plot of signal intensity versus 1/T (Curie Law) for Met Mb F^- and the five-coordinate O^{-2} bridged cytochrome oxidase model compound.	110
igure 4.19	The core size dependence of the high frequency Raman vibrations of Fe^{III} meso-diphenylporphyrin species.	113
igure 5.1	Optical absorption spectra of Bis-NMI and "oxy" ferrous octaethylheme.	131
igure 5.2	Identification of $\nu(Fe^{II}\text{-}O_2)$ for ferrous oxy octaethylheme, protoheme, and heme a.	133
igure 5.3	Raman spectra of Bis-NMI and "oxy" ferrous octaethylheme (low frequency region).	135
igure 5.4	Raman spectra of Bis-NMI and "oxy" ferrous octaethylheme (high frequency region).	136
igure 5.5	Optical absorption spectra of ferryl oxo protoheme, octaethylheme, and tetraphenylheme.	138

gure 5.6 Identification of $\nu(Fe^{IV}=O)$ for ferryl oxo protoheme, octaethylheme, and tetraphenylheme. 140

gure 5.7 Raman spectra of ferryl oxo, μ-oxo dimer and μ-peroxo dimer of protoheme (high frequency region). 141

gure 5.8 Raman spectra of ferryl oxo and four-coordinate ferrous octaethylheme (high frequency region). 145

gure 5.9 Raman spectrum of ferryl oxo tetraphenylheme (high frequency region). 147

gure 6.1 High frequency spectra of photoreduced cytochrome oxidase samples (liquid and frozen). 172

gure 6.2 High frequency Raman spectra of resting cytochrome oxidase (liquid and frozen). 176

gure 6.3 High frequency Raman spectra of 580 nm species of cytochrome oxidase (liquid and frozen). 178

gure 6.4 High frequency Raman spectra of frozen compound C cytochrome oxidase (MVCO + O_2 and pulsed plus peroxide) and pulsed cytochrome oxidase. 180

ure 6.5 High frequency Raman spectrum of frozen "reoxidized" cytochrome oxidase. 182

ure 6.6 High frequency Raman spectrum of CO reacted 580 nm species of cytochrome oxidase. 183

ure 6.7 Low frequency Raman spectra of frozen resting and 580 nm (^{16}O and ^{18}O) cytochrome oxidase. 185

ure 6.8 Intermediate frequency Raman spectra of frozen resting and 580 nm (^{16}O and ^{18}O) cytochrome oxidase. 186

ure 6.9 Upper-intermediate frequency Raman spectra of frozen resting and 580 nm (^{16}O and ^{18}O) cytochrome oxidase. 187

CHAPTER 1

INTRODUCTION

OVERVIEW OF HEME PROTEINS

Heme proteins are well known for their role in oxygen transport emoglobin) and oxygen storage (myoglobin). Less well known are the ltitude of other heme proteins and enzymes which are amazing in their riations of structure and function and their occurrence in nearly all ological systems. The basic structure of a heme can be seen in Figure .. It consists of a central iron ion strongly chelated by the four rrole nitrogens of the conjugated porphyrin macrocycle. What tinguishes one heme from another is the pattern of substitution at labeled peripheral positions. The biochemical function and the sical properties of a heme protein or enzyme are controlled by these g substituents, and specific environmental factors produced by the rounding protein. The latter effects include hydrogen bonding, ation (from amino acid residues) to the axial position of the iron, tron transfer pathways, and hydrophobic or hydrophilic "pockets" ssible to exogenous ligands. It is the variability of the above ined effects which allows for the great variety of heme hemistry.

Heme proteins and enzymes are generally categorized into groups ding to the heme which they contain or their general functional rties (see Adar 1978). Cytochromes b utilize unmodified protoheme

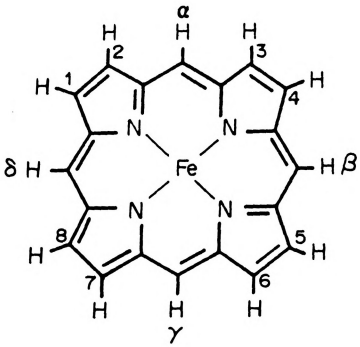

Figure 1.1 The structure of a heme (from Callahan, 1983).

(Figure 1.2a) as the prothetic group, with the heme held in the protein by axial ligation (normally the nitrogen of a histidine residue). Cytochromes c are protoheme containing globular proteins, in which the protoheme is covalently linked to the protein through the thioether linkages to the 2,4 vinyl groups (Figure 1.2b). Although some of the hemes in these proteins will bind exogenous ligands (Andersson et al. 1986; Ondrias 1980), the axial ligation of cytochromes b and c does not change under normal activity. They appear to function primarily as electron carriers with the iron undergoing redox changes between the +2 and +3 states. In contrast to these, there exists a large number of heme enzymes and proteins in which changes in the axial ligation is inherent to normal activity. In these systems, one of the iron axial positions is accessible to exogenous ligands that can bind to or react with the heme iron. The chemistry of these heme systems is generally more complicated than that of the cytochromes b and c and owing to their prominence in biological systems, they have been the subjects of extensive research. Included in this group are the globins, cytochromes P450, peroxidases, catalases, and cytochrome oxidase. Hemoglobin and myoglobin bind O_2 for transport and storage respectively. Cytochromes P450 use O_2 to metabolize various compounds via specific oxygen insertion (Griffin et al. 1979). Peroxidases use peroxide (H_2O_2) as a chemical oxidant. They react with a wide variety of substrates and are functional, for example, in anti-infection defense systems. Catalases remove peroxides from biological systems by catalyzing their disproportionation to O_2 and H_2O (Hewson and Hager 1979). These proteins usually contain protoheme, the most commonly occurring heme, in the active site. Cytochrome oxidases catalyze the exothermic

a)

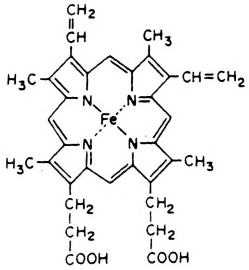

protoheme

b)

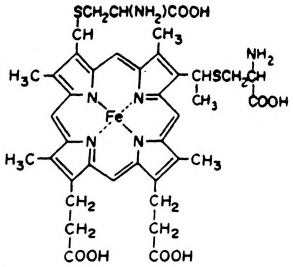

thioester-linked protoheme

Figure 1.2 The structure of protoheme: a) unmodified, b) thioether-linked to the protein.

eduction of O_2 to H_2O, thereby providing the thermodynamic driving
rce for the synthesis of ATP (stored chemical energy). Cytochrome
idase is unusual and complex in that it utilizes two hemes and two
pper ions in the catalytic process (Wikstrom, M. et al. 1981). The
mes of cytochrome oxidase are heme a, the structure of which is seen
Figure 1.3. The common factor in all these heme enzymes is that they
lize oxygen (O_2 or H_2O_2) as a ligand or reaction substrate. Although
se heme systems can bind other small ligands (CO, CN-, NO, etc.),
ctivity is predominantly restricted to oxygen. To understand this
cific and unusual chemistry, the following questions must be
wered: (1) what is the physical nature of the interaction between
s and oxygen; (2) what are the specific mechanisms of these
ferent enzyme reactions; and (3) what factors control the rate and
ificity of these reactions? The results of my research will be
ented in later chapters and the discussion will address these
tions. The remainder of the introduction will summarize the
ts, tools and ideas which have brought this area of science to its
nt state.

STRUCTURE AND REACTIVITY OF MOLECULAR OXYGEN

o understand why molecular oxygen binds to and reacts with hemes
adily, it is useful to examine the structure of molecular oxygen.
rbital diagram of dioxygen is shown in Figure 1.4. The ground
contains a double bond and has two unpaired electrons (triplet
. Conservation of spin requirements severely limit the reactivity
plet species. The lowest singlet state is ~22.3 kcal/mole higher
gy (Jones et al. 1979). Peroxides, which contain two more

eduction of O_2 to H_2O, thereby providing the thermodynamic driving rce for the synthesis of ATP (stored chemical energy). Cytochrome idase is unusual and complex in that it utilizes two hemes and two pper ions in the catalytic process (Wikstrom, M. et al. 1981). The mes of cytochrome oxidase are heme a, the structure of which is seen Figure 1.3. The common factor in all these heme enzymes is that they lize oxygen (O_2 or H_2O_2) as a ligand or reaction substrate. Although se heme systems can bind other small ligands (CO, CN-, NO, etc.), ctivity is predominantly restricted to oxygen. To understand this cific and unusual chemistry, the following questions must be wered: (1) what is the physical nature of the interaction between s and oxygen; (2) what are the specific mechanisms of these ferent enzyme reactions; and (3) what factors control the rate and ificity of these reactions? The results of my research will be ented in later chapters and the discussion will address these tions. The remainder of the introduction will summarize the ts, tools and ideas which have brought this area of science to its nt state.

STRUCTURE AND REACTIVITY OF MOLECULAR OXYGEN

o understand why molecular oxygen binds to and reacts with hemes adily, it is useful to examine the structure of molecular oxygen. bital diagram of dioxygen is shown in Figure 1.4. The ground contains a double bond and has two unpaired electrons (triplet . Conservation of spin requirements severely limit the reactivity let species. The lowest singlet state is ~22.3 kcal/mole higher gy (Jones et al. 1979). Peroxides, which contain two more

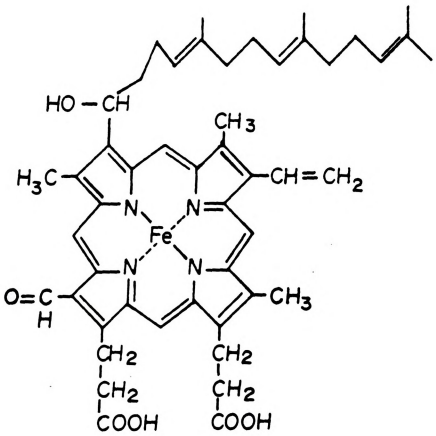

heme a

Figure 1.3 The structure of heme a.

Figure 1.

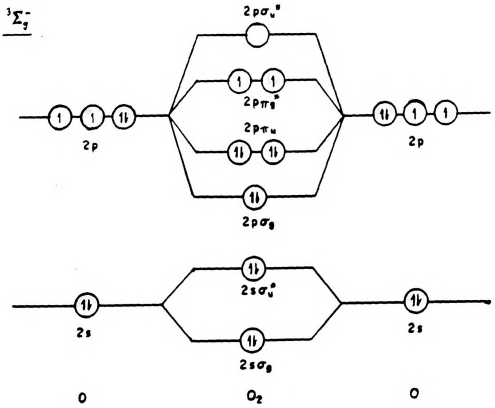

Figure 1.4 The molecular orbital description of dioxygen (O_2) (adapted from Jones et al., 1979).

electrons, are sir

The four electron

stage, to water ha

solution under con

in Figure 1.5. Sev

(1) the overall fo

favorable (large p

(2) the reaction be

electron reduction

high pH). It is the

thermodynamically u

almost inert in the

with a singlet grou

high pH), is a much

The energies of

the oxygen HOMO's (2

of plane orbitals ar

interactions. These

a weak σ donor but a

a delocalization of e

1977) from the iron t

structure of oxygen b

converged on roughly

Williams 1983 pp. 26-

configurations: the f

oxygen, the second is

ctrons, are singly bonded and have no unpaired electrons (singlet).
four electron electrochemical reduction of O_2, through the peroxide
e, to water has been studied by Sawyer and Nanni (1981) in aqueous
tion under conditions of different pH. These results are reproduced
igure 1.5. Several important points can be observed in these data:
the overall four electron process is highly thermodynamically
rable (large positive reduction potential) at all values of the pH;
he reaction becomes more favorable at lower pH values; and (3) one
ron reduction of O_2 is unfavorable at all values of pH (more so at
pH). It is the triplet ground state of O_2, coupled with the
odynamically unfavorable first reduction step, that makes O_2
inert in the absence of a catalyst (Malmstrom 1982). Peroxide,
singlet ground state and exothermic reduction steps (except at
H), is a much more reactive species.

e energies of the iron 3d orbitals in hemes are close to those of
ygen HOMO's ($2P\pi g$). In addition, the symmetries of the iron out
e orbitals are suitable for both σ and π type bonding
tions. These can be seen schematically in Figure 1.6. Oxygen is
σ donor but a stronger π acceptor. The net result of the bond is
alization of electron density (ca. 0.1 e^-, Olafson and Goddard
rom the iron to the oxygen. Calculations of the electronic
e of oxygen bound hemoglobin by a variety of methods have
d on roughly the same physical model (see Gubelmann and
1983 pp. 26-27). Oxyhemoglobin is pictured as a mixture of two
ations: the first is a low spin Fe^{+2} ($S = 0$) bound to singlet
he second is an intermediate spin Fe^{+2} ($S = 1$) bound to

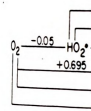

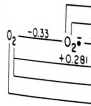

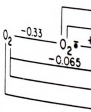

Figure 1.5

STANDARD REDUCTION POTENTIALS FOR DIOXYGEN SPECIES IN WATER

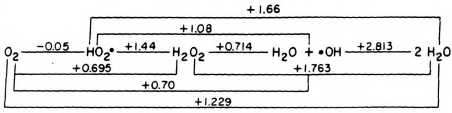

pH 0 (1M H^+)

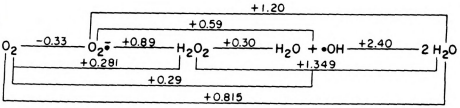

pH 7

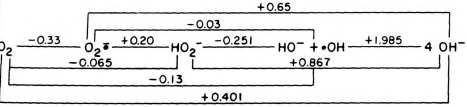

pH 14 (1M OH^-)

Figure 1.5 The one electron reduction potentials of O_2 in solution at different pH values. Potentials are solution versus a normal hydrogen electrode (NHE) (from Sawyer and Nanni, 1981).

triplet oxygen. Th

1.6, with each spe

Since the spins co

are net S = 0 (sin

transfer from the

calculations but it

oxygen can be consi

to reaction has bee

hemoglobin has serv

reactive heme syste

higher energy anti-

(O-O) bond (Gubelma

fundamental step in

O_2 will only bind to

also react with oxid

solution) with O_2 an

given clues as to re

1978; Chin 1980). Th

in the analysis of o

C. PHYSICAL TECHNIC

In an ideal bioch

interest in a pure fo

metals and other non-

obtain a crystal stru

crystalline form, thi

information to begin

riplet oxygen. The latter configuration is the one depicted in Figure
.6, with each species contributing an electron to the σ and π bonds.
.nce the spins couple in the second case, both these configurations
e net S = 0 (singlet). A third configuration corresponding to eletron
ansfer from the iron to the oxygen (Fe^{+3}, O_2^-) can be included in the
lculations but it makes only a minor contribution. The heme bound
ygen can be considered "activated" in that the triplet state barrier
reaction has been removed. This description of oxygen binding to
oglobin has served as a model for the initial binding of oxygen to
ctive heme systems. Transfer of electrons from the heme to the
her energy anti-bonding oxygen orbitals results in cleavage of the
O) bond (Gubelmann and Williams 1983 pp. 20-24). This is the
damental step in the reaction of heme proteins with oxygen. Although
ill only bind to and react with reduced hemes (Fe^{+2}), peroxide will
react with oxidized hemes (Fe^{+3}). The reactions of hemes (in
tion) with O_2 and peroxide have been studied and these results have
n clues as to reasonable mechanisms in the protein species (James
Chin 1980). These mechanisms will be discussed in later chapters
e analysis of our experimental results.

PHYSICAL TECHNIQUES FOR HEME PROTEIN RESEARCH

n an ideal biochemical world, we would isolate the enzyme of
est in a pure form, perform an elemental analysis (to identify
and other non-protein components), sequence all the peptides and
a crystal structure. Although enzymes don't normally function in
lline form, this would give us the necessary structural
ation to begin intelligent investigations of the mechanism. It

Figure 1.6

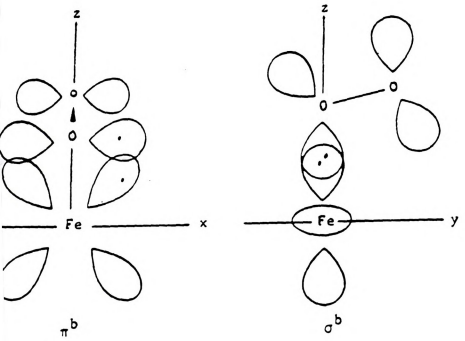

Figure 1.6 The interaction of iron out of plane orbitals with the π^* orbitals of O_2 in Fe^{II} "oxy" heme complexes (from Reed, 1978).

would be better y
intermediates as
studies could be e
preferred. With so
hemoglobin, and my
extent. Unfortunat
molecules, crystal
it seems to be limi
species. Many enzym
cytochrome oxidase,
the isolation and c
been well character
still lacking. In m
most important is th
this is where the in
obtain this informat
resort to less direc
their usefulness, wi

The techniques o
(NMR) spectroscopies
containing proteins,
signal is dominated b
techniques, aqueous s
data collection. Elec
susceptibility are us
signal provides specif

ld be better yet to obtain crystal structures of the reaction
ermediates as well. Once the reaction pathway was known, theoretical
lies could be employed to try to understand why this mechanism is
erred. With some of the simpler heme systems (such as cytochrome c,
globin, and myoglobin) these steps have already occurred to a great
nt. Unfortunately, the biochemical world is still real. For large
cules, crystallography can be a very slow process and at present,
ems to be limited to small proteins and very stable intermediate
es. Many enzymes, especially membrane bound enzymes like
hrome oxidase, have not been successfully crystallized. Although
solation and chemical reactivity of many of the heme enzymes have
well characterized, structural and mechanistic information is
lacking. In most heme enzymes, the structural information that is
mportant is that in the immediate vicinity of the heme, since
s where the important chemistry occurs. Since we cannot always
this information directly by crystallographic means, we must
to less direct techniques. Some of the possible techniques, and
usefulness, will be discussed below.

techniques of infrared (IR) and nuclear magnetic resonance
pectroscopies have been of limited use for the study of heme
ing proteins, as they are not very specific and the observed
is dominated by bands from bulk protein. In addition, for both
ues, aqueous solution systems present technical problems for
lection. Electron paramagnetic resonance (EPR) and magnetic
bility are useful for the study of heme proteins. The observed
rovides specific information about the metal centers because

the signals arise

Although EPR is li

utility for the id

heme proteins (Pei

especially valuabl

the heme and the co

under various condi

electron nuclear do

extensively in heme

ENDOR allows the ob

EPR signal. The tech

environment of paran

limited by the lack

valuable for the stu

al. 1978). Magnetic

technique which has

heme proteins (Babco

direct information ab

It is of limited use

of ^{57}Fe (Munck, E. 19

(XAFS) is a technique

systems. Although int

task, this method is

under favorable condi

Two techniques tha

characterization and s

signals arise from unpaired electrons on the metal centers. ough EPR is limited to odd spin systems, it has been of great ity for the identification of imidazole ligation in a number of proteins (Peisach and Mims 1977). This technique has been an ially valuable tool in the study of cytochrome oxidase since both eme and the copper contain unpaired electrons and can be detected various conditions (Blair et al. 1983). A companion technique, on nuclear double resonance (ENDOR), has not yet been used ively in heme research but shows great promise (Palmer 1979). allows the observation of nuclear transitions via changes in the gnal. The technique gives NMR like resolution in the restricted nment of paramagnetic centers. Magnetic susceptibility is d by the lack of structural detail it provides, but it is le for the study of both odd and even spin systems (Tweedle et 78). Magnetic circular dichroism (MCD) is another magnetic ue which has allowed identification of the iron spin state in oteins (Babcock et al. 1976). Mossbauer spectroscopy provides information about the iron environment and oxidation state but f limited use if the system cannot be enriched in the percentage (Munck, E. 1979). X-ray absorption fine structure spectroscopy s a technique that has been applied extensively to heme Although interpretation of the results has not been a simple is method is capable of providing direct structural information vorable conditions (Powers et al. 1981, 1982).

echniques that have been used extensively for heme ization and structural investigation are optical absorption

and resonance Rama

have used most ext

more detail than t

absorption spectru

cm^{-1}) at ~400 nm i

bands (ϵ=~5 to 20

bands. These consis

transition (0-0), a

(0-1). Of the theor

Gouterman 1978), th

to account best for

HOMO's and 2 LUMO's

a simple Huckel mod

schematically in Fig

atomic orbitals, cer

orbitals. Dashed cir

planes are represent

henes the HOMO's, de

respectively; the LU

symmetry. If one ass

electronic levels sho

strong (allowed) high

(forbidden) low energ

predicts that, as thi

stronger in relation

the X and Y axes is re

components. These prec

esonance Raman spectroscopies. Since these are the techniques I used most extensively in my research, they will be described in detail than the techniques mentioned above. A typical heme ption spectrum is seen in Figure 1.7. The strong band (ϵ=~100 mM^{-1} at ~400 nm is referred to as the "Soret" or "B" band. The weaker (ϵ=~5 to 20 mM^{-1} cm^{-1}) to the red of the Soret are called the "Q" . These consist of the α band, which is a fundamental electronic ltion (0-0), and the β band, which is the first vibronic overtone Of the theoretical treatments applied to heme spectra (see rman 1978), the four orbital model (Gouterman 1961 and 1978) seems ount best for the observed behavior. In this model only the 2 and 2 LUMO's are considered. These orbitals, which are based on le Huckel model (Longuet-Higgins et al. 1950), are shown tically in Figure 1.8. The circles represent contributions of the orbitals, centered on the enclosed atoms, to the molecular ls. Dashed circles represent orbitals of opposite sign and nodal are represented by the heavy lines. Under the ~D_{4h} symmetry of he HOMO's, designated b_1 and b_2, are of a_{2u} and a_{1u} symmetry ively; the LUMO's (c_1 and c_2) are a degenerate set of e_g y. If one assumes that the HOMO's are nearly degenerate, the hic levels should mix through electron interactions, yielding a allowed) high energy transition (Soret) and a weaker en) low energy band (Q) (Gouterman, M. 1959). The theory that, as this degeneracy is relaxed, the Q band will become in relation to the Soret. In addition, if the degeneracy of d Y axes is removed, the Q bands will split into their X and Y ts. These predictions agree with the observed spectra of hemes

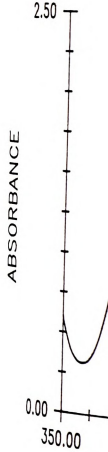

Figure

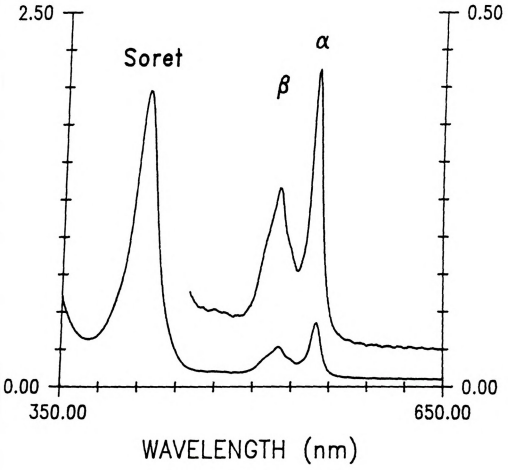

Figure 1.7 The optical absorption spectrum of Fe^{II} cytochrome C.

$c_1(e_g$

$b_1(a_2$

Figure 1.8

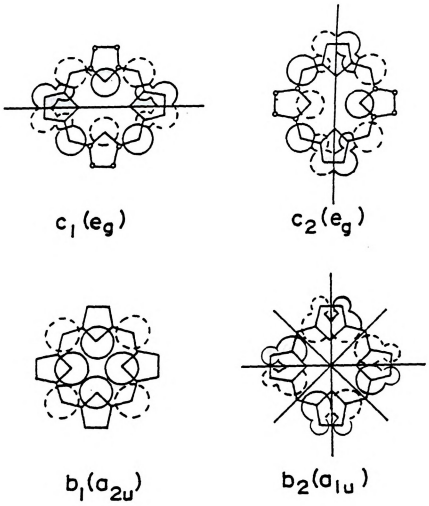

Figure 1.8 The 2 HOMO's and 2 LUMO's of porphyrins, within the 4 orbital model (from Longuet-Higgins, 1950).

with asymmetric r

substituent pertu

other.

Absorption spe

metalloporphyrins

orbitals to the HO

which results in m

specific mixing va

1966). Spectra of

charge transfer bar

region and arise pr

107-114). The charg

weaker and at highe

observed. Other asp

needed in future cha

material, see Callah

Raman spectrosco

information, similar

molecular vibrations

of heme proteins is

give information spec

nature of this resona

When light scatters o

normally be the same

With Raman scattering

with asymmetric ring substitutions. These effects result from the substituent perturbation of one of the HOMO's (or LUMO's) but not the other.

Absorption spectra of hemes are more complicated than other etalloporphyrins owing to the closeness in energy of the iron d rbitals to the HOMO's of the porphyrins (and compatible symmetries), hich results in mixing. This can be seen in Figure 1.9 where the ecific mixing varies with different axial ligation (Zerner et al. 66). Spectra of high spin hemes are also complicated by fairly strong arge transfer bands. These are most often seen in the 500 to 700 nm gion and arise primarily from HOMO to dπ transitions (Spiro 1983, pp 7-114). The charge transfer bands in other heme states are often ıker and at higher energy wavelenghts (near IR) and are typically not erved. Other aspects of heme absorption theory will be discussed as ded in future chapters. For a more detailed discussion of the above erial, see Callahan (1983, Chapter 2).

Raman spectroscopy is a technique which provides structural rmation, similar to IR spectroscopy, through the detection of cular vibrations. The advantage of Raman spectroscopy for the study eme proteins is that it can be used in a resonance condition to information specific to the heme vicinity. To understand the re of this resonance, a brief theoretical discussion is useful. light scatters off a molecule, the scattered frequency will lly be the same as the incident frequency (Rayleigh scattering). Raman scattering, the electromagnetic oscillations of light couple

Orbital Energy (eV)
-8.0
-9.0
-10.0
-11.0
$b_{1g}(d_{x^2-y^2})$
$e_g(\pi)$
$a_{1g}(d_{z^2})$
$e_g(d_\pi)$
$b_{2g}(d_{xy})$
$a_{2u}(\pi)$
$a_{1u}(\pi)$
Fe

Figure 1.9

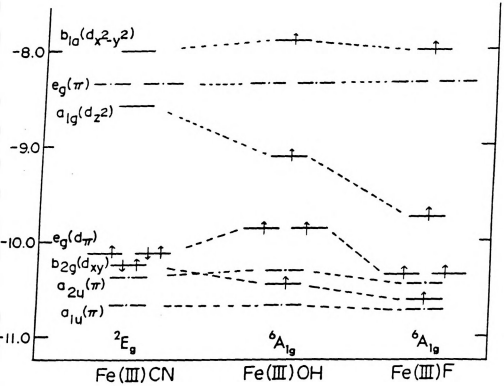

Figure 1.9 Relative energy levels of porphyrin (-·-) and iron (——) orbitals for ferric porphyrin complexes (adapted from Zerner et al., 1966).

with the vibratio

a vibrational fre

note that Raman s

factor of approxi

"anti-Stokes" indi

frequency, respect

temperature or low

originates from th

Raman scattering i

scattered frequency

squared. The polari

dipole moment in re

Albrecht 1970). A s

as the Kramers-Heis

$$(\alpha_{\rho\sigma})_{gf} = \frac{1}{h} \sum_{e}$$

$(\alpha_{\rho\sigma})_{gf}$ is the trans

scattered polarizati

are dipole moment tr

$|e\rangle$, and $|f\rangle$ are the

states , and ν_{eg} and

between the subscript

is a function of the

91-93). The integrals

the intensities of th

the relationships bet

ith the vibrations of the molecule to produce light shifted by + or -
vibrational frequency. This is shown schematically in Figure 1.10;
te that Raman scattering is weaker than the Rayleigh scattering by a
ctor of approximately 10^5. The designations "Stokes" and
nti-Stokes" indicate that the scattered light is of lower or higher
equency, respectively, relative to the incident light. At room
mperature or lower, the Stokes Raman scattering will dominate, as it
ginates from the ground vibrational state. The intensity of the
an scattering is proportional to the incident intensity, the
ttered frequency to the fourth power, and the polarizability
ared. The polarizability is defined as the change in the molecule's
ole moment in response to an applied electric field (Tang and
echt 1970). A second order perturbation expression for this, known
he Kramers-Heisenberg dispersion formula, is seen below.

$$(\alpha_{\rho\sigma})_{gf} = \frac{1}{h} \sum_e \frac{\langle f|\mu_\rho|e\rangle \langle e|\mu_\sigma|g\rangle}{\nu_{eg} - \nu_0 + i\Gamma_e} + \frac{\langle f|\mu_\sigma|e\rangle \langle e|\mu_\rho|g\rangle}{\nu_{ef} + \nu_0 + i\Gamma_e}$$

$_{gf}$ is the transition polarizability tensor, with incident and
ered polarizations indicated by ρ and σ respectively. μ_ρ and μ_σ
ipole moment transition operators of polarization ρ and σ; $|g\rangle$,
and $|f\rangle$ are the wave functions for the ground, excited, and final
s , and ν_{eg} and ν_{ef} are the frequencies for the transitions
en the subscripted states. Γ_e is the transition halfwidth, which
unction of the lifetime of the excited state $|e\rangle$ (Spiro 1983, pp.
. The integrals in the numerators of the two terms evaluate to
tensities of the electronic transitions; the denominators define
lationships between the incident frequency and the frequencies of

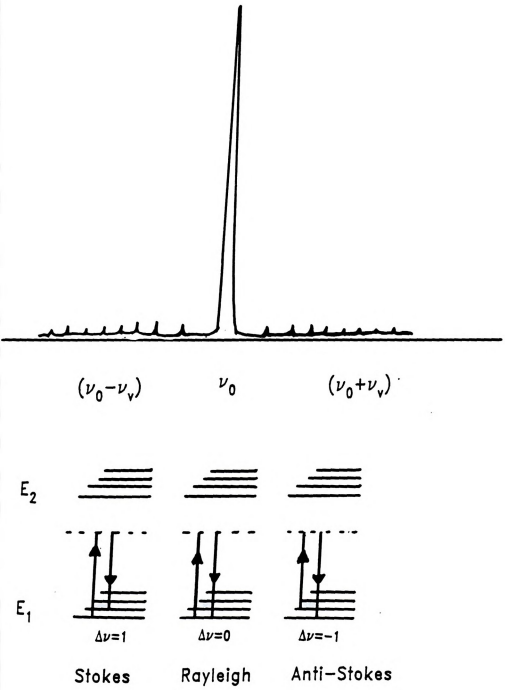

Figure 1.10 Raman (Stokes and anti-Stokes) and Rayleigh light scattering.

the electronic tr

incident frequenc

transition ν_{eg}. T

consider all the

following behavio

incident intensity

a fourth power dep

in energy to an al

polarizability exp

scattering will be

if the excited sta

spectroscopy is sin

selective scatterin

normal Raman is see

bands in the visibl

at wavelengths clos

scattering in the i

from the bulk of the

heme models in solut

enhanced over those

theory (Clark and St

predictions: (1) res

predominantly the to

the Q bands will enh

the polarization of t

light, is characteris

predictions, in conju

the electronic transitions. The resonance effect is observed when the incident frequency is very close to the frequency of the electronic transition ν_{eg}. This will cause the first term to dominate. If we consider all the variables of Raman scattering together we observe the following behavior: (1) Raman scattering increases linearly with incident intensity; (2) blue light scatters better than red light with a fourth power dependence; and (3) if the incident frequency is close in energy to an allowed electronic transition, the first term in the polarizability expression becomes large and the total observed Raman scattering will be dominated by the resonance contribution; especially if the excited state has a long lifetime (small Γ_e). Resonance Raman spectroscopy is simply the use of the resonance effect to obtain selective scattering from a light absorbing species. A comparison with normal Raman is seen in Figure 1.11. Since hemes have strong absorption bands in the visible region of the spectrum, the use of incident light of wavelengths close to these absorption bands results in strong Raman scattering in the immediate heme vicinity with negligible scattering from the bulk of the protein. This process is also advantageous for heme models in solution, since the heme vibrations will be greatly enhanced over those of the solvent. A more detailed analysis of the theory (Clark and Stewart 1979; Spiro 1983) yield the following predictions: (1) resonance with the Soret band will enhance predominantly the totally symmetric heme vibrations; (2) resonance with the Q bands will enhance the non-totally symmetric vibrations; and (3) the polarization of the scattered light, relative to the incident light, is characteristic of the vibrational symmetry. These predictions, in conjunction with calculations of metalloporphyrin

Figure 1.

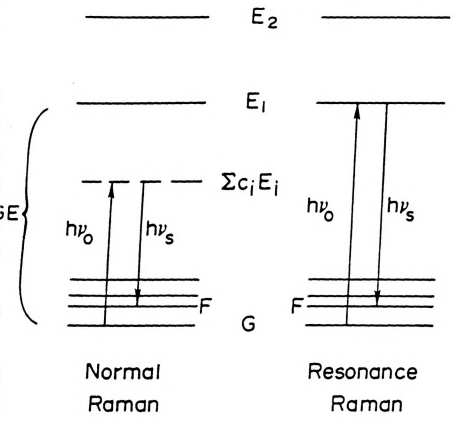

Figure 1.11 A comparison of normal and resonance Raman light scattering (from Ondrias, 1980).

normal modes of

have made possibl

vibrations. This

for the analysis

in heme proteins.

found in Callahan

D. PEROXIDASES,

Peroxidases ar

share many structu

these enzymes has

and Jones (1984).

prothetic group whi

ligated by an axial

to small ligands. P

and the resting for

state. The catalyti

Native Enzyme + H

Compound I +

Compound II +

AH_2 is a substrate t

intermediates. The c

Native Enzyme + H_2O

Compound I + H_2O

normal modes of vibration (Abe et al. 1978; Gladkov and Solovyov 1986) have made possible the assignment of many of the observed heme vibrations. This has made resonance Raman spectroscopy a powerful tool for the analysis of the heme structure and of the immediate environment in heme proteins. A more detailed analysis of the above theory can be found in Callahan (1983, Chapter 2) or Ondrias (1980, Chapter 5).

PEROXIDASES, CATALASES, AND CYTOCHROMES P-450

Peroxidases and catalases are often discussed together because they share many structural and reactive similiarities. The biochemistry of these enzymes has been summarized by Hewson and Hager (1979), and Frew and Jones (1984). Peroxidases and catalases usually contain a protoheme prosthetic group which, except for the subgroup chloroperoxidases, are ligated by an axial histidine imidazole. The heme pocket is accessible to small ligands. Peroxide is the oxidant common to both these systems, and the resting forms of these enzymes have iron in the +3 oxidation state. The catalytic cycle of peroxidases is summarized below:

$$\text{Native Enzyme} + H_2O_2 \text{ ---> Compound I}$$

$$\text{Compound I} + AH_2 \text{ ---> Compound II} + AH$$

$$\text{Compound II} + AH_2 \text{ ---> Native Enzyme} + AH$$

AH_2 is a substrate to be oxidized and compounds I and II are reaction intermediates. The catalytic sequence of catalases is similar:

$$\text{Native Enzyme} + H_2O_2 \text{ ---> Compound I} + H_2O$$

$$\text{Compound I} + H_2O_2 \text{ ---> } O_2 + H_2O + \text{Native Enzyme}$$

In addition, perc

The compounds I a

and they are beli

is an Fe^{IV}=O spec

porphyrin orbital

which are only on

been positively i

(Hashimoto et al.

crystallized (Finz

structural changes

characterized. The

well understood ei

characterized of t

to it frequently.

Cytochromes P-4

insertion of one mo

substrate specifici

review of this fiel

additional recent re

In addition, peroxidases can display catalase activity and vice versa. The compounds I are two oxidizing equivalents above the resting enzyme and they are believed to have a ferryl π-cation radical structure. This is an Fe^{IV}=O species in which an electron has also been removed from a porphyrin orbital to yield a cation radical species. The compounds II, which are only one oxidizing equivalent above the resting enzyme, have been positively identified as ferryl species for some peroxidases, (Hashimoto et al. 1984). Although some of these enzymes have been crystallized (Finzel et al. 1984), the full catalytic cycle and structural changes under turnover conditions have not been well characterized. The factors which control substrate specificity are not well understood either. Horseradish peroxidase is probably the best characterized of this group of enzymes and future chapters will refer to it frequently.

Cytochromes P-450 are a group of heme enzymes which catalyze the insertion of one molecule of oxygen into a substrate. The degree of substrate specificity varies with the particular enzyme. A thorough review of this field can be found in Griffin, et al. (1979) while additional recent results have been discussed by Dolphin, et al.

(1981), Groves (1

catalyzed by this

CYT P-450 + 2e$^-$

where RH is the su

in the C-H bond. I

C-H bond, at a spe

amount of attentio

contain protoheme

occupied by an RS$^-$

common histidine i

mechanisms are sti

that the heme is i

form a species anal

there is a general

1985). Although the

from that of the pe

intermediates may c

E. CYTOCHROME c OX

The enzyme cytoc

major focus of resea

be discussed in grea

perhaps the most com

the process of aerob

study. Several books

1981), Groves (1985), and Eble and Dawson (1986). The basic reaction
ıtalyzed by this class of enzymes is as follows:

$$\text{CYT P-450} + 2e^- + 2H^+ + O_2 + RH \text{ -----> } \text{CYT P-450} + ROH + H_2O$$

ıere RH is the substrate and ROH is the product with oxygen inserted
ı the C-H bond. It is this ability to activate the normally unreactive
H bond, at a specific substrate position, that accounts for the large
ount of attention that cytochromes P-450 have received. These enzymes
ntain protoheme in the active site, but the axial position is
cupied by an RS^- ligand (from a cysteine residue) instead of the more
mmon histidine imidazole. Like the other heme enzymes, their
chanisms are still not well understood. The evidence to date suggests
ıt the heme is initially reduced to Fe^{+2}. It can then bind oxygen to
rm a species analogous to oxymyoglobin. Later steps are not clear but
ere is a general consensus that a ferryl species is involved (Groves
5). Although the chemistry of cytochromes P-450 are quite different
m that of the peroxidases and catalases, their reaction
ermediates may contain some analogous structures.

CYTOCHROME c OXIDASE

The enzyme cytochrome c oxidase (cytochrome oxidase) has been a
r focus of research in the laboratory of G. T. Babcock and it will
iscussed in greater detail than the previous enzyme systems. It is
aps the most complex of the heme enzymes and its dominant role in
rocess of aerobic respiration has made it the subject of intense
. Several books and extensive reviews have been written on the

subject of cytoch
1979; Wikstrom et
is referred to th
summary below wil
function of the e
will be emphasize

Cytochrome oxi
functions at the t
equivalents (elect
increasingly bette
potential) until th
reaction is shown b

$4H^+ + 4CYT\ c^+$

Coupled to oxygen r
gradient which is fu
biochemical energy).
provided by the redu
molecules of ATP per
anaerobic organisms
localized on the inne
protruding on both si
monomer have been rep
in Figure 1.13. This
microscopy of oriente

subject of cytochrome oxidase (see King et al. (ed) 1979; Malmstrom 1979; Wikstrom et al. 1981; and Naqui and Chance 1986) and the reader is referred to them for details of its chemistry or biochemistry. The summary below will provide a brief overview of the structure and function of the enzymes. The role of the metal centers in catalysis will be emphasized.

Cytochrome oxidase (labeled as "Cytochrome a_3" in Figure 1.12) functions at the terminus of the electron transport chain. Reducing equivalents (electrons) from the tricarboxylic acid cycle are passed to increasingly better electron acceptors (more positive reduction potential) until they are used to reduce O_2 to H_2O. The overall reaction is shown below, where CYT stands for cytochrome.

$$4H^+ + 4CYT\ c^{+2} + O_2 \text{ ---> } 2H_2O + 4CYT\ c^{+3}$$

Coupled to oxygen reduction is the generation of a transmembrane pH gradient which is functional in the production of ATP (stored biochemical energy). Because of the large thermodynamic driving force provided by the reduction of oxygen, aerobic organisms can produce 36 molecules of ATP per molecule of glucose as opposed to only 2 for anaerobic organisms (Lehninger 1975 p. 517). Cytochrome oxidase is localized on the inner membrane of the mitochondria with portions protruding on both sides. The shape and dimensions of the enzyme dimer have been reported by Henderson et al. (1977) and can be seen in Figure 1.13. This result was obtained through the use of electron microscopy of oriented membrane layers. Cytochrome oxidase has been

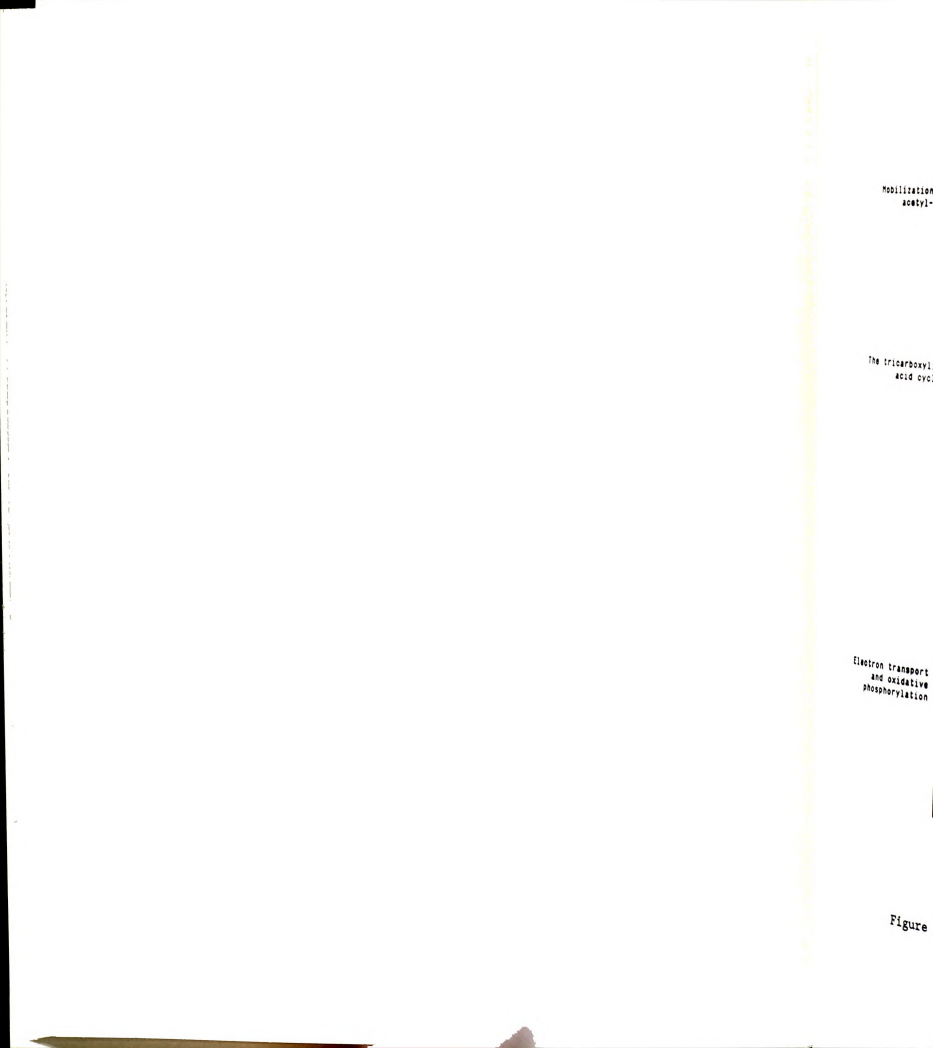
Mobilization
acetyl-
The tricarboxyl
acid cyc
Electron transport
and oxidative
phosphorylation

Figure

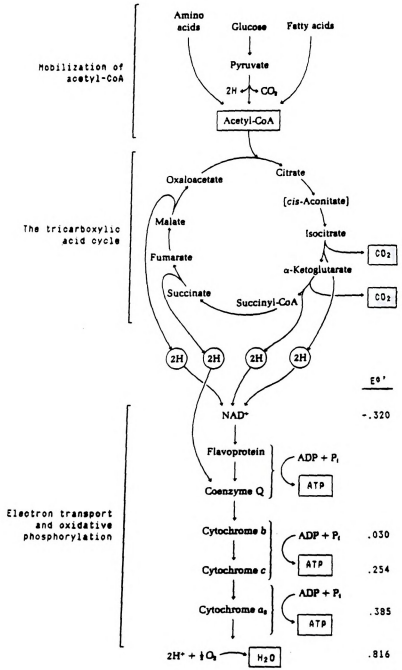

Figure 1.12 Aerobic respiration
(adapted from Lehninger, 1975).

Figure 1.13

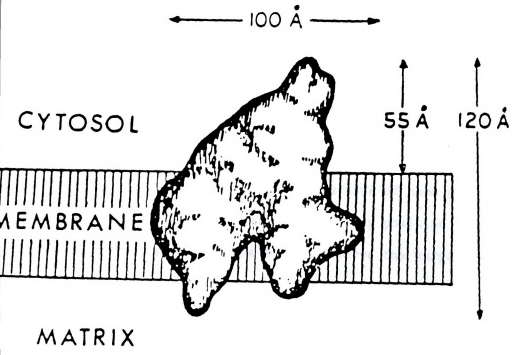

Figure 1.13 The shape of cytochrome oxidase (adapted from Henderson, 1977).

difficult to stu

with a total mol

subunits in euka

composed of only

larger units of

active metal cent

one serving a dif

temperature, the

the study of inte

membrane bound en

isolate and study

The heme of cy

has been shown in

long, partially un

formyl group at ri

anchoring the heme

transfer into the

been postulated to

enzyme (Artzatbanov

substituents is sti

particular heme see

representation of t

can be seen in Figu

et al. (1983), is b

knowledge about the

reasons, the two met

difficult to study for several reasons. It is a very large protein, with a total molecular weight of ~140,000 to ~200,000 and 7 to 12 subunits in eukaryotic cells. Bacterial oxidase is smaller and is composed of only two subunits which are roughly equivalent to the two larger units of the eukaryotic system. Cytochrome oxidase contains four active metal centers: two hemes and two chelated copper ions, with each one serving a different specific function. At physiological temperature, the enzyme can turnover at a rate of ~500 s^{-1}, which makes the study of intermediates difficult. Cytochrome oxidase, like many membrane bound enzymes, easily denatures. This makes it difficult to isolate and study in an active form, relative to other heme enzymes.

The heme of cytochrome oxidase is heme a; the structure of which has been shown in Figure 1.3. The peculiar features of heme a are the long, partially unsaturated "tail" attached to ring position 2, and the formyl group at ring position 8. The tail may serve the purpose of anchoring the heme in the protein, or it may be functional in charge transfer into the heme site (Caughey et al 1975). The formyl group has been postulated to participate in the proton pumping function of the enzyme (Artzatbanov et al. 1979). The purpose of these particular ring substituents is still a very active area of research, as this particular heme seems to be unique to cytochrome oxidase. A schematic representation of the placement and ligation of the four metal centers can be seen in Figure 1.14. This picture, which was proposed by Blair et al. (1983), is based on both his own recent data and cumulative knowledge about the structures of the metal centers. For historical reasons, the two metal centers in the upper half of Figure 1.14 are


cytochrome
c
INTRACRISTAL
SPACE
INNER
MITOCHONDRIAL
MEMBRANE
MATRIX

Figure 1.14

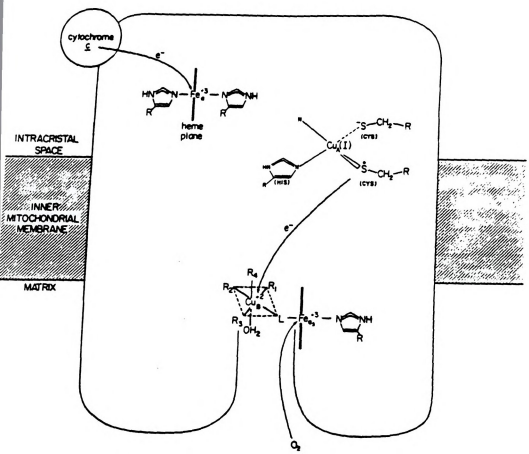

Figure 1.14 The relative locations of the metal centers in cytochrome oxidase (from Blair, 1983).

referred to as

while the lower

figure is drawn

has two imidazol

Cu_A is less cert

(from cysteine)

of these two meta

conditions. They

electron transfer

The distance betw

angstroms. The cy

reduction site. F

catalytic cycle.

bridges and magnet

1978). The identit

have not been dete

two metal systems

sufficiently close

ligands; both amin

under investigatio

oxidase in the ful

Figure 1.15a. This

deconvoluted by Var

heme centers. These

the individual heme

of heme a models (C

et al. 1981) in ter

referred to as cytochrome a (with the individual metals Fe_a and Cu_A) while the lower half is called cytochrome a_3 (with Fe_{a3} and Cu_B). The figure is drawn so that the heme axial ligands are clearly seen. Fe_a has two imidazole ligands from histidine residues. The ligation of the Cu_A is less certain but probably includes one or two sulfur ligands (from cysteine) and probably one or two imidazole ligands. The ligation of these two metal centers does not appear to change during turnover conditions. They appear to function primarily as redox centers for electron transfer (although they may have a role in proton pumping). The distance between these two metal centers has been estimated at ~15 angstroms. The cytochrome a_3 metals have been identified as the O_2 reduction site. Fe_{a3} contains one imidazole ligand throughout the catalytic cycle. A sixth ligand is present in the resting enzyme, which bridges and magnetically couples the Fe_{a3} to the Cu_B (Tweedle et al. 1978). The identity of this bridging ligand and the ligands to the Cu_B have not been determined with any certainty. The distance between these two metal systems has been estimated at ~5 angstroms. This is sufficiently close to allow for a wide variety of possible bridging ligands; both amino acid residues and exogenous ligands are currently under investigation. The optical absorption spectrum of cytochrome oxidase in the fully oxidized and fully reduced states is seen in Figure 1.15a. This composite spectrum of the two hemes has been deconvoluted by Vanneste (1966) into the components of the individual heme centers. These results are seen in Figure 1.15b. These spectra of the individual heme sites have been closely approximated with the use of heme a models (Callahan and Babcock 1981; and Van Steelandt-Frentrup et al. 1981) in terms of a six-coordinate, low-spin heme in cytochrome

a)

b)

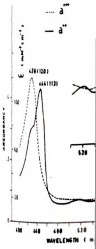

Figure 1

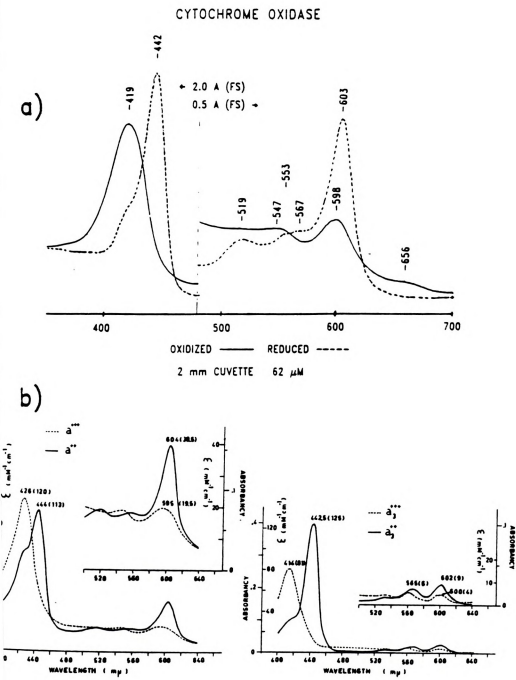

Figure 1.15 a) The optical absorption spectrum of oxidized and reduced cytochrome oxidase, b) The approximation of the spectral contributions from the individual heme centers (from Vanneste, 1966).

a and a high-sp

oxidized enzyme

reproduced in F

the two heme cer

Raman spectra of

line. Resonance

reviewed recentl

further in the l

The catalytic

great deal of res

The scheme presen

intermediates tha

figure only the t

are shown. The fi

oxidation states.

bind oxygen to for

involved as the ox

cleavage of the O-

ferryl intermediat

there is still no

exists as drawn. R

the possibility of

and a high-spin heme in cytochrome $\underline{a}_3$ which is six-coordinate in the xidized enzyme and five-coordinate in the reduced. These spectra are eproduced in Figure 1.16. Note that the different absorption maxima of ne two heme centers make it possible to obtain selective resonance aman spectra of the two centers by careful choice of laser exciting ine. Resonance Raman spectroscopy of cytochrome oxidase has been eviewed recently by Babcock (1986). This topic will be discussed urther in the later chapters in the discussion of my results.

The catalytic cycle of cytochrome oxidase has been the subject of a reat deal of research and the source of a great deal of speculation. ne scheme presented in Figure 1.17 is representative of the types of ntermediates that have been proposed (Blair et al. 1985). In this igure only the two metals of cytochrome $\underline{a}_3$ and the space between them re shown. The first species contains the metals in their resting tidation states. Upon reduction of the metal centers, the heme may nd oxygen to form an "oxy" structure. Bridging structures may be volved as the oxygen is reduced to the level of peroxide. The eavage of the O-O bond may be associated with the formation of a rryl intermediate. Unfortunately, despite a great deal of research, ere is still no definite evidence that any of these intermediates ists as drawn. Results discussed in later chapters will comment on possibility of these structures being correct.

Figure

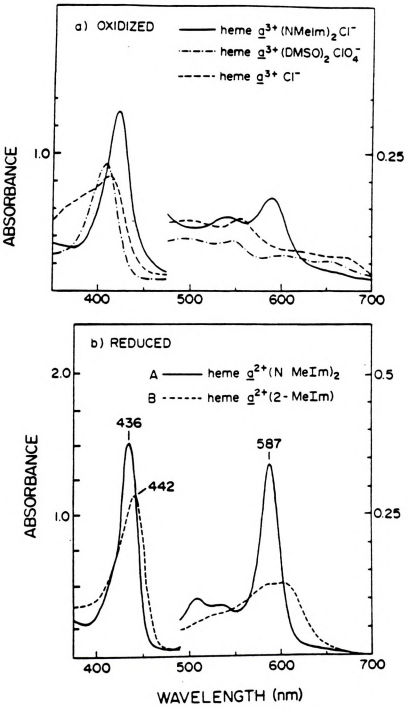

Figure 1.16 Heme a models for the heme centers in cytochrome oxidase (Figure courtesy of G. T. Babcock).

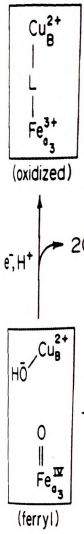

Figure 1.1

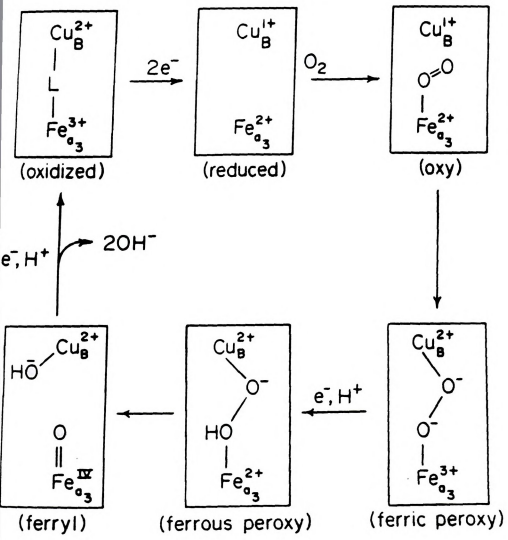

Figure 1.17 A proposed catalytic cycle for oxygen reduction by cytochrome oxidase (Figure courtesy of G. T. Babcock).

A. RESONANCE R

To obtain Ra

include: (1) a h

laser), (2) a sa

other chromatic

detector, and (5

laboratory for r

sources:

sample holders

monochromator:

detector:

data collectior

output device:

The commercially m

Appendix 1. The va

frequencies through

for resonance Raman

CHAPTER 2

EQUIPMENT AND TECHNIQUES

.. RESONANCE RAMAN SPECTROSCOPY

To obtain Raman spectra, several components are necessary. These nclude: (1) a high intensity monochromatic light source (usually a aser), (2) a sample holder, (3) a high resolution monochromator or cher chromatic dispersing component (prism or grating), (4) a light tector, and (5) a data output device. The components available in our boratory for resonance Raman spectroscopy consist of the following:

sources:	Kr ion, Ar ion, tunable dye, and He-Cd lasers
sample holders:	cuvette, capillary, spinning cell, spinning difference cell and low temperature EPR tube
monochromator:	scanning double grating
detector:	photomultiplier tube
data collection:	dedicated computer
output device:	chart recorder and digital plotter

commercially manufactured components of this system are listed in ndix 1. The variety of laser sources provide different excitation uencies throughout the visible region of the spectrum. This allows resonance Raman investigation of hemes utilizing both Soret and

"visible" (Q ba
excellent for s
light or tempera
monochromator ar
resolution, reje
throughput. Alth
samples, a major
was the inabilit
deficiency resul
drive. Difference
two different san
scan to scan vari
problem was solve
computer control
of the data. The
of a Raman differ
collection of Rama
apparatus utilized
software modificat
are described in t

A schematic dr
2.1. The Digital E
Ramalog spectromet
was designed and as
Atkinson and me. Th
spectrometer steppe

"visible" (Q band) excitation. The cuvette and capillary cells are excellent for stable samples, but the alternate cells are necessary for light or temperature unstable samples. The combination of a scanning monochromator and a PMT produces excellent spectra in terms of resolution, rejection of the strong Rayleigh scattering, and light throughput. Although a chart recorder output is sufficient for many samples, a major deficiency of an earlier version of the Raman system was the inability to signal average or reformat data. Another deficiency resulted from the mechanical limitations of the grating drive. Differences in the peak positions of less than 2 cm^{-1}, between two different samples, could not be assigned with confidence since the scan to scan variability of the instrument was ~+/- 1 cm^{-1}. The first problem was solved by the construction of an interface which provided computer control of the instrument and allowed collection and storage of the data. The second limitation was alleviated by the construction of a Raman difference apparatus, which allows for simultaneous collection of Raman spectra of two different samples. The difference apparatus utilized the interface and required only minor hardware and software modifications. The design and operation of these two systems are described in the following paragraphs.

A schematic drawing of the Raman system layout is seen in Figure . The Digital Equipment Corporation (DEC) LSI-11/2 is linked the the analog spectrometer through a house built interface. This interface was designed and assembled by Martin Rabb with assistance from Thomas Hinson and me. The interface allows the computer to actuate the spectrometer stepper motor and drive the gratings. Since the level of


CHART RECORDER
ANALOG OUT
PHOTOMETER
PULSE DISCRIMINATOR

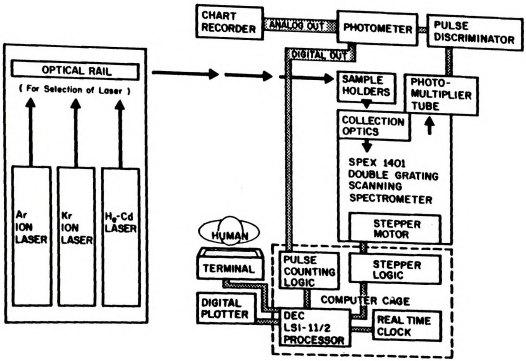

Figure 2.1 Computer interfaced scanning Raman spectrometer system.

light observed f
from the PMT is
single photon. T
and then passed
an analog value
on the ratemeter
these photon pul
logic level pulse
digital counting
over the commerci
ratemeter analog
accuracy. The sof
a menu fashion fo
parameter are dis
photon count valu
and graphics rout
user specifies the
number of scans to
specified time int
counts again, etc.
scan time, the ope
utilize time more
that it allows for
impossible before.
ny experimental wo
identifying were e
noise with only a

light observed for Raman spectroscopy is typically very low, the signal from the PMT is observed as distinct pulses, each corresponding to a single photon. These pulses are shaped by a discriminator/preamplifier and then passed on to a ratemeter where the pulse rate is converted to an analog value which is sent to the chart recorder. A digital output on the ratemeter makes the photon pulses available directly. Since these photon pulses were very similar in shape and size to computer logic level pulses, we connected the raw pulse signal directly to a digital counting chip in the interface. This design was an improvement over the commercial systems available at the time which redigitized the ratemeter analog signal at the loss of collection speed and data accuracy. The software is written in FORTRAN and MACRO and operates in a menu fashion for user convenience. The data file name and all current parameter are displayed continuously; the spectrometer wavenumber and photon count values are updated as available. Some data manipulation and graphics routines are also available directly from the program. The user specifies the scan limits, point spacing, counting time, and the number of scans to be averaged. The computer counts photons for the specified time interval, moves the spectrometer to the next point and counts again, etc. Since the computer is in control during the entire scan time, the operator can now do other things while it is running and utilize time more efficiently. The greatest advantage of this system is that it allows for long signal averaging experiments that were impossible before. Implementation of this capability was essential for my experimental work since many of the peaks I was interested in identifying were extremely weak and could not be resolved from the noise with only a single scan.

The Raman c

which is divide

is spun by a mo

operation, a sy

motor mount eac

(switches from

gating of the P

the accumulatio

different count

subtracted from

the two spectra

result from gra

assignments of

selects the pho

seconds, since

the two channels

mount were desig

designed the dif

design of this e

however the use

the reported mix

channel separati

hardware schemat

found in Centeno

The Raman difference apparatus utilizes a short cylindrical cell
ich is divided down the center to provide two compartments. This cell
spun by a motor drive such that alternate halves are illuminated. In
eration, a synchronization pulse is generated from a circuit on the
or mount each time the cell rotates through the cell divider
itches from one cell half to the other). This pulse activates the
ing of the PMT output from one counter to another. The net result is
accumulation of data from the two different samples in two
ferent counters. The scans can be plotted separately or one
tracted from the other to accentuate the differences. Collection of
two spectra simultaneously eliminates the uncertainty which may
ult from grating slippage. Use of this technique allows confident
gnments of peak differences of $^{-}1$ cm^{-1}. For these spectra, the user
cts the photon counting time in terms of cell rotations rather than
nds, since the cell must complete full rotations for the signals on
two channels to be equivalent. The electronic hardware and motor
t were designed by Martin Rabb and Jose Centeno; Jose and I
gned the difference cell, and I wrote the necessary software. The
gn of this equipment is based on that of Kiefer et al. (1975);
ver the use of digital counting and switching logic, rather than
eported mixture of analog and digital processing, turned the
el separation from a difficult task to a nearly trivial one. The
are schematics and mechanical details of the instrument can be
in Centeno (1987).

B. LOW TEMPER

Many of the
temperatures or
intention was t
spectroscopy, i
them in the sam
possible, it wo
introduce addit
(outside dimens
qualities: (1) t
glass shop; (2)
experiments with
reagents or diff
cylindrical shap
vacuum and the f
(4) quartz is in
transparent in t
definition they
temperature rig
for Raman spectr
equipment (either
could be easily s
draw-backs of usi
events required t
in the small tube
absorption spectr
samples. I had to

. LOW TEMPERATURE SPECTROSCOPY

Many of the compounds I have worked with are stable only at low emperatures or under anaerobic conditions or often both. Since my ntention was to study these compounds with different types of pectroscopy, it was desirable to be able to make them and characterize hem in the same cell. Even if transfering them to different cells was ssible, it would make the experiments more difficult and possibly troduce additional variables. The standard cell chosen was a 4 mm utside dimension) quartz EPR tube. These displayed many positive alities: (1) they were inexpensive and easily manufactured by our ass shop; (2) their small dimensions made it possible to do periments with small volumes of sample, thus conserving valuable gents or difficult to isolate biological substances; (3) the indrical shape of tubing makes it structurally able to withstand uum and the freezing and thawing of aqueous and organic solutions; quartz is inert to esentially all solvent systems and optically nsparent in the UV and visible regions of the spectrum; (5) by inition they could be used for EPR spectroscopy and a low perature rig had already been constructed for the use of these tubes Raman spectroscopy; (6) they could be easily connected to anaerobic pment (either direct seal or heat shrink tubing); and (7) samples d be easily stored in a liquid nitrogen freezer in them. The only -backs of using these tubes were: (1) the sophisticated sequence of ts required to produce most of the samples was difficult to perform he small tubes; and (2) we had no practical way to obtain optical rption spectra of samples in these tubes, especially frozen les. I had to learn to live with the first problem but the second

was eliminated

optical absorpt

the other low t

The original

was designed by

laser beam enter

prisms, and refl

Light scattered

collected by the

contrast to a tr

vertically throu

the scattered li

is held by fricti

spun in the mount

obtain a more hom

degradation that

to the laser beam

gas through coppe

inner passage of

controllable from

thermocouple posi

through the dewar

impractical to at

Although there are

system produces ex

throughout its ful

was eliminated by the design and construction of a low temperature optical absorption rig for samples in EPR tubes. Details of this and the other low temperature rigs are presented below.

The original functional low temperature Raman backscattering system was designed by W. Anthony Oertling and is seen in Figure 2.2. The laser beam enters from below, is horizontally moved by two 90 degree prisms, and reflects off the backscattering mirror on to the sample. Light scattered from the sample at ~180 degrees to incidence is collected by the optics and focused into the monochromator. This is in contrast to a traditional Raman experiment in which the laser passes vertically through the sample (in an optical cuvette for example) with the scattered light collected at 90 degrees to incidence. The EPR tube is held by friction against two O-rings in a plastic "spinner" which is spun in the mounting block by tangential air jets. The tube is spun to obtain a more homogeneous sampling and to minimize the photo or thermal degradation that may occur if the same region were continuously exposed to the laser beam. Temperature is controlled by the flow of nitrogen gas through copper coils (submerged in liquid nitrogen) and through the inner passage of the dewar. The temperature, which is continuously controllable from room temperature to ~-130 C, can be monitored by a thermocouple positioned directly below the EPR tube. Thermal leakage through the dewar walls, transfer tubes, and connections, make it impractical to attempt to use this system at lower temperatures. Although there are reflective losses at each optical surface, this system produces excellent spectra for both liquid and frozen samples throughout its full temperature range. In addition, for room

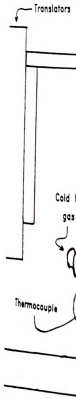
Translators
Thermocouple

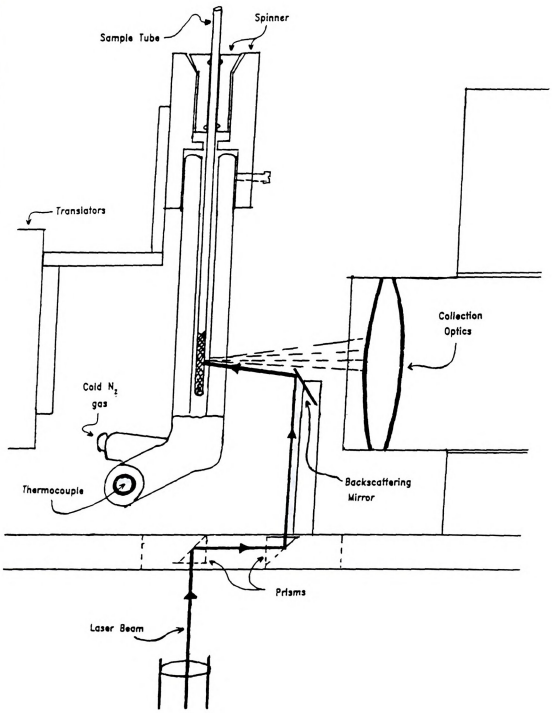

Figure 2.2 Low temperature Raman backscattering Dewar.

temperature wor
reflective loss
absorbing sampl
technique over
can be used, st
solvent scatteri

Although the
use, temperature
not attainable w
liquid nitrogen.
temperature regu
nitrogen interfe
designed and had
operates on a flo
entry surfaces. N
resevoir and dire
The sample is aga
of the sample com
are submerged in
front wall and tha
monitored by an in
Dewar system, desp
or better than the
readily controlled
C) with warmer tem
system is more dif

mperature work, the Dewar flask can be removed to reduce the
flective losses. For resonance Raman spectroscopy of strongly
sorbing samples in organic solvents, backscattering is the preferred
chnique over 90 degree scattering. Since much higher concentrations
n be used, stronger resonance scattering relative to the background
lvent scattering is obtained.

Although the above mentioned Dewar flask works well and is easy to
, temperatures low enough for some of the planned experiments were
attainable with it. We needed to maintain temperatures near that of
uid nitrogen. Immersion Dewar systems are effective but offer no
perature regulation and the spontaneous bubbling of the liquid
rogen interferes with the signal collection. For this reason, I
igned and had constructed the Dewar system in Figure 2.3. It
rates on a flowing gas principle but it is designed to minimize heat
y surfaces. Nitrogen gas flows through the coils in the central
voir and directly out through the tube imbedded in the sidewall.
sample is again suspended and spun in this tube. Because the back
he sample compartment is the reservoir and all connection points
submerged in liquid nitrogen, the only heat leakage surface is the
t wall and that seems to be neglegible. Again, temperature is
tored by an imbedded thermocouple and regulated by gas flow. This
system, despite its awkward appearance, produces signal equal to
tter than the original Dewar arrangement. The temperature is
ly controlled in the range of -192 C to -182 C (liquid N_2 = -196
th warmer temperatures possible with some effort. Since this
n is more difficult to set up, it is not normally used for routine

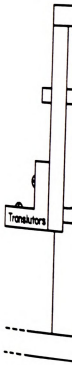

Figure

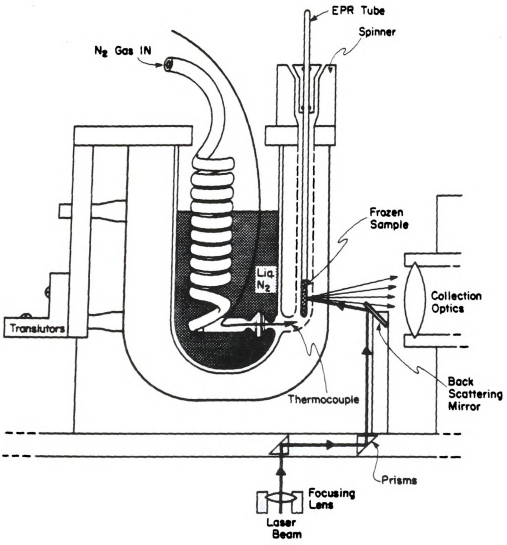

Figure 2.3 Liquid nitrogen temperature backscattering Dewar system.

work with the

obtain Raman s

intermediates.

The basis o

rig is a system

use of EPR tube

problem. The wi

spectrometer is

mm) and curved e

sample giving er

with the acquisi

which has a focu

still poor relati

was considerably

minimized by the

down to a width o

the sample to rec

more of it would

shown in Figure 2.

Using a clear liqu

transmitted relati

much smaller than

instrument to achi

baseline with this

pathlength calibrat

centered. This rig

ork with the more stable compounds, but it has added the capability to
otain Raman specta of highly unstable compounds and enzyme
ntermediates.

The basis of the low temperature optical absorption spectroscopy
g is a system like the original Raman Dewar arrangement. However, the
e of EPR tubes for absorption spectra presented a slightly different
oblem. The width of the light beam in the average absorption
ectrometer is ~2 to 4 mm. The narrow inside diameter of the tubes (~3
and curved edges allowed light from the spectrometer to bypass the
ple giving erroneous absorption values. The situation was improved
h the acquisition of a Perkin-Elmer Lambda 5 spectrophotometer,
ch has a focused beam width of ~1 mm, however light throughput was
ll poor relative to the light bypassing the sample. The situation
considerably worse with frozen samples. These problems were
imized by the use of a cylindrical lens to focus the incident light
to a width of ~0.2 mm at the sample. Another lens was added after
sample to recollimate the light diverging from the sample so that
of it would reach the detector. A drawing of this Dewar system is
n in Figure 2.4. Inset in the top is a schematic of the light path.
g a clear liquid as a blank, approximately 15% of the light is
mitted relative to the unhindered reference beam. Although this is
smaller than hoped, there is still enough dynamic range in the
ument to achieve good spectra even with concentrated samples. The
ine with this rig is flat over most of the visible range and the
ength calibrates to 3 mm, indicating that the beam is narrow and
ed. This rig has been an essential part of my research. Positive

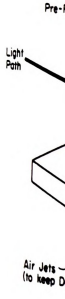

Figure 2.4

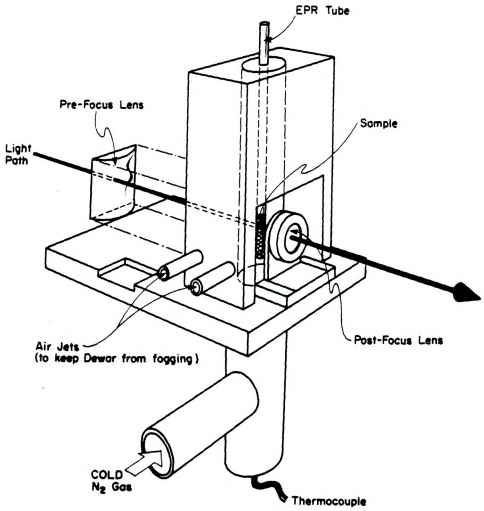

Figure 2.4 Low temperature Dewar system for optical absorption spectroscopy.

identificatio

more confident

temperature sy

spectrum can b

decomposition

C. ANAEROBIC

Many of the

sensitive. Sinc

the basic requi

anaerobic/vacuu

it offered a hig

anaerobic train

This design is b

(personal commun

highly reduced m

selectable rough

The anaerobic pa

oxygen scrubbing

trap or solvent s

pressure releases

anaerobic line is

alternately evacua

used with this car

tight and able to

manifold.

identification of sample species by their absorption spectra allows more confident interpretation of their Raman spectra. With this low temperature system, the absorption spectrum taken after a Raman spectrum can be compared with the one taken before as a test for sample decomposition in the laser beam.

ANAEROBIC TECHNIQUES

Many of the compounds I have worked with have been oxygen and water nsitive. Since the normal atmosphere contains large amounts of both, e basic requirement for such work is a well made glove box or a good aerobic/vacuum train. The latter was chosen for my experiments since offered a higher degree of anaerobicity at a lower cost. The aerobic train I designed for this purpose is shown in Figure 2.5. s design is based on one designed and used by Dr. John Ellis rsonal communication) at the University of Minnesota for work with hly reduced metal species. The vacuum part consists of alternately ectable rough or oil diffusion pumps with two cold traps in series. anaerobic part consists of an Ar gas source, BASF (R3-11 catalyst) gen scrubbing column (generously donated by Dr. James Dye), moisture or solvent saturation bubbler, Ar gas reservoirs, and mercury pool sure releases. The connecting unit between the vacuum line and the robic line is the Schlenk manifold which allows an apparatus to be rnately evacuated or pressurized with Ar gas. The specific vessel with this can take on any variety of forms but it must be vacuum and able to attach to the ground glass joint on the Schlenk old.

Figu

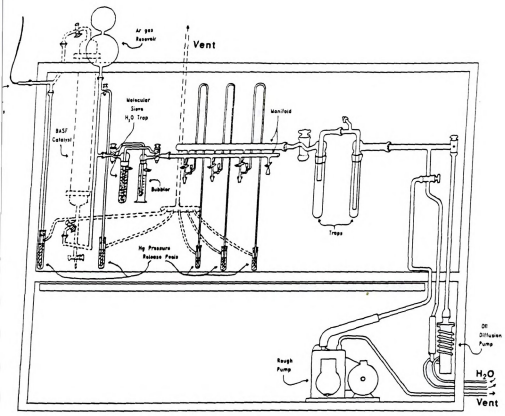

Figure 2.5 Anaerobic/vacuum system.

Examples

flasks are see

manifold and f

over the septu

the flask is u

removed to all

attached high v

removed from th

reattached late

an EPR tube, wh

Scientific) high

allows modular p

experiment. Othe

glass shop for e

expensive. The o

Solution from th

tube arm. When th

collapse on itsel

tightly sealed an

anaerobicity. Unl

non-destructive.

tube reused. This

of Raman samples,

removed from the m

When a flask i

must be purged of

Examples of some of my more versatile and frequently used anaerobic flasks are seen in Figure 2.6. The upper flask attaches directly to the manifold and features only a septum port. The plate of glass is clamped over the septum to assure a complete seal during the vacuum cycles. If the flask is under a positive pressure of Ar gas, this plate can be removed to allow syringe access to the flask. The lower flask has an attached high vacuum stopcock. When this is closed, the cell can be removed from the manifold without risk of air contamination and reattached later as needed. This flask also features a syringe port and EPR tube, which are connected to the main body with FLOTITE (Pope Scientific) high vacuum heat shrink tubing. This is useful because it allows modular pieces to be assembled quickly for a specific experiment. Otherwise, specific cells would have to be made by the glass shop for each experiment, which would be both time consuming and expensive. The other advantage is that it allows for easy "seal-offs". Solution from the main body of the flask can be poured into the EPR tube arm. When the bridging part of the FLOTITE is heated, it will collapse on itself. If it is crimped while warm, the tube will be totally sealed and can be cut off the main body without loss of hydrobicity. Unlike a traditional glass seal off, this is nondestructive. The FLOTITE can be easily removed later and the EPR tube reused. This procedure was especially useful for the preparation of human samples, since the EPR tube cannot be spun unless it is sealed from the main body of the flask.

When a flask is first attached to the manifold, the sample within the tube is purged of oxygen by "freeze, pump, thaw" cycles. As the name

Figu

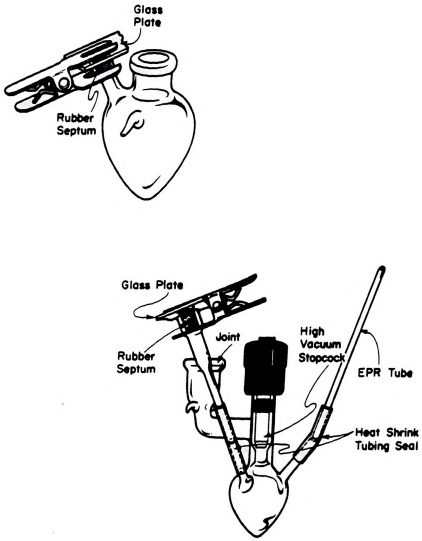

Figure 2.6 Anaerobic glassware.

implies, the
completely fr
pumped out un
nitrogen is re
Ar gas simply
evaporation as
gases to be re
or other volati
depends on the
the sensitivity
cycles are perf

Although hig
septum ports, ca
syringe needles
under a positive
septum will cause
the second end is
above atmosphere)
anaerobically. If
the higher pressu
transfer these sol
do complex anaerob

implies, the cell is immersed in liquid nitrogen until the sample is completely frozen. While still immersed in the liquid N_2, the flask is pumped out under vacuum for ~5 to 30 minutes. Finally, the liquid nitrogen is removed and the cell is filled with Ar gas as it thaws. The Ar gas simply provides an inert atmosphere which minimizes solvent evaporation as the solution thaws. This allows for oxygen and other gases to be removed from the sample without losing much of the solvent or other volatile components of the sample. The number of cycles used depends on the sample size, the surface area of the frozen sample and the sensitivity of the final product to oxygen. Ordinarily 5 to 12 cycles are performed.

Although high quality gas tight syringes can be used with the septum ports, cannulae are generally more useful. These are long syringe needles with points on both ends. If a flask is maintained under a positive Ar gas pressure, insertion of the cannula through the septum will cause Ar gas to flow out preventing air from flowing in. If the second end is inserted in a flask of lower pressure (but still above atmosphere), Ar gas will flow from one to the other, still anaerobically. If the cannula point is pushed below the fluid level in the higher pressure flask, liquid will be transferred. The ability to transfer these solutions anaerobically is the final tool necessary to complex anaerobic chemistry as will be described in later chapters.

D. ELECTROCH

One powerf

electrochemist

the technique

oxidase, is mo

reagents commor

the ring substi

undesirable sin

porphyrin which

Previous reducti

the careful titr

results and wast

system since the

there is no faci

electrodes. Sinc

the literature se

designed my own e

Current flows bet

wire acts as a ps

separaced by glas

but to prevent la

solutions are free

then poured in uni

reduction potentia

determined by perf

plot of current flo

flow only during an

D. ELECTROCHEMISTRY

One powerful synthetic tool often overlooked by chemists is electrochemistry. For some of the reactions I performed, it was clearly the technique of choice. Heme a, the prosthetic heme in cytochrome oxidase, is more difficult to study than most hemes because the reagents commonly used to reduce Fe^{+3} to Fe^{+2} can also easily reduce the ring substituent formyl group (see Figure 1.3). This is very undesirable since it is the π-conjugation of this group into the porphyrin which gives heme a some of its unique characteristics. Previous reduction schemes (Vansteelandt-Frentrup et al. 1981) required the careful titration of reductant, which often produced unpredictable results and wasted heme a. Electrochemistry is ideal for this heme system since the reduction potential can be specifically adjusted and there is no facile mechanism for formyl reduction on simple platinum electrodes. Since none of the electrochemistry cell designs reported in the literature seemed to meet my specific needs (Kadish 1983), I designed my own electrochemistry cell. This cell is seen in Figure 2.7. Current flows between the working and counter electrodes while a silver wire acts as a pseudo reference electrode. These compartments are separated by glass frits to allow electronic contact and ion transport but to prevent large amounts of mixing. The sample and electrolyte solutions are freeze, pump, thawed in their individual side arms and then poured in unison into their electrochemistry compartments. The reduction potential of heme a relative to the pseudo-reference is determined by performing cyclic voltammetry (Figure 2.8 a), i.e., a plot of current flow versus electrode potential. Since current will flow only during an oxidation or reduction process, we can determine

Figure 2.

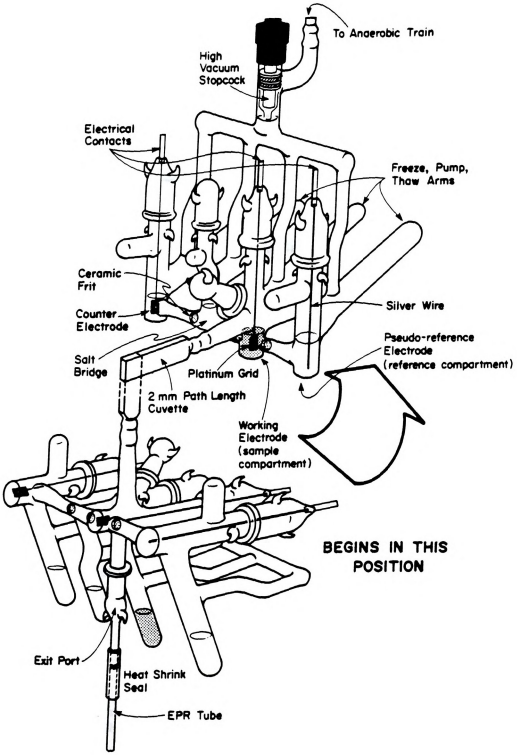

Figure 2.7 Electrochemistry cell for small volume anaerobic work.

b)

ABSORBANCE

0

Figure 2.8

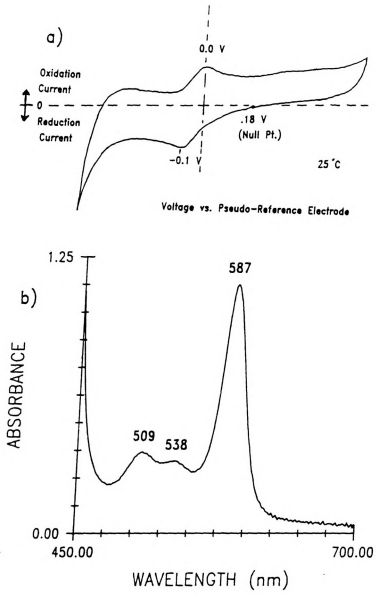

Figure 2.8 A. Cyclic voltammagram of bis 1-methylimidazole heme a (Fe^{III}) in CH_2Cl_2 (electrolyte TBAP .1M)
B. Optical absorption spectrum of bis 1-methylimidazole heme a in CH_2Cl_2, which was reduced at -0.2 V (vs. pesudo reterence).

the potential

suitable pote

compartment,

end point, th

checked by opt

out through th

removed by a h

material can b

solvent used i

well for any s

perchlorate was

for other hemes

Overall, this t

previous heme a

technique for s

e potential of these processes from the peaks on the plot. If a itable potential is applied to the working electrode in the sample mpartment, current will flow until all the heme a is reduced. At the d point, the sample can be poured into the attached cuvette arm and ecked by optical absorption (Figure 2.8 b). The sample can be poured t through the port under the side arm into an attached flask and moved by a heat shrink seal. Approximately 90 % of the starting terial can be recovered from the cell. Methylene chloride was the lvent used in the above experiments but the technique works equally ll for any solvent in which the heme is soluble. Tetrabutylammonium rchlorate was the electrolyte used. This process worked equally well r other hemes and produced consistently high quality results. erall, this technique represents a fundamental improvement over evious heme a reduction techniques. It is also a generally useful chnique for specific reductions or oxidations of other heme systems.

RESO

A. INTRODUCT

A wide var
in their activ
chemistry of th
present and the
investigate bot
seen in the fir
can furnish thi
conjunction wit
ligand binding
ligands indicate
weakly ligated h
provides informa
well as whether
the more informa
comparison of li
species relative
specific structur
information about
site opposite the
can detect the ir

CHAPTER 3

RESONANCE RAMAM CHARACTERIZATION OF CYANIDE BOUND HEME PROTEINS AND MODEL COMPOUNDS

INTRODUCTION

A wide variety of enzymes containing hemes or other iron porphyrins their active sites have been identified. Since the specific emistry of the enzyme is a function of the type of iron porphyrin esent and the surrounding protein environment, it is important to vestigate both if the enzyme mechanism is to be understood. We have en in the first chapter that a variety of spectroscopic techniques n furnish this type of information. One tool frequently used in njunction with these various spectroscopic techniques is exogenous and binding studies. The ability of a heme protein to bind exogenous ands indicates a solvent accessible heme environment and a vacant or kly ligated heme axial position. The type of ligand that will bind vides information on the size of the pocket and access pathway as as whether the environment is hydrophobic or hydrophilic. One of more informative uses of ligand binding studies involves the arison of ligand binding strength and geometry in the protein ies relative to free solution models. These studies can indicate ific structural constraints in the heme pocket as well as rmation about the proximal ligand, the ligand binding to the axial opposite the exogenous ligand. Since resonance Raman spectroscopy etect the iron-ligand stretching and bending vibrations for some

ligands, it c

addition, by

intermediate

Studies of th

changes durin

the intermedia

A thorough

spectroscopy w

review is a co

frequencies fo

model compounds

exogenous ligan

vibrations in t

this ligand bee

stretching vibra

sample of insect

frequencies betw

sterically hinde

al. (1985) also

cyano-metmyoglobi

model and enzyme

NMR (Behere et al

crystallography (

Oertling et al. (

cyano-myeloperoxi

previously reporte

ligands, it can provide the type of information described above. In addition, by careful choice of nonreactive exogenous ligands shortlived intermediate species which are difficult to study can be mimicked. Studies of these types can provide information about conformational changes during enzyme turnover and are much easier than working with the intermediates themselves.

A thorough review of ligand binding studies in which Raman spectroscopy was used, has appeared (Spiro, 1983). Included in this review is a compilation of the observed iron-ligand stretching frequencies for a variety of ligands with different heme proteins and model compounds. Although CN^- (cyanide) has been a commonly used exogenous ligand for protein studies, there are no reports of its vibrations in this review. Only recently have the Raman properties of this ligand been investigated. Yu et al. (1984) report the $\nu(Fe^{+3}\text{-}CN)$ stretching vibration at 453 cm^{-1} and a bending mode at 412 cm^{-1} in a sample of insect cyano-methemoglobin. Stretching vibrations at frequencies between 453 and 445 cm^{-1} have been reported in a series of sterically hindered model compounds (Tanaka, T. et al. 1984). Sitter et al. (1985) also report a similar stretching frequency (454 cm^{-1}) for a cyano-metmyoglobin sample. These studies have been complemented with model and enzyme investigations in which IR (Yoshikawa et al. 1985), NR (Behere et al. 1985), Mossbauer (Lukas and Silver 1986), and X-ray crystallography (Scheidt et al. 1980, 1983) were used. Recently, Ortiz de Montellano et al. (1986) observed an Fe^{+3}-CN vibration in cyano-myeloperoxidase at 360 cm^{-1}. This is much lower than all previously reported frequencies for CN^- heme species. Since the

prosthetic po

(a porphyrin

and Babcock et

low Fe^{+3}-CN vi

Since no resul

porphyrin stru

undertook such

complexes of i

and heme a are

protein and mod

deuteroporphyri

chemical stabil

is in good reso

B. MATERIALS A

1-methylimid

hydride and stor

without further

and Fe(III)deute

The dimethyl este

the chlorin with

methylene chlorid

complexes of the

Approximately 0.0

buffered detergent

(Sigma)) to produc

was dissolved in m

osthetic porphyrin in this enzyme has been postulated to be a chlorin
porphyrin with a reduced pyrrole ring) by Sibbert and Hurst (1984)
d Babcock et al. (1985), it was not known whether this anomalously
w Fe^{+3}-CN vibration was due to porphyrin effects or protein effects.
nce no results have been reported in which the effects of the
rphyrin structure on the binding of CN^- were characterized, we
dertook such a study. In this chapter, the Raman spectra of cyanide
mplexes of iron deuteroporphyrin (deuteroheme), iron deuterochlorin,
l heme a are compared with previously reported Raman spectra of
otein and model species and cyano-horseradish peroxidase. The
teroporphyrin system was chosen because of its availability, its
mical stability, and the fact that its Soret optical absorption peak
in good resonance with our 406.7 nm laser line.

MATERIALS AND METHODS

1-methylimidazole (Aldrich) was vacuum distilled over calcium
ride and stored over molecular sieves. All other materials were used
hout further purification. Fe(III)deuteroporphyrin dimethyl ester
Fe(III)deuterochlorin were generously supplied by Dr. C. K. Chang.
dimethyl ester of Fe(III)deuterochlorin was prepared by refluxing
chlorin with trifluoroacetic anhydride under nitrogen in a
ylene chloride/methanol mixture (Wang et al., 1958). Bis-cyanide
exes of the porphyrins and chlorin were prepared as follows.
ximately 0.004 g of solid KCN (Fisher) were dissolved in 1 ml of a
ted detergent solution (0.1 M phosphate, pH 8.4, 0.2% W/V Brij 35
a)) to produce a final pH of 10.7. The iron porphyrin or chlorin
ssolved in methylene chloride and vortexed with the cyanide

solution unde

transfer to t

bis-cyanide c

mono-l-methyl

bis-cyanide c

the above solu

in optical abs

Horseradish pe

phosphate buff

addition of a

samples were pr

^{15}N, Cambridge

Optical abs

5 UV/visible sp

air reference.

Ramalog scanning

photomultiplier

operation is ach

built interface.

406.7 nm excitat

contained in a sp

The Raman spectro

for all scans.

olution under a stream of argon. As the methylene chloride evaporates,
ransfer to the aqueous solution results. The formation of the
is-cyanide complex was confirmed by optical absorption spectra. The
ono-1-methylimidazole, mono-cyanide complexes were prepared from the
is-cyanide complexes by the addition of 20 μl of 1-methylimidazole to
he above solution. This was again verified by characteristic changes
n optical absorption and resonance Raman spectra (see below).
orseradish peroxidase (Sigma type IV) was dissolved in a 20 mM
hosphate buffer at pH 7.5. The CN^- complex was produced by the
ddition of a few crystals of KCN. The final pH was 7.8. $C^{15}N$ labeled
amples were produced by identical methods in which $KC^{15}N$ was used (99%
^{15}N, Cambridge Isotope Laboratories).

Optical absorption spectra were obtained with a Perkin-Elmer Lambda
UV/visible spectrophotometer by using a 0.5 cm quartz cuvette with
r reference. Resonance Raman spectra were obtained with a Spex 1401
nalog scanning double monochromator; a cooled RCA C31034
otomultiplier tube was the detector. Data collection and instrument
eration is achieved from a DEC LSI-11/2 computer through a house
lt interface. All spectra were recorded by using 20 mW of power at
.7 nm excitation (Spectra-Physics model 164 Kr^+ ion). Samples were
tained in a spinning cell; a 90 degree scattering geometry was used.
Raman spectrometer was calibrated to the 1004 cm^{-1} line of toluene
all scans.

C. RESULTS

The struc

shown in Figu

except that t

protons. The

increase the

any acid/base

distinguished

alteration res

degeneracy. It

differences in

these perturbat

bis-imidazole,

are shown in Fi

spectra of the

relative to tho

also one less pe

and the peak bet

systems retain t

Q bands (bands t

between the bis-

distinguishes the

the red of 600 nm

The low frequ

porphyrin species

system, a band occ

. RESULTS

The structures of the iron deuteroporphyrin and deuterochlorin are hown in Figure 3.1. The deuteroporphyrin is similar to protoporphyrin xcept that the vinyl groups at positions 2 and 4 are replaced by rotons. The dimethyl ester (of the proprionic acid groups) is used to crease the solubility of this species in organic solvents and block y acid/base chemistry of the group. The deuterochlorin is stinguished by the reduced pyrrole ring at positions 3 and 4. This teration results in reduced ring conjugation and a loss of the X, Y generacy. It is expected that if the CN^- binding is sensitive to fferences in porphyrin structure, we should see differences due to se perturbations. The optical absorption spectra of the bis-cyanide, -imidazole, and mixed ligand compounds of the porphyrin and chlorin shown in Figures 3.2 and 3.3, respectively. The peaks in the ctra of the bis-cyanide complexes are considerably red shifted ative to those of the bis-imidazole species. In each case there is one less peak in the 500 to 700 nm range with bis-cyanide ligation the peak between 330 and 340 nm is much stronger. The mixed ligand ems retain the shape of the bis-cyanide complexes but the Soret and nds (bands to the red of the Soret) are intermediate in location een the bis-cyanide and bis-imidazole cases. The feature which most nguishes the chlorin from the porphyrin is the additional band to ed of 600 nm.

he low frequency region resonance Raman spectra of the three yrin species are presented in Figure 3.4. In the mixed ligand n, a band occurs at 451 cm^{-1} which is not present in either of the

F

b

Figure 3

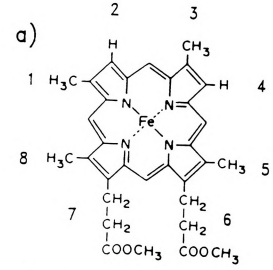

Fe^{III} Deuteroporphyrin DME

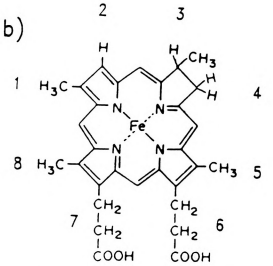

Fe^{III} Deuterochlorin

Figure 3.1 The structures of iron deuteroporphyrin DME and iron deuterochlorin.

Figure 3.

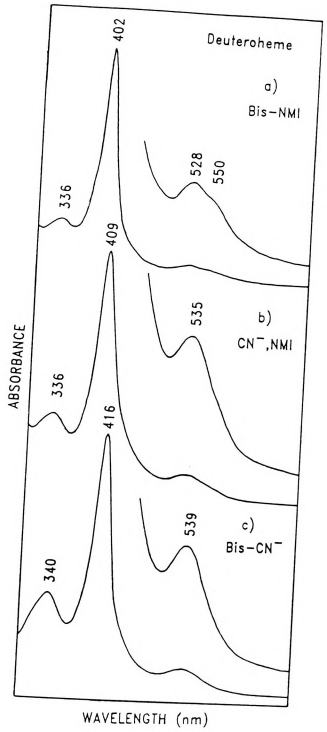

Figure 3.2 Optical absorption spectra of bis-NMI, CN^-/NMI, and bis-CN^- ligated Fe^{III} deuteroporphyrin.

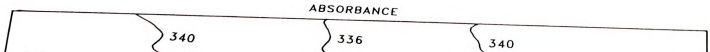

Figure 3.1

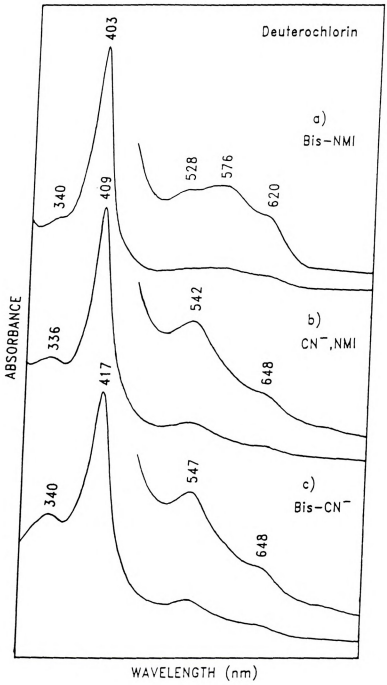

Figure 3.3 The optical absorption spectra of bis-NMI, NMI/CN^-, and bis-CN^- ligated Fe^{III} deuterochlorin.

Figure 3.

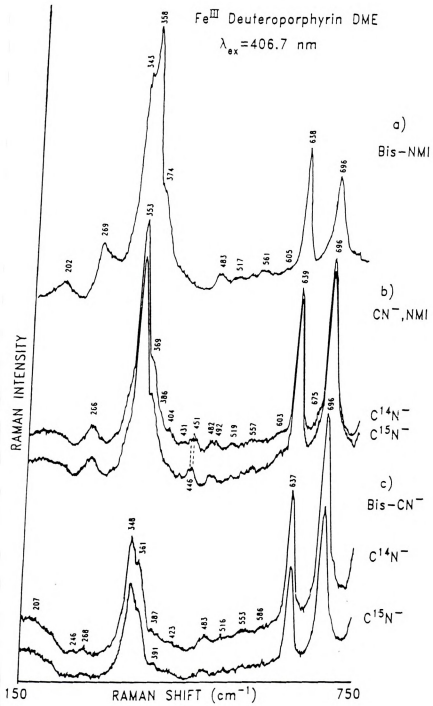

Figure 3.4 Raman spectra of bis-NMI, NMI/CH$^-$, and bis-CN$^-$ ligated Fe^{III} deuteroporphyrin.

other specie

We assign th

also seen in

plot of this

3.6. The ν(Fe

was observed

bis-cyanide s

shifts to 454

in the porphyr

asymmetric str

below. Duplica

produced resul

isotope sensit

spectrum of na

in Figure 3.8.

shifted relativ

patern is very

spectra of the

frequency regio

to 452 cm^{-1} upo

ν(Fe-CN) stretch

D. DISCUSSION

The results

previously repor

species (Kerr et

from the myelope

other species and which shifts to 446 cm^{-1} upon substitution of $C^{15}N$. We assign this band to the ν(Fe-CN) stretching frequency. The band is also seen in the mixed ligand chlorin system (Figure 3.5). An expanded plot of this region for the mixed ligand systems can be seen in Figure 3.6. The ν(Fe-CN) peak for the mixed ligand heme a system (not shown) was observed at 447 cm^{-1}. In Figure 3.7 we expand the spectra for the bis-cyanide samples. The chlorin exhibits a band at 458 cm^{-1} which shifts to 454 upon isotope substitution. This band is completely absent in the porphyrin spectrum. We assign this band to the ν(NC-Fe-CN) asymmetric stretching frequency for reasons which will be discussed below. Duplicate experiments run with the Fe deuterochlorin DME produced results identical to the unesterified species. No other isotope sensitive modes are observed in these samples. The absorption spectrum of native and CN bound horseradishperoxidase (HRP) are shown in Figure 3.8. Although the spectrum of the CN bound species is red shifted relative to the deuteroporphyrin mixed ligand system, the basic pattern is very similar. Figure 3.9 shows the low frequency Raman spectra of the native and CN^-HRP. Again, looking at the expanded low frequency region (Figure 3.10) we see a peak at 457 cm^{-1} which shifts 452 cm^{-1} upon isotope substitution. We assign this peak to the Fe-CN) stretching frequency.

DISCUSSION

The results from the mixed ligand systems are consistent with the viously reported results for models (Tanaka et al. 1984) and protein cies (Kerr et al., 1984; Yu et al., 1984). They are quite different m the myeloperoxidase results, however. The presence of the isotope

Figure 3.5

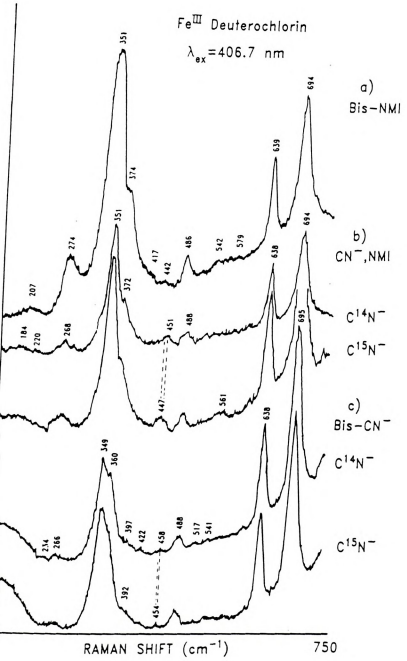

Figure 3.5 Raman spectra of bis-NMI, NMI/CN^-, and bis-CN^- ligated Fe^{III} deuterochlorin.

Figure 3.6

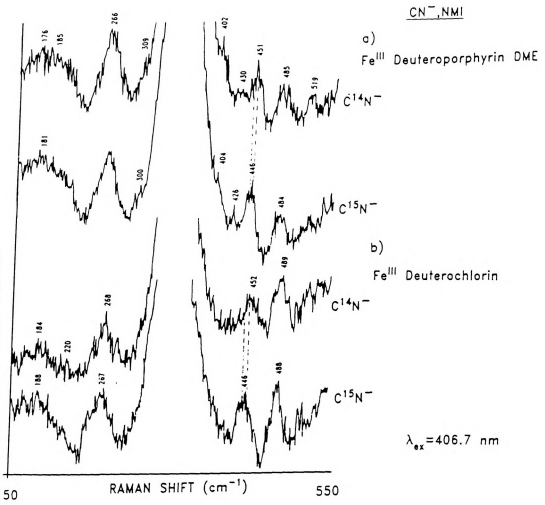

Figure 3.6 Raman spectra of NMI, CN^- NMI/CN^- ligated Fe^{III} deuteroporphyrin and deuterochlorin with isotope labeled CN^-.

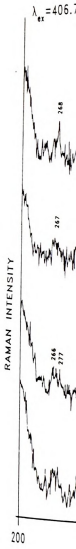

Figure 3.7

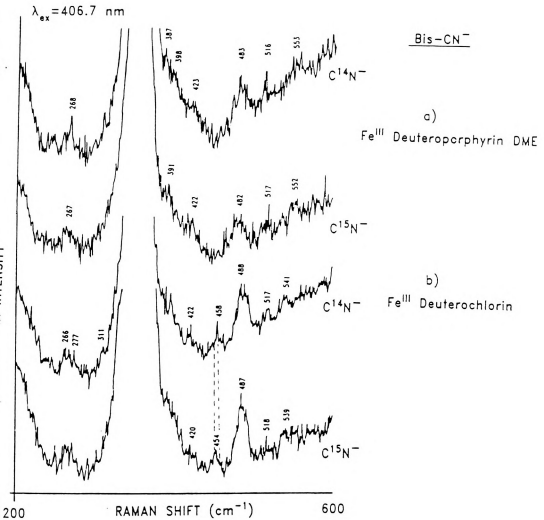

Figure 3.7 The Raman spectra of bis-CN^- Fe^{III} deuteroporphyrin and deuterochlorin with isotope labeled CN^-.

Figure 3.

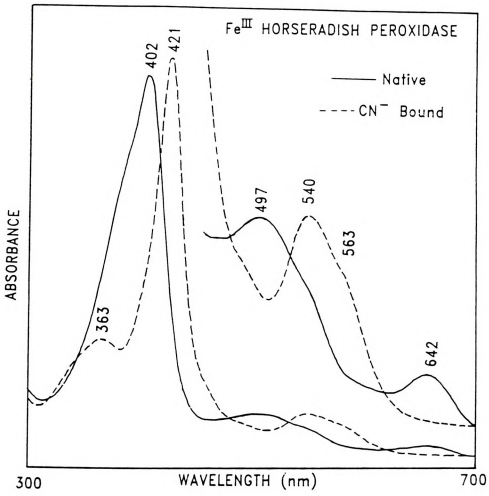

Figure 3.8 The optical absorption spectra of native and CN^- bound horseradish peroxidase.

Figure

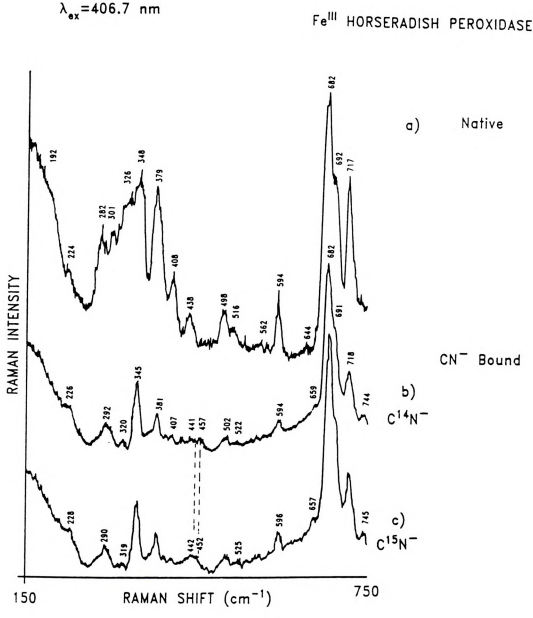

Figure 3.9 The Raman spectra of native and CN^- bound horseradish peroxidase.

λ_{ex}=406.7 n

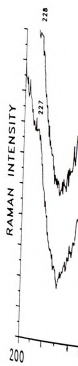

Figure 3.

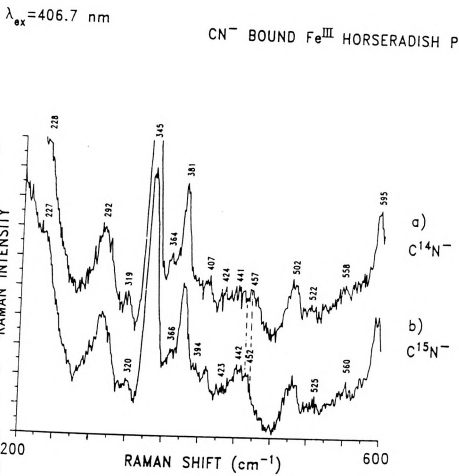

Figure 3.10 Raman spectra of CN^- bound horseradish peroxidase with isotope labeled CN^-.

sensitive ba

in the heme

restrictions

basis of sym

IR allowed a

reduction of

(Gallucci et

lowering of t

the symmetric

458 cm^{-1} band

its presence

of a simple ha

upon isotope s

= m(CN)/2). Th

asymmetric str

shift. In the

broken due to

X-ray crystallo

displacement of

cyanide. With t

become Raman al

Although the

Raman allowed, t

reasonable expla

for out of plane

frequency must b

sensitive band in the bis-cyanide chlorin samples, which is not present in the heme samples, may be explained on the basis of symmetry restrictions. Bis-cyanide hemes have an effective D_{4h} symmetry. On the basis of symmetry, a Raman allowed ν(NC-Fe-CN) symmetric stretch and an IR allowed asymmetric stretch are predicted. In the chlorin system, the reduction of the pyrrole ring results in an S_4 buckling of the ring (Gallucci et al., 1982; Strauss et al., 1983, 1985) and an overall lowering of the symmetry to C_2. The loss of the planar symmetry makes the symmetric and asymmetric stretches both Ramam and IR allowed. The 458 cm^{-1} band is therefore most likely the asymmetric stretch based on its presence in the chlorin and not in the porphyrin. In addition, use of a simple harmonic oscillator approximation predicts a 9 cm^{-1} shift upon isotope substitution for the symmetric stretch (with Reduced mass = m(CN)/2). The observed shift of 5 cm^{-1} is more consistent with an asymmetric stretch which is expected to display a smaller isotope shift. In the mixed ligand systems, the plane of symmetry is also broken due to the different ligands on opposite sides of the heme. X-ray crystallographic data (Scheidt et al., 1980, 1983) indicates a displacement of the iron out of plane (~.03 angstroms) toward the cyanide. With the loss of planar symmetry, these Fe-CN vibrations become Raman allowed.

Although the ν(NC-Fe-CN) symmetric vibrations of the bis-CN^- are Raman allowed, they are not observed in any of the samples. A reasonable explanation for this observation may be as follows. In order for out of plane ligand modes to be resonance enhanced, the excitation frequency must be in resonance with a metal to ligand charge transfer

transition c

enhanced por

vibrations,

vibrates out

the other po

Fe is expecte

coupling of t

One conce

the 458 cm^{-1}

actually from

impurity, e.g.

be asymmetric

Raman allowed

band in the op

the sample was

observed signal

experiments. Ir

and further red

species. The Ra

had a peak of g

out the possibi

five-coordinate

CN^- concentratio

the hydroxy comp

titration to low

homogeneous opti

transition or the ligand-metal vibration must couple with the resonance enhanced porphyrin transitions (Spiro, 1983). With asymmetric vibrations, the porphyrin core size is expected to change as the iron vibrates out of plane. This may couple the vibration effectively with the other porphyrin modes. In the case of the symmetric vibration, the Fe is expected to remain centrally located and there may be only weak coupling of the Fe-ligand vibrations with the porphyrin vibrations.

One concern that arose during the course of this work was whether the 458 cm^{-1} band observed with the bis-CN^- deuterochlorin sample was actually from the bis-cyanide species or whether it could be due to an impurity, e.g., HO-Fe-CN, H_2O-Fe-CN, or Fe-CN. All these species would be asymmetric (lack planar symmetry) and would be expected to have a Raman allowed ν(Fe-CN) stretching frequency. The broadness of the Soret and in the optical spectra of the bis-cyanide samples suggested that the sample was probably not homogeneous. The possibility that the observed signal was due to impurities was ruled out by additional experiments. Increasing the CN^- concentration decreased the broadness and further red shifted the Soret as expected for the bis-cyanide species. The Raman spectrum of the sample higher in CN^- concentration had a peak of greater intensity at 458 cm^{-1}. This would seem to rule out the possibility that this peak is associated with a five-coordinated sample or the H_2O complex. However, the increase in CN^- concentration is associated with an increase in pH which may favor the hydroxy complex. This possibility was rendered unlikely by titration to lower pH to produce a sample which also had a more homogeneous optical spectrum and a stronger 458 cm^{-1} band. This

observation

bis-cyanide

presence of

presence of

the loss of

pyrrole ring

properties of

O^{2-} ligand bi

in which the

withdrawing a

ν(Fe-ligand)

ligand heme a

detergent emul

2 in heme a, a

(positions 6 a

which weakens

be a porphyrin

hemes (Kerr et

to 453 cm^{-1}) ob

porphyrin effec

The frequen

consistent with

of previous wor

cm^{-1}) is higher

This observatio

steric constrai

observation also indicates that the 458 cm^{-1} band is due to the bis-cyanide sample. The optical inhomogeneity is most likely due to the presence of some residual μ-oxo dimer which is broken up in the presence of high CN^- concentrations or upon lowering the pH. Other than the loss of planar symmetry, it is clear that the reduction of a pyrrole ring to produce a chlorin has little effect on the binding properties of CN^-. This is consistent with results from other O_2 and O^{2-} ligand binding studies (Tsubaki et al. 1980; Kean and Babcock 1986) in which the heme peripheral substituents were varied in their electron withdrawing ability with little or no resultant change in the ν(Fe-ligand) frequency. The slightly lower frequency of the mixed ligand heme a sample (447 cm^{-1}) may result from a difference in detergent emulsification. The long hydrophobic "tail" on ring position 2 in heme a, across from the hydrophilic proprionic acid groups (positions 6 and 7), may result in a different solubilization geometry which weakens the CN^- binding. Alternately, this frequency lowering may be a porphyrin substituent effect as has been observed for CO ligated hemes (Kerr et al., 1983). The near constant ν(Fe-CN) frequency (~451 to 453 cm^{-1}) observed for mixed ligand models and protein species makes porphyrin effects seem less likely.

The frequency of the ν(Fe-CN) stretching frequency of the CN-HRP is consistent with the results of our model compounds and with the results of previous work. It is interesting to note that the frequency (457 cm^{-1}) is higher than that in both models and most other heme proteins. This observation is indicative of a slightly stronger bond or less steric constraint in the HRP species. Yoshikawa et al. (1985) have

implicated a

histidine re

effect is ex

sufficient t

configuratio

frequency in

speculate as

strict steric

a large decre

implicated a hydrogen bonding interaction between a protonated histidine residue and the CN^- nitrogen atom in HRP. Although this effect is expected to be weak in the Fe(III) protein, it may be sufficient to stabilize the CN^- in a more strongly binding configuration. It is predicted that the anomalously low ν(Fe-CN) frequency in myeloperoxidase is due to protein effects. We can only speculate as to the nature of these but it would seen probable that strict steric constraints would have to be involved to account for such a large decrease in frequency.

A. INTRODUC

Synthetic

the understan

heme containi

interpretatio

have been synt

structure and/

references wit

function of he

protic or apro

specific steri

been successful

hemoglobins, Wa

Babcock, 1981;

sophisticated m

rigid structure

models would id

(octaethylporphy

naturally occurr

Unfortunately, t

to the floppines

CHAPTER 4

CHARACTERIZATION OF CYTOCHROME $\underline{a}_3$ MODEL COMPOUNDS

A. INTRODUCTION

Synthetic hemes (iron porphyrins) have played an important role in the understanding of the chemistry and ligand binding properties of heme containing proteins. Not only have they been important in the interpretation of spectroscopic data of heme proteins, but heme models have been synthesized which mimic heme enzymes in some aspects of their structure and/or function (see Lever and Gray eds., 1983, and references within). Some of the variables important in the specific function of heme proteins are the following: specific axial ligation, protic or aprotic environment, proximity of other metal centers, and specific steric constraint. Axial ligation and general environment have been successfully reproduced in simple solution studies (i.e., hemoglobins, Walters et al., 1980; cytochrome oxidase, Callahan and Babcock, 1981; cytochrome P-450, Sakurai and Yoshimura, 1985) but more sophisticated modeling requires covalent attachment of the porphyrin to rigid structures which can mimic very specific protein effects. These models would ideally utilize β-substituted porphyrins (octaethylporphyrin (OEP) types), since they are the type found in all naturally occurring heme proteins (Smith and Williams, 1970). Unfortunately, the models in this class often suffer from disorder due to the floppiness of the side chains used for the covalent attachment

(Young and

types) have

1978a; Colln

1985; Schaef

ease of synt

their substi

difficulty o

and Chang, 19

the four pher

spectrum (Gou

Raman spectru

the physiolog

structural ana

spectroscopic

the TPP models

Young and Chan

phenyl groups

phenyl substitu

of the OEP type

compromise for

rigidity of the

the naturally o

important tool

characteristics

reported. We hav

species to deter

spectra, more cl

(Young and Chang, 1985). Meso-substituted tetraphenylporphyrins (TPP types) have found extensive use for model construction (Burke et al., 1978a; Collman et al., 1983; Kerr et al., 1983; Schappacher et al., 1985; Schaeffer et al., 1986; and Bruice et al., 1986) because of their ease of synthesis, chemical stability and the increased rigidity of their substituent groups. The problem with making TPP models is the difficulty of selectively derivatizing the phenyl substituents (Young and Chang, 1985). From a spectroscopic point of view, the presence of the four phenyl substituents produces changes in the optical absorption spectrum (Gouterman, 1978) and dramatic alterations in the resonance Raman spectrum (Burke et al., 1978; Chottard et al., 1981) relative to the physiological (OEP type) hemes, making it difficult to infer structural analogies in heme proteins just from comparison of spectroscopic data. A heme type that may represent an improvement over the TPP models is the meso-diphenylporphyrin (Gunter et al., 1981; Young and Chang, 1985). Models with different derivitization of the two phenyl groups can be easily prepared and separated, and with only two phenyl substituents, the optical absorption spectra are more like those of the OEP type hemes. These meso-diphenyl derivatives represent a good compromise for heme protein models because they exhibit the structural rigidity of the TPP types but have optical characteristics similar to the naturally occurring hemes. Although Raman spectroscopy is an important tool for the study of heme proteins, the Raman spectral characteristics of these meso-diphenylporphyrins have not yet been reported. We have undertaken the Raman characterization of these species to determine if the Raman spectra, like the optical absorption spectra, more closely resemble the OEP type hemes than do the TPP

types. Since

species have

Chang, 1985)

different ax

spectra of F

The appl

particular i

the oxygen re

To model this

must be able

the heme and

between the t

al., 1978). A

(Berry et al.

were used, hav

overall failed

In addition, a

unambiguously

reproduced the

centers in oxi

et al., 1980;

meso-diphenylp

synthesized oth

oxidase, which

resonance Ramar

Interpretation

types. Since the optical absorption spectra of only a few ligation species have been previously reported (Gunter et al., 1981; Young and Chang, 1985), the first part of this study establishes the effects of different axial ligation on both the optical and resonance Raman spectra of Fe^{+3} meso-diphenyl porphyrins.

The application of meso-diphenylporphyrin derivatives that is of particular interest to us is their use in the synthesis of models of the oxygen reduction site of cytochrome oxidase (Gunter et al., 1981). To model this center (in the resting oxidase) accurately, these models must be able to chelate a copper ion in close proximity to the iron of the heme and display strong anti-ferromagnetic exchange coupling between the two metal centers through a bridging ligand (Tweedle et al., 1978). Although previous models, in which either TPP type hemes (Berry et al., 1980) or meso-diphenyl type hemes (Gunter et al., 1981) were used, have succeeded in this copper binding, the models have overall failed to mimic the magnetic coupling properties of the enzyme. In addition, actual ligand binding states of these models could not be unambiguously assigned. Some iron and copper containing species have reproduced the strong magnetic coupling that occurs between the metal centers in oxidase, but none of them contains the heme structure (Okawa et al., 1980; Morgenstern-Badarau and Wickman, 1985). Using the meso-diphenylporphyrin structure as a basis, Koo and Chang (1987) have synthesized other models of the oxygen reduction center of cytochrome oxidase, which we have characterized by using optical absorption, resonance Raman, and EPR spectroscopies as structural tools. Interpretation of these results was made possible by the previous

characteriz

second part

characterist

suitability

spectroscopi

B. MATERIA

1-methyl

hydride and

distilled ov

further purif

Asaad Salehi

The copper-li

by Myoung Seo

hemes, as pre

chloride and

ligation was

with aqueous

M, pH 8.4), to

chloride or di

was produced b

DMSO solution

characteristic

toluene/tetrahy

methylene chlo

mixture of tolu

produced by the

characterization of the simpler meso-diphenylporphyrin species. In the second part of this chapter, I will discuss the structural characteristics of these cytochrome oxidase model species and their suitability as oxidase models, as established by the observed spectroscopic results.

B. MATERIALS AND METHODS

1-methylimidazole (Aldrich) was vacuum distilled over calcium hydride and stored over molecular sieves. Methylene chloride was distilled over calcium hydride. All other materials were used without further purification. Meso-diphenyletioporphyrins were synthesized by Asaad Salehi and Myoung Seo Koo as described in Young and Chang (1985). The copper-ligating cytochrome oxidase model compounds were synthesized by Myoung Seo Koo (Koo, 1986; Koo and Chang, 1987). These various hemes, as prepared, generally consisted of a mixture of five-coordinate chloride and hydroxide ligated species. Homogeneous hydroxide ion ligation was induced by shaking the heme solution (methylene chloride) with aqueous KOH (~1 M) followed by washing with phosphate buffer (.1 M, pH 8.4), total solvent evaporation, and re-solution in methylene chloride or dimethyl sulfoxide (DMSO). Homogeneous chloride ligation was produced by bubbling HCl vapor through the methylene chloride or DMSO solution until the absorption spectrum remained constant and characteristic of chloride ligated hemes. Samples in toluene/tetrahydrofuran (THF) were prepared by evaporation of the methylene chloride from the desired sample and resolution in a 50:50 mixture of toluene/THF. Bis-N-methylimidazole ligated heme samples were produced by the addition of excess N-methylimidazole to the methylene

chloride so

spectrum wer

Optical

5 UV/visible

air referenc

regulating D

1401 Ramalog

photomultipli

achieved from

All spectra w

excitation (S

in a spinning

collected by

spectrometer

scans. EPR spe

noted) by usi

a Bruker ER 2C

and high spin

observed EPR s

solutions of c

respectively.

hepes butter a

equation: g=(7

is the magnetic

chloride solution until no further changes in the optical absorption spectrum were observed.

Optical absorption spectra were obtained with a Perkin-Elmer Lambda 5 UV/visible spectrophotometer by using a 0.5 cm quartz cuvette with air reference, or in a 4 mm O.D. EPR tube suspended in a temperature regulating Dewar. Resonance Raman spectra were obtained with a Spex 1401 Ramalog scanning double monochromator and a cooled RCA 31034C photomultiplier tube. Data collection and instrument operation were achieved from a DEC LSI-11/2 computer through a house built interface. All spectra were recorded by using 20 mW of power at 406.7 nm excitation (Spectra-Physics model 164 Kr ion). Samples were contained in a spinning EPR tube (at room temperature) and the signal was collected by utilizing a ~170 degree scattering geometry. The Raman spectrometer was calibrated to the 1004 cm-1 line of toluene for all scans. EPR spectra were recorded at ~10 K (or specific temperature as noted) by using an Oxford Instruments ESR 9 liquid helium cryostat and a Bruker ER 200D X-Band spectrometer. Concentrations of ligated copper and high spin hemes were estimated by double integration of the observed EPR signal and comparison with the signals from standard solutions of copper (II) EDTA (1 mM) and metmyoglobin fluoride (.1 mM) respectively. Both of these standards were prepared in 50 mm aqueous hepes butter at pH 7.4 The "g" values were calculated by using the equation: $g=(714.47*\nu)/H$, where ν is the frequency in gigahertz and H is the magnetic field in gauss.

C. MESO-D

The str

Figure 4.1a

butyl(benzam

porphine), c

blocked/bloc

groups preve

(under alkal

coluamido, (p

imidazole/blo

one simple bl

species are d

macrocycles,

different exo

investigated

in this group

of the phenyl

simplify the d

single capital

imidazole/bloc

ligands are in

Figure 4.1b.

In Figure 4

and six-coordin

are both five-c

consistent with

C. MESO-DIPHENYLPORPHYRIN RESULTS

The structures of the diphenylporphyrin derivatives are shown in Figure 4.1a. The top species (Trans-5,15-bis [o-(p-tert-butyl(benzamido)) phenyl]-2,8,12,18 tetraethyl-3,7,13,17 tetramethyl porphine), called Trans bis(p-tert-butyl(benzamido))DPE or more simply blocked/blocked, represents the simplest structure. These blocking groups prevent aggregation of the heme and formation of μ-oxo-dimers (under alkaline conditions). The second structure (Trans[(N-imidazolyl) toluamido, (p-tert-butyl)benzamido]DPE), referred to as imidazole/blocked, has one intramolecular ligating imidazole group and one simple blocking group. The schematic diagrams for these different species are depicted to the right of each one. With these two basic macrocycles, a variety of heme species can be made by the addition of different exogenous ligands to the system. The species that were investigated are shown in Figure 4.1b in short hand notation. Included in this group is a macrocycle with an imidazole group attached to both of the phenyl substituents to yield a imidazole/imidazole structure. To simplify the discussion, each of parent macrocycles has been assigned a single capital letter designation: blocked/blocked, A; imidazole/blocked, B; and imidazole/imidazole, C. Additional axial ligands are indicated in parentheses after the letter as is shown in Figure 4.1b.

In Figure 4.2, optical absorption spectra are shown for the five- and six-coordinate species of macrocycle A. Species A(Cl^-) and A(OH^-) are both five-coordinate high-spin species and these spectra are consistent with those previously published (Young and Chang, 1985).

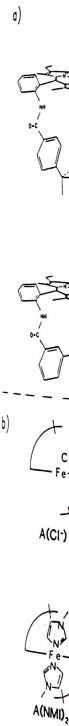

Figure 4.

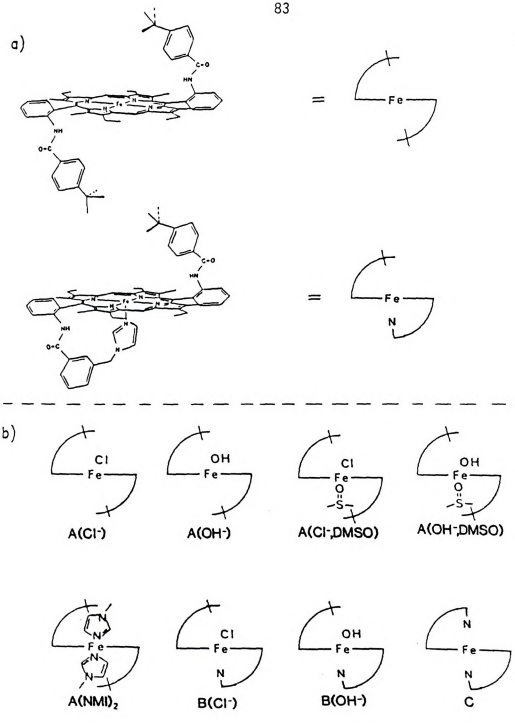

Figure 4.1 Structures of Fe^{III} meso-diphenylporphyrin species.

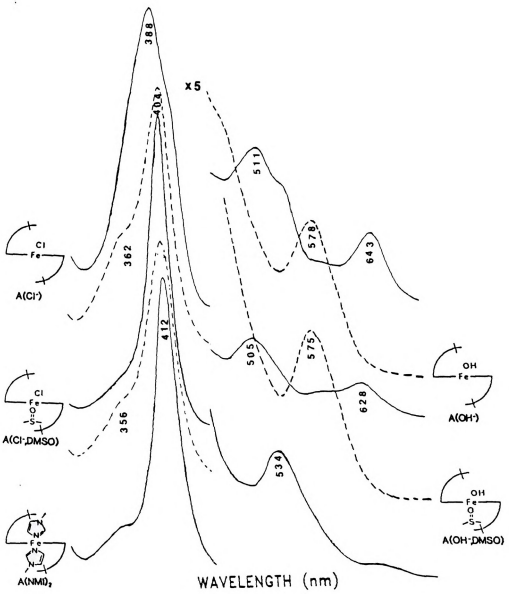

Figure 4.2 Optical absorption spectra of Fe^{III} meso-diphenylporphyrin species.

Species A(C

The differe

the similar

five-coordi

ligand to fo

spectrum in

$A(NMI)_2$. The

visible band

spectrum of

that the cova

its ligation

In Figure

species are c

six-coordinat

has a spectrum

visible regio

described as s

band nearly id

are quite diff

$A(OH^-,DMSO)$ is

new bands appe

similarity of t

six-coordinate

probably reflec

species owing t

species. These

Species A(Cl^-,DMSO) and A(OH^-,DMSO) are both six-coordinate high-spin. The differences between the spectra of A(Cl^-,DMSO) and A(OH^-,DMSO) and the similarities of the spectra to those of their respective five-coordinate analogues, suggests that DMSO is not a strong enough ligand to form $A(DMSO)_2$ when Cl^- and OH^- are present. The final spectrum in Figure 4.2 is that of the bis-(N-methylimidazole) species, $A(NMI)_2$. The narrow red shifted Soret band (412 nm) and the single weak visible band (534 nm) identify this species as low-spin. The absorption spectrum of C (not shown) is identical to that of $A(NMI)_2$, indicating that the covalently attached ligand is not significantly weakened in its ligation strength relative to free solution NMI.

In Figure 4.3, the optical spectra of macrocycle B six-coordinate species are compared with the corresponding spectra of the six-coordinate DMSO ligated species (A(Cl^-,DMSO), A(OH^-,DMSO)). B(Cl^-) has a spectrum similar to that of A(Cl^-,DMSO) in both the Soret and visible regions, indicating that B(Cl^-) is probably accurately described as six-coordinate high-spin. B(OH^-) has a Soret absorption band nearly identical to that of A(OH^-,DMSO) but the visible regions are quite different. The strong band at ~575 nm in the spectrum of A(OH^-,DMSO) is almost completely absent in the spectrum of B(OH^-) and new bands appear at ~492 and ~620 nm in the B(OH^-) spectrum. The similarity of the Soret regions suggests that these species are both six-coordinate high-spin. The differences in the visible region probably reflect different charge transfer absorptions in the two species owing to the different ligands trans to the OH^- in the two species. These differences will be discussed in more detail below.

Figure 4

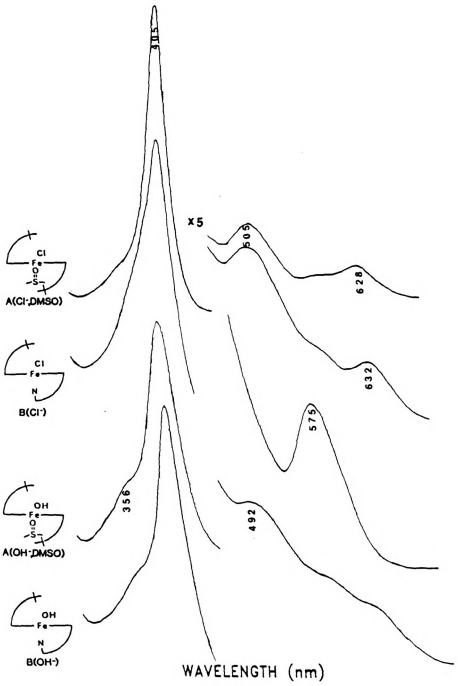

Figure 4.3 Comparison of the optical absorption spectra of six-coordinate high-spin Fe^{III} meso-diphenylporphyrin species.

The hig
macrocycle
those which
the heme spe
presented in
of frequency
arrows. With
species are
spectra. Thi
vibrational
verifies the
previously un
figures are s
consecutively
represents a
figures. Assig
similarity to
assignments ar
could not be a
types. The imp

The Raman s
absorption spec
confirms the pr
of the imidazol
$B(Cl^-)$ and $B(OH$
those of the DMS

The high frequency resonance Raman spectra of the complexes of macrocycle A are shown in Figure 4.4. The peaks marked with arrows are those which are sensitive to or characteristic of the axial ligation of the heme species. The low frequency region, for these same species, is presented in Figure 4.5. Again, peaks which show significant variation of frequency or intensity with change of ligation are marked with arrows. With the exception of A(Cl^-,DMSO) and A(OH^-,DMSO), all the species are easily distinguished from each other by their Raman spectra. This spin or ligation state sensitivity of the normal vibrational modes allows us to make initial mode assignments and it verifies the potential of Raman spectroscopy to identify species of previously undetermined ligation. The peaks observed in these two figures are summarized in Table 4.1 with the peaks being numbered consecutively from high to low frequency. An asterisk (*) in the table represents a peak which is marked with an arrow in either of the figures. Assignments are made for some of these peaks based on their similarity to peaks observed with OEP or TPP type hemes and these assignments are also included in Table 4.1. Most of the observed peaks could not be assigned by direct comparison with these other porphyrin types. The implications of this will be discussed below.

The Raman spectrum of the macrocycle C heme, like the optical absorption spectrum, was identical to that of species $A(NMI)_2$. This confirms the previous observation that there is no detectable weakening of the imidazole ligand in the strapped species. The Raman spectra of B(Cl^-) and B(OH^-) (see next section) were also essentially identical to those of the DMSO ligated analogs A(Cl^-,DMSO) and A(OH^-,DMSO), despite

The hig

macrocycle

those which

the heme spe

presented ir

of frequency

arrows. With

species are

spectra. This

vibrational

verifies the

previously un

figures are s

consecutively

represents a

figures. Assig

similarity to

assignments ar

could not be a

types. The imp

The Raman s

absorption spec

confirms the pr

of the imidazol

B(Cl^-) and B(OH^-

those of the DMS

The high frequency resonance Raman spectra of the complexes of macrocycle A are shown in Figure 4.4. The peaks marked with arrows are those which are sensitive to or characteristic of the axial ligation of the heme species. The low frequency region, for these same species, is presented in Figure 4.5. Again, peaks which show significant variation of frequency or intensity with change of ligation are marked with arrows. With the exception of A(Cl^-,DMSO) and A(OH^-,DMSO), all the species are easily distinguished from each other by their Raman spectra. This spin or ligation state sensitivity of the normal vibrational modes allows us to make initial mode assignments and it verifies the potential of Raman spectroscopy to identify species of previously undetermined ligation. The peaks observed in these two figures are summarized in Table 4.1 with the peaks being numbered consecutively from high to low frequency. An asterisk (*) in the table represents a peak which is marked with an arrow in either of the figures. Assignments are made for some of these peaks based on their similarity to peaks observed with OEP or TPP type hemes and these assignments are also included in Table 4.1. Most of the observed peaks could not be assigned by direct comparison with these other porphyrin types. The implications of this will be discussed below.

The Raman spectrum of the macrocycle C heme, like the optical absorption spectrum, was identical to that of species $A(NMI)_2$. This confirms the previous observation that there is no detectable weakening of the imidazole ligand in the strapped species. The Raman spectra of B(Cl^-) and B(OH^-) (see next section) were also essentially identical to those of the DMSO ligated analogs A(Cl^-,DMSO) and A(OH^-,DMSO), despite

Figure

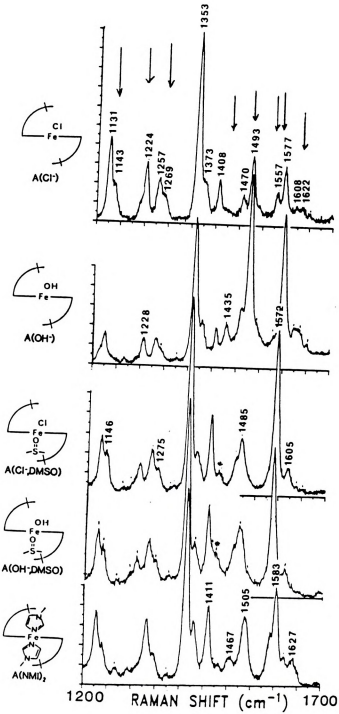

Figure 4.4 High frequency Raman spectra of Fe^{III} meso-diphenylporphyrin species.

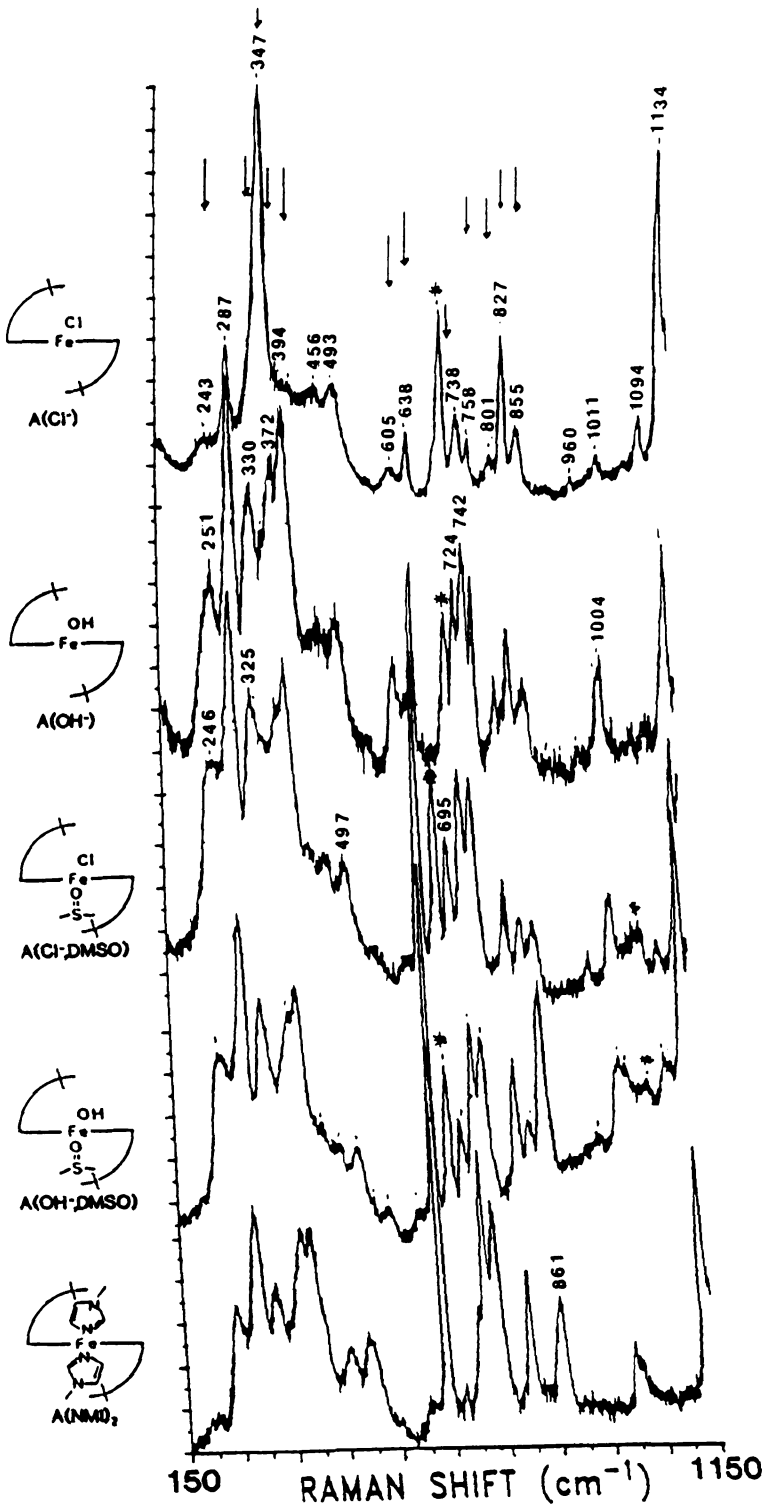

Figure 4.5 Low frequency Raman spectra of Fe^{III} meso-diphenylporphyrin species.

Table 4.1:

Peak #	(C
1	164
*2	162
3	160
*4	157
*5	155
6	151
*7	149
8	147
*9	-
10	140
11	137
12	135
13	-
*14	126
15	125
*16	122
17	120
18	116
*19	114
20	113
21	109
22	106
23	101
24	-
25	96
26	91
*27	85
*28	82
*29	80
*30	75
31	73
*32	-
33	67
*34	63
*35	60
36	55
37	49
38	45
*39	39
40	?
ν(Fe-Cl)	347
*41	-
42	287
*43	243

Table 4.1: Raman Peaks of Fe^{III} Meso-Diphenylporphyrins.

Peak #	(Cl^-)	(OH^-)	$(Cl^-$, DMSO)	$(OH^-$, DMSO)	$(NMI)_2$	compo-sition	equiv mode
1	1640	1640	1640	-	-	substituent	?
*2	1622	1618	1626	-	1627	CaCm?	ν_{10}
3	1608	1606	1605	1603	1605	phenyl	A
*4	1577	1579	1572	1570	1583 1571	CbCb	ν_2
*5	1557	1555	-	-	-	?	?
6	1511	1511	-	1507	-	?	?
*7	1493	1492	1484	1486	1505	CaCm	ν_3
8	1470	1472	1472	1471	1467	?	?
*9	-	1435	-	-	1438?	?	?
10	1408	1410	1407	1406	1411	?	?
11	1372	1374	1372	1372	1375	?	?
12	1353	1354	1352	1352	1356	CaCN	ν_3
13	-	1313	1316	1310	1308	?	?
*14	1269	1269	1275	1275	1274	CaCN	ν_{13}
15	1257	1260	1260	1258	1257	Cm-Phenyl?	
*16	1224	1228	1231	1229	-	(phenyl-H)	C
17	1209	1209	1211	1213	1211	Cm-phenyl	?
18	1169	1180	1189	1181	1181	?	?
*19	1143	-	1146	1145	1147	?	?
20	1134	1135	1137	1135	1135	?	?
21	1094	1088	1095	1097	1093	?	?
22	1064	1061	1061	1058	1065	?	?
23	1011	1004	1004	1007	1010	Ca-Cm	ν_6
24	-	948	-	-	1000	phenyl	F
25	960	961	958	958	-	?	?
26	910	922	913	-	-	?	?
*27	855	855	855	857	861	?	?
*28	827	827	829	827	-	?	?
*29	801	800	802	802	802	?	?
*30	758	759	-	-	-	?	?
31	738	742	743	742	741	?	?
*32	-	724	722	722	722	?	?
33	674	674	?	?	671	?	?
*34	638	638	637	639	640	phenyl	G
*35	605	604	604	607	607	?	?
36	558	550	545	550	548	?	?
37	493	493	497	496	498	?	?
38	456	457	462	463	460	?	?
*39	395	394	391	390	393	(porphyrin)	ν_8?
40	?	372	373	374	377	?	?
ν(Fe-Cl)	347						
*41	-	330	325	323	325	?	?
42	287	290	287	287	291	(porphyrin)	?
*43	243	251	246	244	248	(porphyrin)	?

the fact th

absorption

clearly dis

and A(OH$^-$))

verifies tha

high-spin ir

absorption a

spin and lig

D. CYTOCHR

The meso

of compounds

oxidase. Thi

macrocycle t

held in close

(trans-5-[(p

(2-(2-pyridyl

4.6a along wi

to by the sho

designation D

imidazole gro

by the letter

studied and t

Cl^- and OH^- e

species which

expected to f

addition of O

the fact that there were some differences in the corresponding optical absorption spectra. The Raman peak positions (see Table 4.1) are also clearly distinct from those of the five-coordinate high-spin (A(Cl^-) and A(OH^-)) and six-coordinate low-spin ($A(NMI)_2$) species. This verifies that these species of macrocycle B are indeed six-coordinate high-spin in nature. These results establish the utility of optical absorption and resonance Raman spectroscopy for the characterization of spin and ligation states of meso-diphenylhemes.

D. CYTOCHROME OXIDASE MODEL COMPOUND RESULTS

The meso-diphenylporphyrin can be used as a basis for the synthesis of compounds which model the oxygen reduction site of cytochrome oxidase. This is accomplished by the addition of a copper chelating macrocycle to one of the phenyl groups, so that a copper ion can be held in close proximity to the heme iron. This structure (trans-5-[(p-tert-butyl(benzamido)]-15-[o-(6-(N,N-bis (2-(2-pyridyl)ethyl)amido)methyl nicotinamido]DPE) is shown in Figure 4.6a along with its shorthand diagram. For simplicity, it is referred to by the shorthand name blocked/chelate and it is given the letter designation D. A companion species, imidazole/chelate, has a ligating imidazole group attached to the other phenyl group and it is designated by the letter E. Various ligated species of these two macrocycles were studied and these are drawn schematically in Figure 4.6b. These include Cl^- and OH^- exogenous ligands with and without chelated copper. For species which have a chelated copper, a μ-oxo bridge (Fe-O-Cu) is expected to form between the two metal centers (see below) upon addition of OH^- and these species will be referred to as oxygen

a]

b]

E

Fi

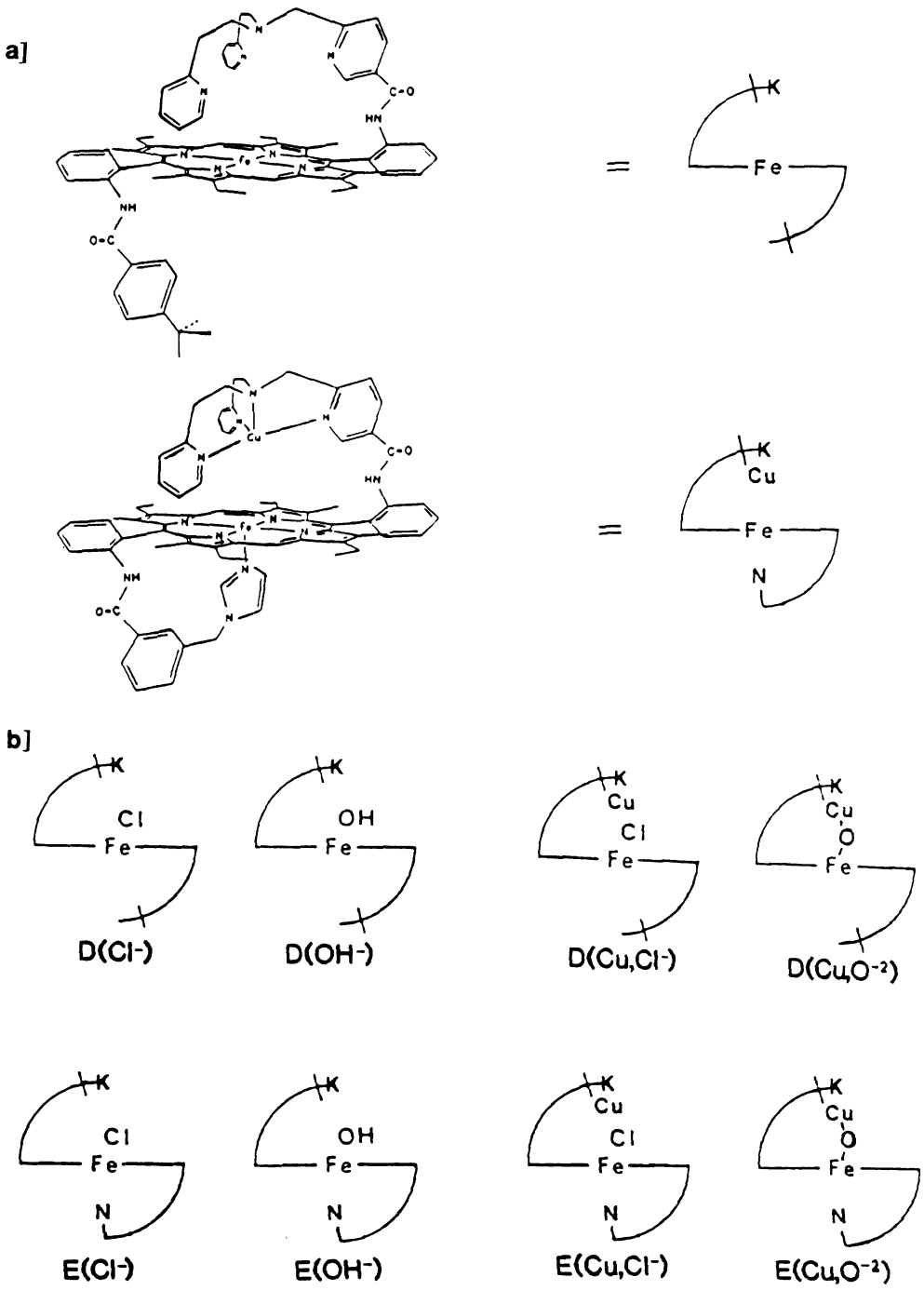

Figure 4.6 Structures of meso-diphenylporphyrin cytochrome oxidase model compounds.

bridged. Fo

the exogeno

ambiguous a

In Figu

changing on

ligand. It

D(Cu,Cl^-), i

nearly ident

high-spin sp

(and oxygen

4.8. Note, h

progressivel

and then the

series of si

and E(Cu,Cl^-

absorption pr

ligand streng

four species

oxygen bridge

the previous

these differe

these, the pe

and intensity

six-coordinat

discussed belo

bridged. For several of the five-coordinated species, the position of the exogenous ligand (i.e. above or below the heme plane) is possibly ambiguous and these possibilities will be discussed below.

In Figure 4.7, we examine the effects on the absorption spectrum of changing one of the phenyl derivatives while maintaining a Cl^- axial ligand. It is evident that the three species ($A(Cl^-)$, $D(Cl^-)$, and $D(Cu,Cl^-)$, including one with ligated copper ($D(Cu,Cl^-)$), produce nearly identical spectra which are characteristic of five-coordinate high-spin species. A similar phenomenon is observed with OH^- ligated (and oxygen bridged) species ($A(OH^-)$, $D(OH^-)$, and $D(Cu,O^{-2})$) in Figure 4.8. Note, however, with these samples that the band at ~570 nm becomes progressively broader and weaker upon addition of the chelating group and then the bound copper. In Figure 4.9 the spectra are shown for a series of six-coordinate Cl^- bound species ($A(Cl^-,DMSO)$, $B(Cl^-)$, $E(Cl^-)$ and $E(Cu,Cl^-)$). Again there is little difference between the optical absorption properties of these species, and thus, despite the stronger ligand strength of the attached imidazole versus the solution DMSO, all four species appear to be high-spin. The final series, OH^- ligated (or oxygen bridged) six-soordinate species, is shown in Figure 4.10. Unlike the previous series, there is significant variation in the spectra of these different species. Although the Soret peak is similar in all of these, the peaks to the red of the Soret vary considerably in position and intensity. We suggest that these species are still all six-coordinate high-spin; the variation in the optical spectra will be discussed below.

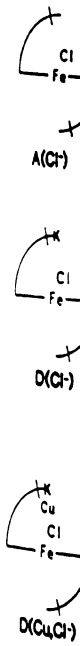

Figure 4

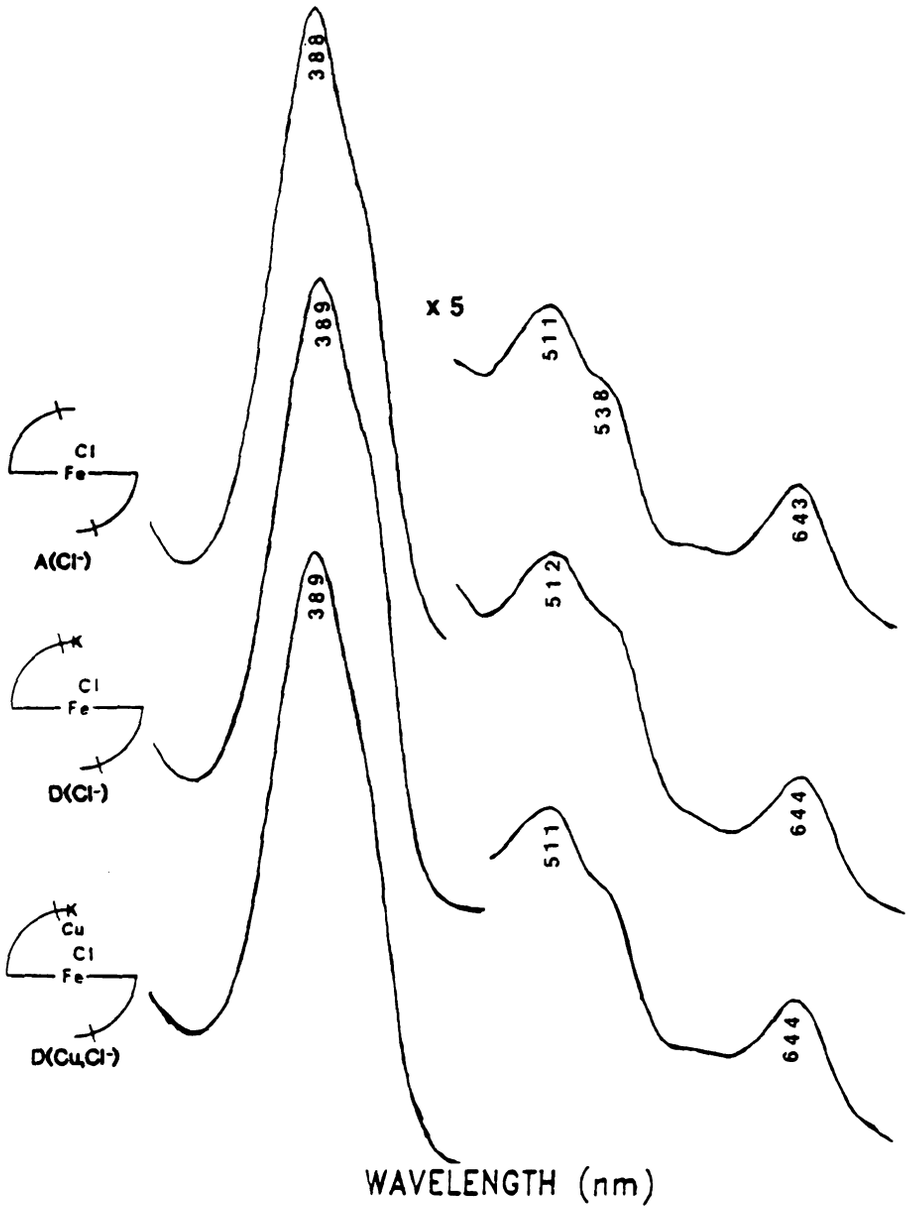

Figure 4.7 Comparison of the optical absorption spectra of five-coordinate, Cl^- ligated Fe^{III} meso-diphenylporphyrin species.

Figure

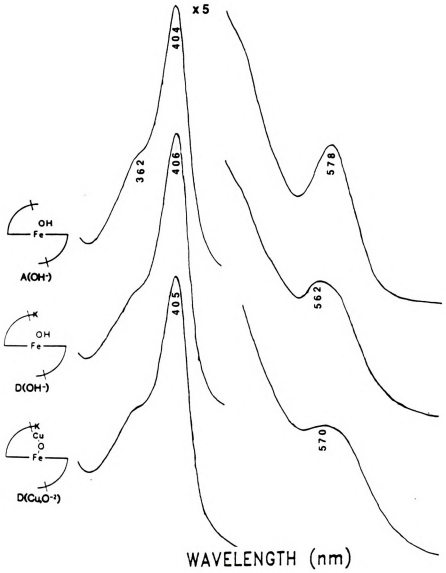

Figure 4.8 Comparison of the optical absorption spectra of five-coordinate, OH^- ligated/ O^{-2} bridged Fe^{III} meso-diphenylporphyrin species.

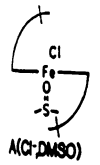

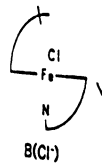

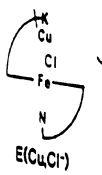

Figur

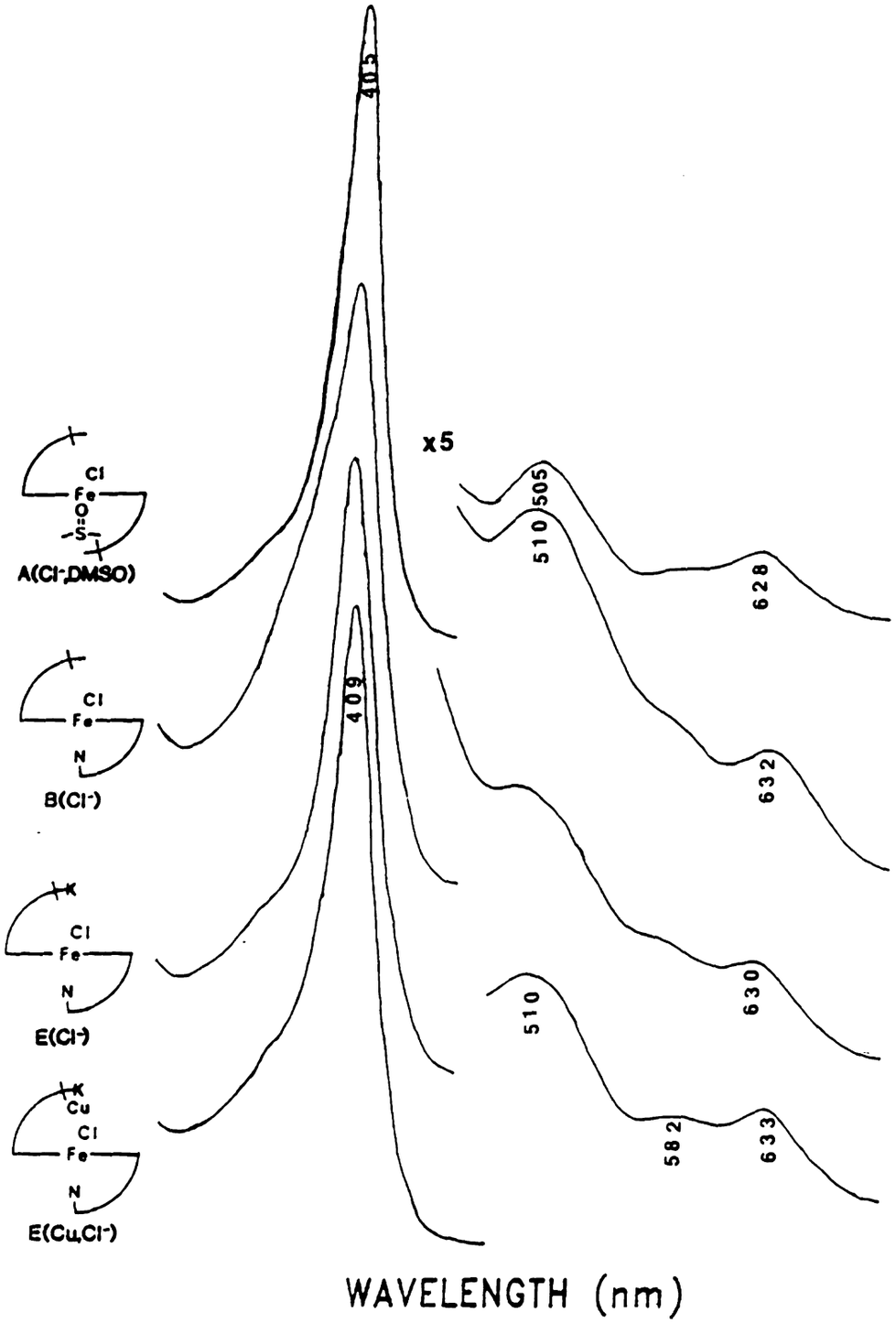

Figure 4.9 Comparison of the optical absorption spectra of six-coordinate, Cl^- ligated Fe^{III} meso-diphenylporphyrin species.

Figure

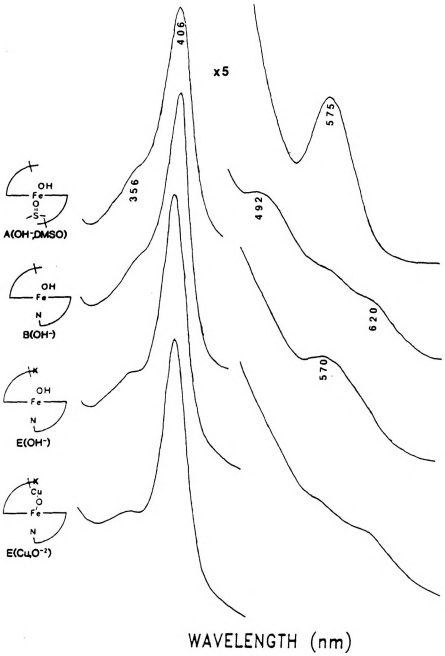

Figure 4.10 Comparison of the optical absorption spectra of six-coordinate, OH^- ligated/ O^{-2} bridged Fe^{III} meso-diphenylporphyrin species.

In Fig

demonstrat

optical ab

and six-co

This same t

shown). The

effects on

OH^- ligated

respective

A(OH^-,DMSO)

species wit

OH^- (or O^{-2}

Figures 4.1

intensity ar

OH^- ligation

for the Rama

Despite

meso-dipheny

types, both

these cytochr

confidently e

species. The

indicate vari

are not detec

six-coordinate

resting form

In Figures 4.11 through 4.14, the high frequency Raman results demonstrate the same pattern that was observed in the corresponding optical absorption spectrum; all the oxidase model species, both five- and six-coordinate, have spectra characteristic of high spin species. This same trend is also reflected in the low frequency Raman data (not shown). The presence of the chelating group and bound copper have small effects on the optical absorption spectra of those species which are OH^- ligated or oxygen bridged, but no distinctions are observed in the respective Raman spectra. Although the Raman spectra of A(Cl^-,DMSO) and A(OH^-,DMSO) could not be clearly distinguished, the six-coordinate species with a ligating imidazole do show a distinction between Cl^- and OH^- (or O^{-2}) ligation. Examination of the peaks marked with arrows in Figures 4.13 and 4.14 (peak 7 from Table 4.1), shows a gain of intensity and a shift to higher frequency on going from Cl^- ligation to OH^- ligation. The low frequency region (not shown) is nearly identical for the Raman spectra of all the six-coordinate species.

Despite the fact that the optical and Raman spectra of these meso-diphenylporphyrins seem to be distinct from both the OEP and TPP types, both techniques have been valuable to the characterization of these cytochrome oxidase model compounds. We have been able to confidently establish the spin and ligation state of these various species. The small changes in the optical absorption spectra may indicate variation in charge transfer transitions, yet these effects are not detected in the respective Raman spectra. The fact that the six-coordinate species are high-spin is encouraging because in the resting form of cytochrome oxidase, the heme is six-coordinate

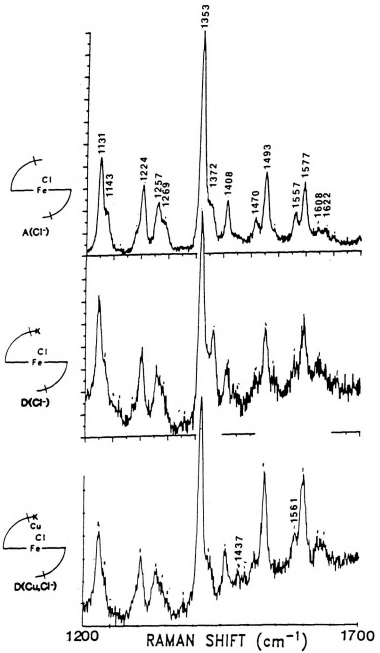

Figure 4.11 Comparison of the high frequency Raman spectra of five-coordinate, Cl^- ligated Fe^{III} meso-diphenylporphyrin species.

Figur

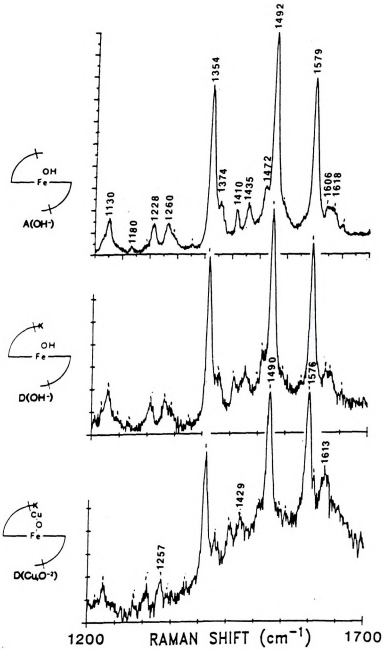

Figure 4.12 Comparison of the high frequency Raman spectra of five-coordinate, OH^- ligated/ O^{-2} bridged Fe^{III} meso-diphenylporphyrin species.

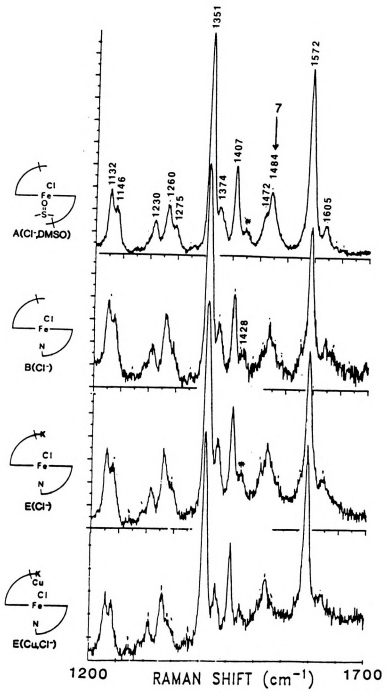

Figure 4.13 Comparison of the high frequency Raman spectra of six-coordinate, Cl^- ligated Fe^{III} meso-diphenylporphyrin species.

Figur

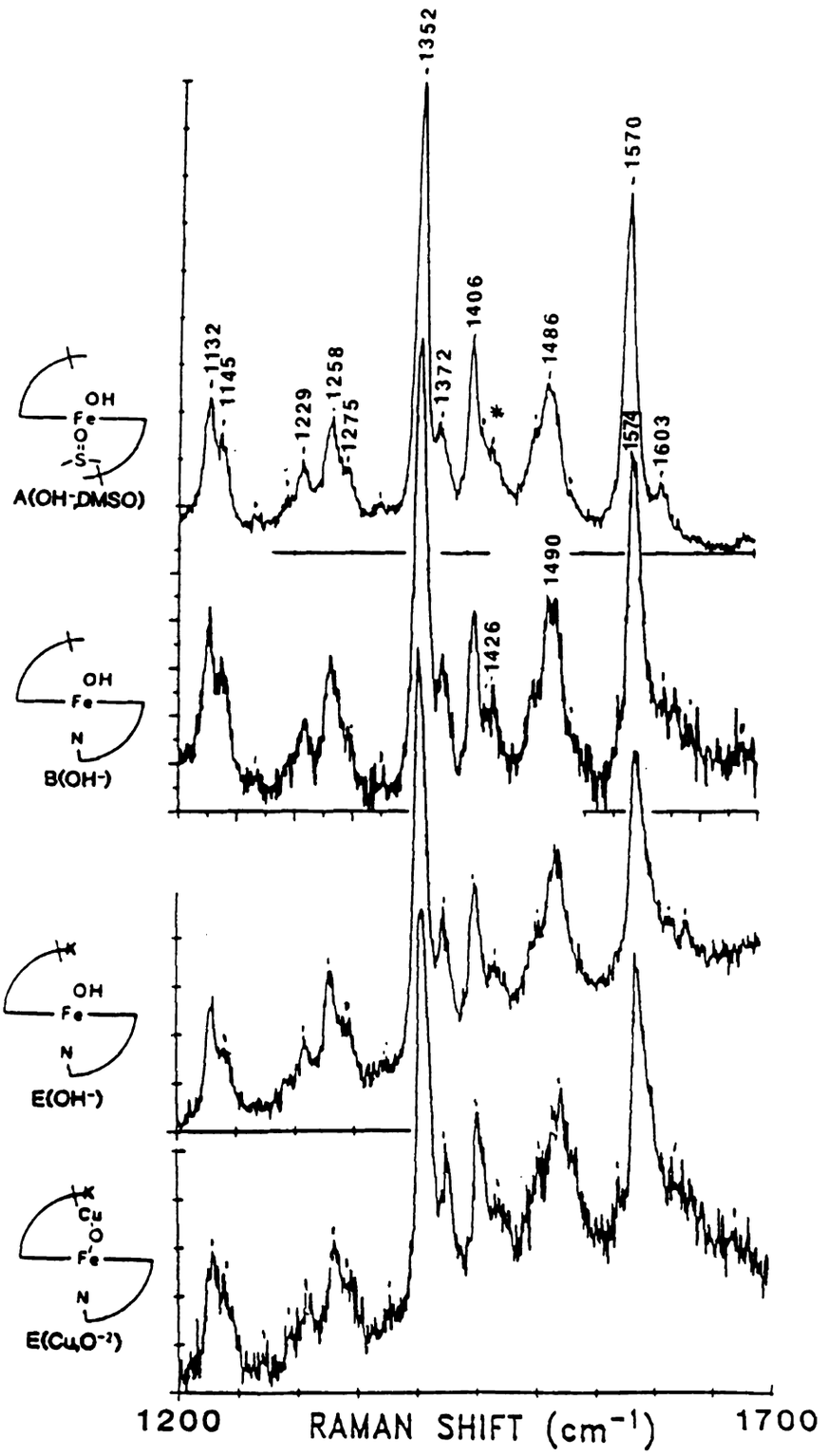

Figure 4.14 Comparison of the high frequency Raman spectra of six-coordinate, OH^- ligated/ O^{-2} bridged Fe^{III} meso-diphenylporphyrin species.

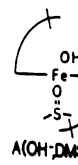

A(OH-DM

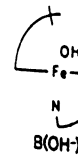

B(OH-)

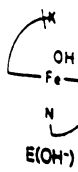

E(OH-)

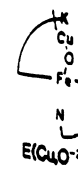

E(Cu$_4$O-

Figure 4.

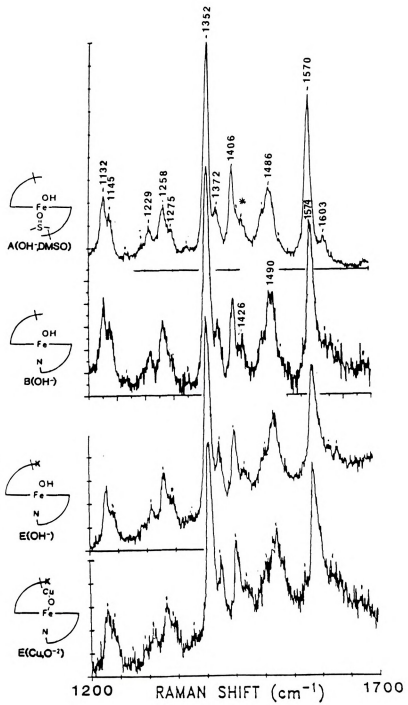

Figure 4.14 Comparison of the high frequency Raman spectra of six-coordinate, OH^- ligated/ O^{-2} bridged Fe^{III} meso-diphenylporphyrin species.

high-spin. Opti
however, cannot
between metal c
coupling simila
EPR to study th

The EPR spec
demonstrated by
prominent featur
smaller signal a
compounds (A(Cl
fluoride as demo
signal is an ind
signals are over
a glass forming
(Figure 4.15c).
with chelated co
attributed mostl

The concentr
calculated by do
rhombic signals
metmyoglobin fluo
intensities for
and D(Cu,Cl⁻)) a
favorably with th
spectra (~.25 mM)

high-spin. Optical absorption and resonance Raman spectroscopy, however, cannot establish whether there is magnetic exchange coupling between metal centers. To determine if our models exhibit exchange coupling similar to that observed with cytochrome oxidase, we have used EPR to study these model compounds.

The EPR spectrum of a typical high spin heme (see discussion) is demonstrated by that of metmyoglobin fluoride (Figure 4.15a). The prominent features are the large signal with a value of g=~6 and a much smaller signal at g=~2. The EPR specra of the five-coordinate Cl^- bound compounds (A(Cl^-), D(Cl^-)) are similar to that of the metmyoglobin fluoride as demonstrated in Figure 4.15(b-d). The splitting of the g=6 signal is an indication of some rhombicity (see discussion) but the signals are overall narrow and fairly homogeneous. Samples prepared in a glass forming solvent (toluene/THF) exhibited the narrowest lines (Figure 4.15c). The spectrum of the five-coordinate Cl^- ligated species with chelated copper (D(Cu,Cl^-)) exhibits a strong g=2 signal which is attributed mostly to a signal from the copper (Figure 4.15e).

The concentrations of the EPR detectable high-spin hemes were calculated by double integration of the g=6 signals (or the split rhombic signals near g=6). These values, standardized against metmyoglobin fluoride, are reported in Table 4.2. The integrated intensities for the five-coordinate Cl^- bound species (A(Cl^-), D(Cl^-), and D(Cu,Cl^-)) are consistently high (above .150 mM) and compare favorably with the concentrations estimated from the optical absorption spectra (~.25 mM). The EPR spectra of the five coordinate OH^- ligated

Figure 4.1

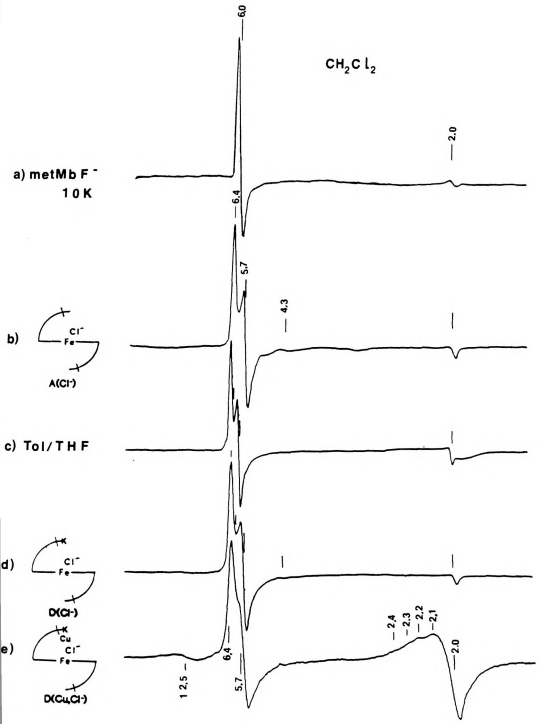

Figure 4.15 EPR spectra of Met Mb F^- and five-coordinate, Cl^- ligated Fe^{III} meso-diphenyl porphyrin species.

Table 4.2: Comp
Conc
EPR

Species
A(Cl^-)
A(Cl^-)
D(Cl^-)
D(Cu,Cl^-)
E(Cl^-)
E(Cu,Cl^-)
A(OH^-)
A(OH^-)
D(OH^-)
D(Cu,O^{-2})
E(OH^-)
E(Cu,O^{-2})

Table 4.3: Slope
Frequ

Peak	K (Slo
1	-
2	304.3
3	-
4	214.2
5	-
6	121.2
7	357.1
8	-
9	130.4
10	89.3

Table 4.4: Compar
Types.

Mode	#	
p CbCb	ν_2	
p CaCm	ν_3	
p CaN	ν_4	
Depolarized mode		

Table 4.2: Comparison of High-Spin Fe^{III} Meso-Diphenylporphyrin Concentrations as Determined by Optical Absorption and EPR Spectroscopy.

Species	Solvent	Conc mM (Optical)	Conc mM (EPR)	EPR Temp K
A(Cl^-)	CH_2Cl_2	.25	.195	10
A(Cl^-)	Tol/THF	.25	.180	10
D(Cl^-)	CH_2Cl_2	.25	.255	11
D(Cu,Cl^-)	CH_2Cl_2	.25	.186	11
E(Cl^-)	CH_2Cl_2	.25	.144	11
E(Cu,Cl^-)	CH_2Cl_2	.25	.099	12
A(OH^-)	CH_2Cl_2	.25	.086	11
A(OH^-)	Tol/THF	.25	.104	11
D(OH^-)	CH_2Cl_2	.25	.115	11
D(Cu,O^{-2})	CH_2Cl_2	.25	.031	11
E(OH^-)	CH_2Cl_2	.25	.051	11
E(Cu,O^{-2})	CH_2Cl_2	.25	.023	11

Table 4.3: Slope and Intercept Values for the Core Size Dependent High Frequency Raman Peaks of Fe^{III} Meso-Diphenylporphyrins.

Peak	K (Slope)	A(Intercept)	Composition	Mode
1	-	-	?	?
2	304.3	7.33	CaCm?	ν_{10}?
3	-	-	phenyl	A
4	214.2	9.37	CbCb	ν_2
5	-	-	?	?
6	121.2	14.47	CbCb?	?
7	357.1	6.20	CaCm	ν_3
8	-	-	?	?
9	130.4	13.0	CbCb?	?
0	89.3	17.79	?	?

Table 4.4: Comparison of the Vibrations of Three Different Porphyrin Types.

Mode	#	$Fe^{III}OEP(NMI)_2$	$Fe^{III}DPP(NMI)_2$	$Fe^{III}TPP(NMI)_2$
CbCb	ν_2	1599	1583	1568
CaCm	ν_3	1505	1505	1545?
CaN	ν_4	1375	1356	1370

Depolarized mode

species ($A(OH^-)$

(extending to h

broad g=2 signa

solvent resulte

some of this ca

unusual and wil

five-coordinate

bridged species)

the iron and cop

the Cl^- bound sp

integrated conce

ligated compound

the decrease in

fact that the si

its broadness. Ho

($D(Cu,O^{-2})$) is st

(Table 4.2), whic

The EPR spect

has a more rhombi

species and a rat

the six-coordinat

displays a simila

intensity of the

corresponding five

copper ($E(Cu,Cl_-)$

species. The EPR s

species (A(OH^-), D(OH^-)) are characterized by very broad g=6 bands (extending to higher g values than the other samples), and very large, broad g=2 signals (Figure 4.16). Again, the use of toluene/THF as a solvent resulted in a more resolved line shape (Figure 4.16b). Although some of this can be attributed to rhombic distortion, these spectra are unusual and will be discussed further below. The spectrum of the five-coordinate species with chelated copper (D(Cu,O^{-2})) (an oxygen bridged species) has a prominent copper signal (Figure 4.16), but both the iron and copper signals are weak in comparison to the spectrum of the Cl^- bound species with chelated copper (Figure 4.15). The integrated concentrations of high-spin heme are lower for these OH^- ligated compounds than for the Cl- ligated species (Table 4.2). Part of the decrease in intensity (see discussion) may be attributed to the fact that the signal extended beyond the integration window owing to its broadness. However, the value for this oxygen bridged compound (D(Cu,O^{-2})) is still much lower than that of the OH^- ligated species (Table 4.2), which also exhibit a broad signal.

The EPR spectrum of the six-coordinate Cl^- bound species (E(Cl^-)) has a more rhombic g=6 signal than the corresponding five coordinate species and a rather large g=2 signal (Figure 4.17a). The spectrum of the six-coordinate Cl^- species with chelated copper (E(Cu,Cl^-)) displays a similar g=6 signal and a g=2 copper signal. The integrated intensity of the high-spin heme for (E(Cl^-)) is less than for the corresponding five-coordinate compound, while the sample with chelated copper (E(Cu,Cl_2)) exhibits the smallest value of all the Cl^- ligated species. The EPR spectra of the six-coordinate OH^- ligated species are

Figure 4.1

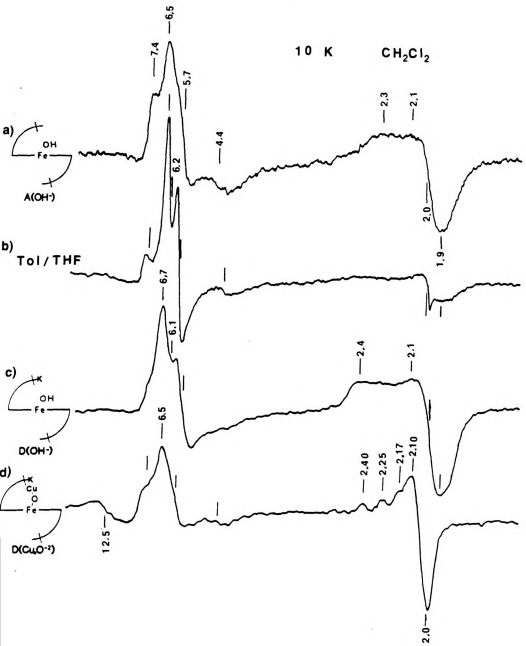

Figure 4.16 EPR spectra of five-coordinate, OH^- ligated/ O^{-2} bridged Fe^{III} meso-diphenylporphyrin species.

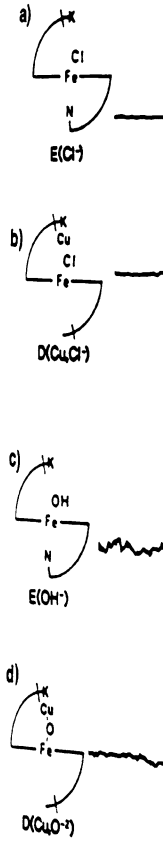

Figure 4.

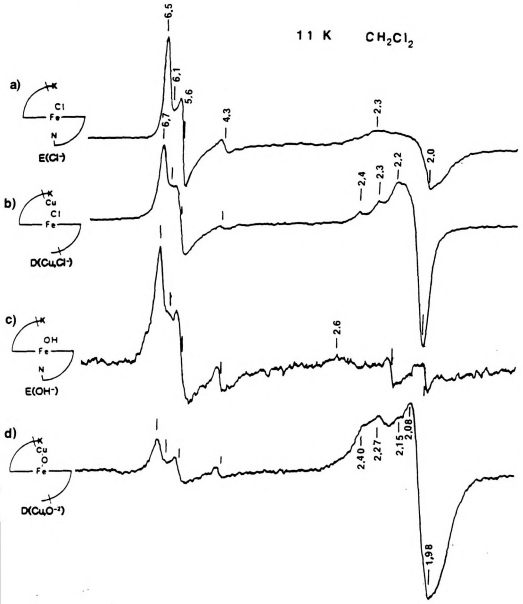

Figure 4.17 EPR spectra of six-coordinate Fe^{III} meso-diphenylporphyrin species.

unusual. The s
displays a bro
features (Figu
indicate the p
spectrum of the
displays a very
which does not
values of the i
are low. These

To obtain a
high-spin heme,
(five-coordinate
to insure inclus
concentration of
the bulk solutio
at least .25 mM.
equilibria, the
function of tempe
temperature depen
by Curie law and
(see Figure 4.18)
consistent with a
high-spin hemes (
signal and the abs
lines in the spect
this temperature r

unusual. The spectrum of the imidazole/chelate species (E(OH$^-$)) displays a broad multifeatured g=6 signal and several other noisy features (Figure 4.17c). The appearance of a broad signal at g=$\sim$2.6 may indicate the presence of a low-spin component in the sample. The spectrum of the corresponding species with chelated copper (E(Cu,O^{-2})) displays a very small g=6 signal but a comparatively large g=2 signal, which does not appear to be a simple copper signal (Figure 4.17d). The values of the integrations of the g=6 signals for both these species are low. These spectra will be further discussed below.

To obtain a more accurate indication of the loss of detectable high-spin heme, a careful study was done with compound (D(Cu,O^{-2})) (five-coordinate oxygen bridged). By using a large integration window to insure inclusion of all the high-spin (g=$\sim$6) signal, the effective concentration of detectable high-spin iron integrated to $\sim$.05 mM while the bulk solution concentration (from optical absorption spectra) was at least .25 mM. To test for temperature dependent spin state equilibria, the integrated value of the g=6 signal was determined as a function of temperature over the range of $\sim$4 K to $\sim$20 K. The observed temperature dependence of this signal roughly followed that predicted by Curie law and paralleled that of the metmyoglobin fluoride standard (see Figure 4.18). The observed deviations from linearity are consistent with a zero-field splitting of $\sim$10 cm^{-1} which is typical of high-spin hemes (Palmer, 1985). The temperature dependence of the g=6 signal and the absence of low-spin (g=3) and intermediate-spin (g=4.75) lines in the spectra indicate that no spin state equilibria exist over this temperature range. Integration of the g=2 signal, which is


40
Ø ≡ metMbF⁻ .093 mM
Ø

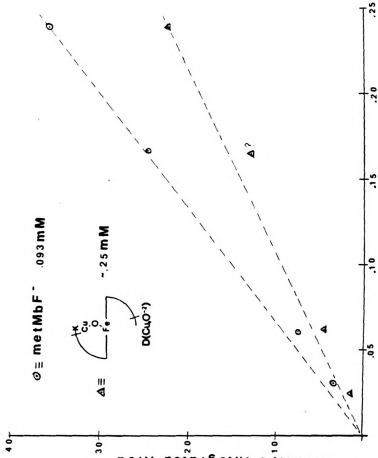

Figure 4.18 A plot of signal intensity versus 1/T (Curie Law) for Met Mb F^- and the five-coordinate O^{-2} bridged cytochrome oxidase model compound.

expected to or

concentration

copper signal

a nearby metal

E. DISCUSSION

Meso-diphen

between those o

through 4.3, th

axial ligand ty

the bis-imidazol

presence of an a

of Cl^- ligation

characteristic o

does not seem to

which has a trans

in the charge tra

imidazole ligand

character. This s

region of $B(OH^-)$

(Makinen and Chur

six-coordinate hi

position). With o

symmetry of the me

similar drop in sy

breakdown of X and

bands. This does n

expected to originate predominantly from the copper, yielded a concentration of ~.07 mM (against a copper (II) EDTA standard). This copper signal exhibited fast relaxation behavior which is indicative of a nearby metal center (Goodman and Leigh, 1985).

E. DISCUSSION

Meso-diphenylporphyrins exhibit optical absorption properties between those of the OEP type and TPP types. As is seen in Figures 4.2 through 4.3, the optical absorption bands are also quite sensitive to axial ligand type and coordination number, and with the exception of the bis-imidazole ligated species, all appear to be high-spin. The presence of an absorption band between ~630 and ~645 nm is diagnostic of Cl^- ligation while a strong band at ~570 to ~580 nm is characteristic of the OH^- ligation, although this latter generalization does not seem to apply well to the six-coordinate OH^- ligated species which has a trans imidazole ligand ($B(OH^-)$). This may reflect a change in the charge transfer absorption bands owing to the addition of the imidazole ligand (Asher and Schuster, 1979) and less iron out of plane character. This seems reasonable since the peak pattern in the visible region of $B(OH^-)$ bears a strong resemblance to that of metmyoglobin (Makinen and Churg, 1983) which contains imidazole ligated six-coordinate high-spin heme (with H_2O ligated to the other axial position). With only two phenyl porphyrin substituents, the effective symmetry of the metalloporphyrin is reduced from D_{4h} to D_{2h}. A similar drop in symmetry for free base porphyrins results in a breakdown of X and Y axis degeneracy. and a splitting of the visible bands. This does not occur for the meso-diphenylporphyrins because the

phenyl substitu

Y axes (through

on both axes. S

(Gouterman, 196

axes and split

substituents do

The Raman

both OEP and TP

porphyrin ring

the normal coor

Abe and Kitagawa

limitation, assi

with extensive c

1978; Stein et a

make some assign

al., 1975; and C

Stong et al., 19

porphyrin core s

straight line wi

composition. The

of different met

with iron porphy

and Gouterman, 1

through 10 are pl

Gouterman, 1983)

The core size (ce

phenyl substituents, unlike the free base hydrogens, are off the X and Y axes (through the pyrrole nitrogens) and exert an equal perturbation on both axes. Since the optical transition dipoles are along these axes (Gouterman, 1961), free base perturbations remove the degeneracy of the axes and split the observed absorption peaks, but the two phenyl substituents do not.

The Raman spectra of the meso-diphenyl hemes were distinct from both OEP and TPP type hemes. The presence of the phenyl groups on the porphyrin ring seriously perturbs the vibrational properties such that the normal coordinate assignments (mode composition and frequency) of Abe and Kitagawa (1978) are not directly applicable. Despite this limitation, assignments for the vibrations of OEP type hemes, along with extensive characterization of the TPP type hemes (Burke et al., 1978; Stein et al., 1984; and Blom et al., 1986), should allow us to make some assignments. It has been demonstrated for OEP (Spaulding et al., 1975; and Choi et al., 1982) and TPP (Huong and Pommier, 1977; Strong et al., 1980) type hemes that a plot of frequency versus porphyrin core size, for porphyrin modes over 1450 cm^{-1}, produces a straight line with a slope and intercept characteristic of mode composition. The porphyrin core size can be varied either by insertion of different metals (Spaulding et al., 1975, and references within), or with iron porphyrins, by variation of spin and ligation state (Scheidt and Gouterman, 1983). In Figure 4.19, the frequencies of peaks 1 through 10 are plotted versus the estimated core size (Scheidt and Gouterman, 1983) for the ferric meso-diphenylporphyrins of Figure 4.4. The core size (center to pyrrole nitrogen distance) increases for the

Figure

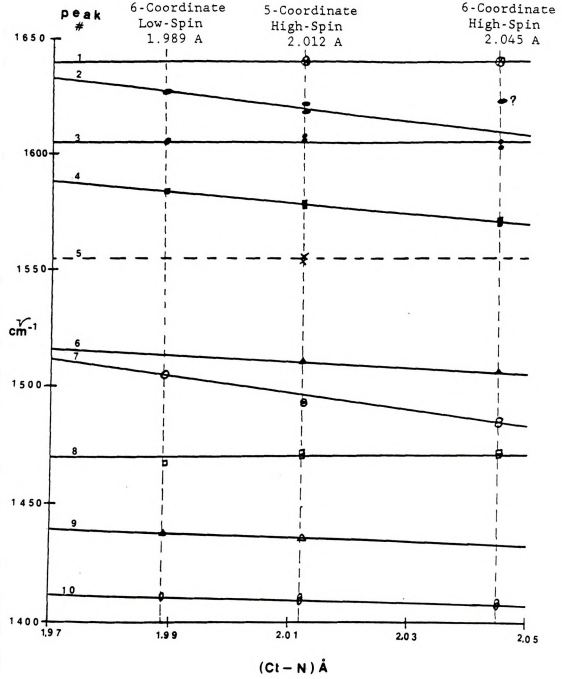

Figure 4.19 The core size dependence of the high frequency Raman vibrations of Fe^{III} meso-diphenylporphyrin species.

series six-co

and intercept

the estimated

analogous OEP

those for both

type porphyrin

mode compositi

both the OEP a

Despite the

modes of the fe

exhibit overall

Peak 4 (see Tab

spin state (and

frequency range

probably has a v

hemes. Peak 7 is

intensity with va

frequency range (

(Table 4.3) all i

hemes. Peak 12 sh

Oertling, unpubli

the spin state an

frequency region w

dependence and thi

These three modes

species of OEP, me

series six-coordinate low-spin to six-coordinate high-spin. The slope and intercept values from this plot are listed in Table 4.3, along with the estimated dominant mode component and the assignment of the analogous OEP mode. The slope values for this plot are much lower than those for both the OEP (Choi et al., 1982) and TPP (Stong et al., 1980) type porphyrins (and the intercepts, higher) which suggests that the mode compositions may be altered or significantly perturbed relative to both the OEP and TPP types.

Despite the unusual core size dependences of the high frequency modes of the ferric meso-diphenylporphyrins, three of these modes exhibit overall behavior similar to modes in their OEP counterparts. Peak 4 (see Table 4.1) undergoes changes in frequency with changes in spin state (and ligation) in the range of 1570 to 1583 cm^{-1}. Its frequency range and core size dependence (Table 4.3) indicate that it probably has a vibrational composition comparable to ν_2 in OEP type hemes. Peak 7 is also is most notable for the dramatic changes in intensity with variation in the axial ligand. This behavior, its frequency range (1483 to 1505 cm^{-1}), and the core size dependence (Table 4.3) all indicate a close correspondence to ν_3 in the OEP type hemes. Peak 12 shifts to ~1345 cm^{-1} upon reduction of the heme (W. A. Oertling, unpublished results) but exhibits only a small dependence on the spin state and ligand type. This is the only peak in the high frequency region which exibits any significant oxidation state dependence and this property makes it analogous to ν_4 of the OEP types. These three modes are listed in Table 4.4 for the bis-NMI ferric species of OEP, meso-diphenylporphyrin, and TPP species. No consistent

trends are rev

for the three

perturbations

different mode

of these vibra

For hemes w

vibrations with

and A_{2g} (AP), w

or anomalously

99). Of these,

enhanced with Sc

Upon addition of

lowered to D_{2h}.

A_g (D_{2h}) and B_{1g}

being polarized

polarized)(McCla

enhanced by Sore

totally symmetric

depolarized (B_{2g})

Our results indic

meso-diphenylporp

the TPP types. In

for the three porp

we would expect to

frequencies of OEP

Therefore, it appe

trends are revealed by comparison of the frequencies across the series for the three different modes. This may result from the different perturbations of ν_2, ν_3, and ν_4 by the phenyl substituents owing to the different mode composition types (C_b-C_b, C_a-C_m, and C_a-N respectively) of these vibrations.

For hemes with D_{4h} symmetry, resonance Raman spectroscopy enhances vibrations with the following characters: A_{1g} (P), B_{2g} (DP), B_{1g} (DP), and A_{2g} (AP), with the predicted polarizations (polarized, depolarized, or anomalously polarized) as indicated in parentheses (Spiro, 1983, Pg 99). Of these, the totally symmetric A_{1g} modes are most strongly enhanced with Soret excitation and will normally dominate the spectrum. Upon addition of meso diphenyl substitution, the symmetry will be lowered to D_{2h}. A_{1g} and B_{2g} vibrations (D_{4h}) will now both transform as A_g (D_{2h}) and B_{1g} and A_{2g} as B_{1g} (Wilson et al., 1955), with A_g modes being polarized and B_{1g} modes modes being depolarized (or anomalously polarized)(McClain, 1971). The net result is that more modes should be enhanced by Soret excitation in D_{2h} symmetry since more of them are now totally symmetric in nature; some of the modes that were previously depolarized (B_{2g}) in D_{4h} should be polarized (A_g) under D_{2h} symmetry. Our results indicate approximately the same number of modes for the meso-diphenylporphyrins as for the OEP types, but many more than for the TPP types. In addition, there are very few direct mode correlations for the three porphyrin types. If only symmetry effects were involved, we would expect to see a closer correlation between the vibrational frequencies of OEP types and those of the meso-diphenylporphyrins. Therefore, it appears that, in addition to symmetry effects, the

specific effe

determination

meso-diphenyl

for these var

more of the m

Although t

porphyrin ring

been able to a

size or oxidat

other vibratio

for ferric mes

state sensitivi

Although we hav

be used to inte

compounds. Thus

4.5 (asterisk i

ferric meso-dip

substituent mod

TPP types (Burk

the phenyl subst

above.

The optical

show a strong re

meso-diphenylpor

phenyl substitue

specific effects of phenyl substitution are also involved in the determination of the specific vibrational patterns observed for the meso-diphenylporphyrins. Excitation profiles and depolarization ratios for these various meso-diphenylporphyrin may be necessary to assign more of the modes and establish the actual extent of symmetry lowering.

Although the interaction of the phenyl substituents with the porphyrin ring makes vibrational mode assignments difficult, we have been able to assign three of the high frequency modes through the core size or oxidation state dependence of their frequencies. Many of the other vibrations observed in Figures 4.4 and 4.5 (listed in Table 4.1) for ferric meso-diphenlyporphyrins also display ligation and/or spin state sensitivity through variations of intensity and/or frequency. Although we have not been able to assign most of them, they can still be used to interpret the Raman spectra of previously uncharacterized compounds. Thus, the peaks marked with arrows in the Figures 4.4 and 4.5 (asterisk in Table 4.1) serve as spin and ligation standards for ferric meso-diphenylporphyrins. We have also assigned several phenyl substituent modes (see Table 4.1) on the basis of those observed in the TPP types (Burke et al., 1974). This further affirms the interaction of the phenyl substituents with the porphyrin macrocycle as suggested above.

The optical absorption spectra of the cytochrome oxidase models show a strong resemblance to those of the simpler meso-diphenylporphyrin species. The presence of the chelating pyridine phenyl substituent, as well as the bound copper produced very little

perturbation
species (Figu
general red sh
group and then
visible region
modeling cytoc
oxidase is six
seems to be on
in close proxi
bound or oxyge
particularly a
that the result
be explained as
characteristic
This idea is st
(1986) with "ba
covalently strap
of this band wit
six-coordinate A
sixth ligand, in
OH^-. Addition of
plane or out of
and decrease of
bands at 492 and
hydrogen bond to
strength and stab
the OH^-. This res

perturbation of the optical spectra of the five-coordinate Cl^- bound species (Figure 4.7). The six-coordinate Cl^- bound species show a general red shift of the Soret peak upon addition of the chelating group and then bound copper (Figure 4.9) but no major changes in the visible region. These results are encouraging from the perspective of modeling cytochrome oxidase. The heme of cytochrome $\underline{a}_3$ in cytochrome oxidase is six-coordinate and high-spin in the resting state and there seems to be only a small perturbation from the presence of the copper in close proximity (Blair et al., 1982). The optical spectra of the OH^- bound or oxygen bridged species exhibit more varied behavior, particularly among the six-coordinate species (Figure 4.10). We beleive that the results from these OH^- ligated and oxygen bridged species can be explained as follows. The presence of the 578 nm band is characteristic of displacement of the iron towards the ligating OH^-. This idea is strongly supported by the results of Schaeffer et al. (1986) with "basket-handle" porphyrins, in which alkoxo groups are covalently strapped across iron axial positions. The strong intensity of this band with the five-coordinate A(OH^-) species and the six-coordinate A(OH^-,DMSO), which has the weakly coordinating DMSO sixth ligand, indicate displacement of the iron toward the ligating OH^-. Addition of the imidazole ligand (B(OH^-)) pulls the iron back into plane or out of plane toward the imidazole, resulting in a blue shift and decrease of intensity of the ~578 nm band and the appearance of bands at 492 and 620 nm. The chelating pyridine groups (E(OH^-)) may hydrogen bond to the OH^- axial ligand, thereby increasing its ligating strength and stabilizing a structure with the iron out of plane toward the OH^-. This results in the reappearance of a peak at ~570 nm. The

addition of c

and induces t

species is ap

constraints,

decrease in i

five-coordinat

consistent wit

heme plane. Th

chelating pyri

complex may ha

out of plane t

the ligation s

Some of the br

D(Cu,OH^-) may b

opposite to the

no steric const

peak at ~570 nm

These resul

of cytochrome o

an absorption ba

states) which is

copper in the cy

that the absorpt

to the comparabl

this 655 nm band

~620 nm bands of

addition of copper to the chelating group removes this hydrogen bond and induces the formation of the μ-oxo species. The iron in the μ-oxo species is apparently back in plane, probably owing to simple steric constraints, as evidenced by the appearance of the 620 nm peak. The decrease in intensity and wavelength of the ~578 nm band in the five-coordinate series A(OH^-), D(OH^-), D(Cu,OH^-) (Figure 4.8) is consistent with increased steric constraint pushing the iron into the heme plane. This is not inconsistent with hydrogen bonding to the chelating pyridines. The optimum geometry for this hydrogen bonded complex may have the iron out of plane toward the OH^- but perhaps less out of plane than for the unconstrained species (A(OH^-), even though the ligation strength of the hydrogen bonded complex may be stronger. Some of the broadness of the visible bands of the species D(OH^-) and D(Cu,OH^-) may be accounted for by OH^- ligating to the axial position opposite to the chelating group. In this case the OH^- would encounter no steric constraints and would display a peak at 578 nm along with peak at ~570 nm (or less) from the constrained species.

These results have interesting implications for the interpretation of cytochrome oxidase absorption spectra. Cytochrome oxidase exhibits an absorption band at ~655 nm in the resting enzyme (and some ligated states) which is associated with ligand coupling between the iron and copper in the cytochrome a_3 site (Beinert et al., 1976). If we consider that the absorption spectra of heme a species are red shifted relative to the comparable meso-diphenyl hemes (Fe^{III} Heme a Cl^-, ~ 670 nm), this 655 nm band in cytochrome oxidase could correspond to the ~630 or ~620 nm bands of the respective Cl^- or OH^- bound six-coordinate

meso-diphenyl

different pos

One possibili

in resting oxi

result in the

that O^{-2}, or a

enzyme with th

bridging, or p

loss of the 65

Despite the

meso-diphenyl h

of Cl^- or OH^- l

as was discusse

meso-diphenylpo

structures of t

spectra of the

high-spin (Figu

Raman spectral

4.13 and 4.14).

a broadness of p

sample inhomogen

This may result

(macrocycle deco

in a low spin co

meso-diphenyl hemes. If this analogy is correct, it suggests two different possibilities for the bridging ligand in cytochrome oxidase. One possibility is that a halide ligand bridges the two metal centers in resting oxidase, and displacement by other exogenous ligands could result in the loss of the 655 nm band. The other possibility suggests that O^{-2}, or a similar ligand, bridges the metal centers in the resting enzyme with the iron in plane. Exogenous ligands which disrupt this bridging, or pull the iron out of plane, could likewise result in the loss of the 655 nm band.

Despite the inability to assign most of the Raman lines of the meso-diphenyl heme species, the Raman spectra are consistent in terms of Cl^- or OH^- ligation, five- or six-coordinate, and high- or low-spin, as was discussed above. As such, the Raman spectra of the simpler meso-diphenylporphyrins allow for straightforward analysis of the structures of the more complex cytochrome oxidase models. The Raman spectra of the D species indicate that they are all five-coordinate high-spin (Figures 4.11 and 4.12). The species made from E have the Raman spectral characteristics of six-coordinate high-spin (Figures 4.13 and 4.14). The spectra of the species E(OH^-) and E(Cu,OH^-) exhibit a broadness of peaks 4 ($\tilde{}$1573 cm^{-1}) and 7 ($\tilde{}$1490) which may indicate sample inhomogeneity, such as a small population of low-spin species. This may result from extraneous pyridine or imidazole ligands (macrocycle decomposition products) or a small percentage of the sample in a low spin configuration.

Optical a

establish whe

iron and copp

whether there

a reasonable

established; l

to other techn

spectroscopic

bridging in th

six-coordinate

indicate that

well as some c

E(Cu,Cl$^-$) (Koo,

model compounds

between the met

The EPR der

ligand symmetry

lineshape commo

with g perpendi

symmetry is cle

Perturbations wh

distortion) caus

from the two non

spectra of the f

which display a

indicates that th

Optical absorption or Raman spectroscopy cannot definitively establish whether the bound Cl^- or OH^- (O^{-2}) is bridging between the iron and copper in those species with chelated copper and if so, whether there is magnetic coupling between the two metal centers. To be a reasonable model for resting oxidase, both of these aspects must be established; ligand bridging and magnetic coupling. We therefore turn to other techniques which may give us this information. IR spectroscopic studies (Koo, 1986) suggest that oxygen (O^{-2}) is probably bridging in the five-coordinate model D(Cu,O^{-2}) and possibly with the six-coordinate model E(Cu,O^{-2}) also. Magnetic susceptibility studies indicate that there may also be magnetic coupling in these species, as well as some coupling with the six-coordinate Cl^- ligated species E(Cu,Cl^-) (Koo, 1986). We have utilized EPR spectroscopy on some of the model compounds to verify the presence and extent of magnetic coupling between the metal centers of the copper chelating species.

The EPR derivative line shapes expected for hemes of different ligand symmetry and spin state are discussed by Palmer (1985). The lineshape common to the high spin ferric hemes is the axial symmetry with g perpendicular (g_x=g_y) at ~6 and g parallel (g_z) at ~2. Axial symmetry is clearly demonstrated with the Mb F^- (Figure 4.15a) sample. Perturbations which remove the equivalency of the X and Y axes (rhombic distortion) cause a splitting of the g=6 signal into individual signals from the two non-equivalent axes. This phenomenon is seen in the spectra of the five-coordinate Cl^- bound species (Figure 4.15b-e), which display a small splitting of the g=6 signal. Palmer (1985) indicates that this behavior arises most often from changes in the type

or orientatio

meso-diphenyl

some extent i

aromatic meso

compounds (Fi

(Figure 4.17a

This is obser

signal and a

resulting lin

different axi

distortion. I

relative to t

premature to

solvent instea

for both sampl

Since the THF

line shape is

there is also

solvent system

compounds are

the "glass" pr

CH_2Cl_2 (which

that similar u

bound TPP type

low-spin charac

hydrogen bondi

or orientation of axial ligands. In the case of these meso-diphenylporphyrins, since this rhombic distortion is present to some extent in all observed species, asymmetry induced by the two aromatic meso substituents may also occur. With the OH^- ligated compounds (Figure 4.16) and some of the six-coordinated compounds (Figure 4.17a,d), we see a much greater distortion of this pattern. This is observed as a broadening and loss of intensity of the g=6 signal and a dramatic increase in the intensity of the g=2 signal. The resulting line shape most closely resembles a composite of the two different axial symmetries, or perhaps a more severe rhombic distortion. In this case, the specific orientation of the axial ligand, relative to the meso substituents, may be responsible. It is also premature to rule out aggregation effects. The use of a toluene/THF solvent instead of CH_2Cl_2 in two cases, resulted in sharper line shapes for both samples and less distortion in the spectrum of the ^-OH sample. Since the THF weakly ligates, it is difficult to say if the sharper line shape is due to the "glass" quality of the solvent, or whether there is also a ligation effect. It is also difficult to say which solvent system would be more prone to aggregation. Although these compounds are less soluble in Toluene/THF overall, the THF ligation and the "glass" properties upon cooling may cause less aggregation than CH_2Cl_2 (which crystallizes upon freezing). It is interesting to note that similar unusual line shapes have been reported for OH^- and RO^- bound TPP type hemes (Schaeffer et al., 1986). The appearance of some low-spin character in the spectrum of E(OH^-) may confirm that there is hydrogen bonding to the pyridine chelating group and increased ligation

strength towa

rule out ligat

Although w

spin iron (III

study, the EPR

chelated speci

signals is ind

ligand bridgin

errors in the

4.2, these err

low integratio

six-coordinate

comparison wit

magnetic coupl

careful study

$(D(Cu,O^{-2}))$, wh

integration val

values. For D(C

value of .05 mm

this is taken i

much less for s

determined conc

$(D(Cu,O^{-2}))$ our

centers which a

relaxation of t

be exchange cou

strength toward the iron. However, the signal is not strong enough to rule out ligation by extraneous pyridine or imidazole.

Although we have focused primarily on the identification of high spin iron (III) through the detection of the g=6 signal in this EPR study, the EPR detection of the copper II (g=2) signal for copper chelated species is also of importance. Absence or attenuation of these signals is indicative of coupling between metal centers by means of ligand bridging or aggregation effects. Although there may be large errors in the absolute values of the integrations reported in Table 4.2, these errors should be systematic. Considering this, the unusually low integration values for both the five- ($D(Cu,O^{-2})$) and six-coordinate ($E(Cu,O^{-2})$) copper chelated oxygen bridged compounds, in comparison with their copperless counterparts, is strong evidence for magnetic coupling between the metal centers in these compounds. The careful study of the five-coordinated oxygen bridged species ($D(Cu,O^{-2})$), which uses a larger integration window, confirms that the integration values in Table 4.2 are probably lower than the true values. For $D(Cu,O^{-2})$, the value in Table 4.2 is ~38% lower than the value of .05 mm obtained with the larger integration window. Even if this is taken into account, the EPR detectable high-spin heme is still much less for several species than the corresponding optically determined concentration. These results suggest that for species ($D(Cu,O^{-2})$) our sample contains ~20% non-bridged or non-coupled metal centers which are still in close enough proximity to enable fast relaxation of the copper copper center. The other ~80% is presumed to be exchange coupled to yield an even spin species which is undetectable

under convent

susceptibilit

discussed bro

non-coupled h

(opposite sid

chelating gro

would not nec

and would only

Although no ot

are confident

bridged specie

bridged compou

and additional

Based on th

Raman, and EPR

meso-diphenyl

properties of t

The model that

be the oxygen b

six-coordinate

magnetic coupli

under conventional EPR conditions. This analysis is consistent with the susceptibility results and also correlates with the previously discussed broadness in the optical absorption spectra. This ~20% non-coupled heme may be accounted for by backside OH^- ligated heme (opposite side to the chelating group) or by heme in which the Cu or chelating group are absent. Small quantities of these different species would not necessarily be distinguished in the optical or Raman spectra and would only contribute to the observed broadness or inhomogeneity. Although no other species have been this carefully characterized, we are confident that coupling also occurs for the six-coordinate oxygen bridged species. A similar coupling may occur in the six-coordinate Cl^- bridged compound, but the evidence for this species is not as strong and additional studies are required.

Based on the combined results of optical absorption, resonance Raman, and EPR spectroscopies, we conclude that some of these meso-diphenyl substituted hemes mimic the geometry and spectroscopic properties of the oxygen reduction site in resting cytochrome oxidase. The model that most accurately represents the structure in oxidase may be the oxygen bridged six-coordinate species $E(Cu,O^{-2})$ in that it is six-coordinate high-spin, like oxidase, and it displays apparent magnetic coupling between Fe^{3+} and Cu^{2+} through a bridging ligand.

CHA

A. INTRODUC

Heme prote

processes. Hem

their intrinsi

for a wide var

probably the m

Adar, 1978, an

and storage, r

Cytochrome oxi

the thermodynar

reduction of ox

P-450, members

to metabolize v

(Griffin et al.

biochemical oxi

their dispropor

Although, most

center, cytochr

been identified

Tsubaki et al.,

variation, in th

CHAPTER 5

CHARACTERIZATION OF "OXY" AND "OXO" HEMES AS MODELS OF HEME PROTEIN REACTION INTERMEDIATES

A. INTRODUCTION

Heme proteins perform prominent roles in many biochemical processes. Hemes are especially important in aerobic organisms, where their intrinsic affinity and reactivity toward oxygen has been utilized for a wide variety of specialized functions. Hemoglobin and myoglobin, probably the most extensively studied of all the heme proteins (see Adar, 1978, and references within), are utilized for oxygen transport and storage, respectively, in mammals and some other higher organisms. Cytochrome oxidase terminates the electron transport chain and provides the thermodynamic drive for aerobic respiration through the catalytic reduction of oxygen to water (Wikstrom et al., 1981). Cytochromes P-450, members of the group of heme containing oxygenases, utilize O_2 to metabolize various compounds through specific oxygen insertion (Griffin et al., 1979). Peroxidases use peroxides as specific biochemical oxidants, whereas catalases remove peroxides by catalizing their disproportionation to H_2O and O_2 (Hewson and Hager, 1979). Although, most heme proteins utilize protoheme as the prosthetic center, cytochrome oxidase uses heme a and additional heme types have been identified in various other proteins (see Adar, 1978, pg. 180; Tsubaki et al., 1980). The specific biochemical purposes of heme variation, in these various enzyme systems, is not well understood.

The centr
mechanisms by
the intermedi
structural fa
Although the
have been obt
Love, 1974; T
studies have
stable interme
conditions or
less direct te
expected to be
may not be pos
enzyme samples
extremely valu
such as solven
1975), axial l
restrictions (
et al., 1981;
bonding (Mispel
with model stud
used to interpr
complicated pro

Two species
"ferrous oxy" a
($Fe^{II}.O_2$) is ex

The central goals of heme protein research are to elucidate the mechanisms by which these reactions occur, as well as the structures of the intermediate species, and to determine the heme and protein structural factors which determine the specificity of a given reaction. Although the structures of some of the above mentioned heme proteins have been obtained with X-ray crystallographic techniques (Padlan and Love, 1974; Takano, 1977; Fermi, 1975; Poulos et al., 1980), these studies have generally been limited to resting enzyme states or highly stable intermediate species. Structures of these systems under turnover conditions or in less stable states have so far been probed only by less direct techniques. Since a variety of environmental factors are expected to be involved in the specific chemistry of a given enzyme, it may not be possible to separate these effects in experiments with enzyme samples. For this reason, model compound studies have been extremely valuable in elucidating heme reaction mechanisms. Factors such as solvent polarity (Brinigar et al., 1974; Chang and Traylor, 1975), axial ligation (Kerr et al., 1983; Collman et al., 1983), steric restrictions (Yu et al., 1983), heme peripheral substitution (Traylor et al., 1981; Kerr et al., 1983; Kean et al., 1987), and hydrogen bonding (Mispelter et al., 1983), can often be varied independently with model studies. The results of these various studies may then be used to interpret results obtained from experiments with the more complicated protein species.

Two species of great interest in heme chemistry research are the "ferrous oxy" and "ferryl oxo" species. The ferrous oxy species (Fe^{II}-O_2) is exemplified by hemoglobin and myoglobin, which bind O_2

reversibly wh

intermediate

Chance, 1986,

(Babcock et a

been identifi

(Champion et

ferrous perox

III), which ma

1983). Althoug

oxy species of

reactive. Unde

crucial to the

Ferryl oxo

cycle of cytoc

the oxygen don

intermediates

Jones, 1984).

hemes can also

Irvine, 1952; D

Peisach, 1981).

enzymes and the

expected that h

and chemical re

species. Compar

protein species

reversibly when the heme is in a ferrous (Fe^{+2}) state. The initial intermediate in the reaction of cytochrome oxidase (see Naqui and Chance, 1986, and references therein) is a ferrous oxy compound (Babcock et al., 1984, 1985) and a ferrous oxy species has recently been identified as a reaction intermediate of cytochrome P-450 (Champion et al., 1986). Dioxygen binding can also be easily induced in ferrous peroxidase samples to produce a ferrous oxy species (compound III), which may be involved in plant growth regulation (Smith et al., 1983). Although the ferrous oxy complexes of the globins are stable, oxy species of other proteins and most free solution hemes are very reactive. Understanding the factors which control this reactivity is crucial to the understanding of heme chemistry.

Ferryl oxo species (Fe^{IV}=O) have been postulated in the catalytic cycle of cytochrome c oxidase (Wikstrom, 1981; Blair et al., 1985), as the oxygen donating species in cytochrome P-450 (Groves, 1985), and as intermediates in the reactions of catalases and peroxidases (Frew and Jones, 1984). Addition of peroxide to the normally unreactive globin hemes can also induce the formation of ferryl species (George and Irvine, 1952; Dalzial and O'Brian, 1954; Aviram et al., 1978; Uyeda and Peisach, 1981). Given the diverse chemistry catalyzed by these various enzymes and the lack of reactivity of the globin species, it is expected that heme pocket modulation strongly influences the structure and chemical reactivity of these oxy (Fe^{II}-O_2) and oxo (Fe^{IV}=O) species. Comparison of the properties of these species for each given protein species and between different protein systems should help

characterize

their diverse

Resonance

study of ferr

recently been

several ferryl

species (Terne

1986a,b; Sitte

and five- and

al., 1984; Pro

al., 1987), th

5.6). This is

perturbations

also vary in p

and references

smaller range

in the optical

species (see Ta

spectra are sen

these changes s

this paper, we

six-coordinate

contain 1-methy

protoheme and h

octaethylheme,

characterize these different heme pockets and provide insights into their diverse reactivities.

Resonance Raman spectroscopy has been applied extensively to the study of ferrous oxy species (both protein and model compounds) and has recently been used for the identification and characterization of several ferryl oxo species. In a comparison of ferryl peroxidase species (Terner et al., 1985; Hashimoto et al., 1984; Hashimoto et al., 1986a,b; Sitter et al., 1986), ferryl myoglobin (Sitter et al., 1985a), and five- and six-coordinate ferryl oxo heme model compounds (Bajdor et al., 1984; Proniewicz et al., 1986; Schappacher et al., 1986; Kean et al., 1987), the frequency of $\nu(Fe^{IV}=O)$ varies by $\sim$85 cm^{-1} (see Table 5.6). This is indicative of a high sensitivity of this bond to perturbations in the local environment. Observed values of $\nu(Fe^{II}-O_2)$ also vary in protein species and heme model compounds (see Spiro, 1983 and references within; Van Wart and Zimmer, 1985) but over a much smaller range ($\sim$10 cm^{-1}). In addition, there are distinct differences in the optical spectra of various ferrous oxy and ferryl oxo protein species (see Table 5.5 and cited references). Optical absorption spectra are sensitive to subtle changes in the heme environment and these changes should also correlate with the observed Raman results. In this paper, we present optical absorption and resonance Raman data for six-coordinate ferrous oxy and ferryl oxo heme model compounds which contain 1-methylimidazole in the trans axial position. Octaethylheme, protoheme and heme a were used for the ferrous oxy models, and octaethylheme, protoheme, and tetraphenylheme were used for the ferryl

oxo models. T

reactivity of

B. MATERIAL

Methylene

to use. Tolue

1972). Toluen

molecular sie

purification.

anhydrous copp

over calcium h

Chemical Inc.)

were stored in

purification.

without furthe

protoporphyrin

(FeTPP), and i

by W. Anthony C

from bovine hea

et al., 1976).

complexes, (NMI

Chang (1974) an

procedures are

μM) were prepar

~100-fold excess

line glassware,

pressure of argo

oxo models. These results provide insight into the structure and reactivity of the heme proteins mentioned above.

B. MATERIALS AND METHODS

Methylene chloride was dried by reflux over calcium hydride prior to use. Toluene was distilled from benzophenone ketyl (Gordon and Ford 1972). Toluene-d_8 (Cambridge Isotope Laboratories) was dried over molecular sieves (4 and 5 angstrom) and used without further purification. Dimethylformamide (DMF) was vacuum distilled over anhydrous copper sulfate. 1-methylimidazole (NMI) was vacuum distilled over calcium hydride. Sodium dithionite (a generous gift from Virginia Chemical Inc.) and tetrabutylammonium borohydride (TBAB, from Aldrich) were stored in vacuum dessicators and used without further purification. Iron protoporphyrin IX (Sigma, bovine hemin) was used without further purification for preparation of the oxy models. Iron protoporphyrin IX dimethylester (FePPIXDME), iron tetraphenyporphyrin (FeTPP), and iron octaethylporphyrin (FeOEP) were generously provided by W. Anthony Oertling (Michigan State University). Heme a was isolated from bovine heart cytochrome c oxidase as previously described (Babcock et al., 1976). The procedures for the preparation of the oxy heme complexes, $(NMI)Fe^{II}\text{-}O_2$, were based on those reported in Brinigar and Chang (1974) and Babcock and Chang (1979). The details of the procedures are as follows. Solutions of the various hemes (~50 to 250 μM) were prepared in methylene chloride or DMF which contained an ~100-fold excess of NMI. These were then purged of oxygen, in Schlenk line glassware, by using 5 to 10 freeze-pump-thaw cycles. A positive pressure of argon gas was maintained over the sample during the thaw

stages. Fe^{III}

addition of a

reduced by ti

reductions we

Oxygen bindin

samples (~45

monitored opt

displacement

illumination

hemes, (NMI)Fe

et al. (1983)

carried out in

box. Although

for FePPIXDME

protoheme was

Isotopic label

achieved by the

respective synt

obtained with a

temperature opt

built optical D

were contained

temperature by

with a Spex 140

detector) by usi

model 164 Kr^+ ic

in EPR tubes, we

stages. $Fe^{III}OEP$ in methylene chloride was reduced to $Fe^{II}OEP$ by the addition of a slight excess of solid TBAB. The hemes in DMF were reduced by titration with a degassed aqueous dithionite solution. These reductions were monitored by using optical absorption spectroscopy. Oxygen binding was achieved by the addition of oxygen to the cooled samples (-45 to -70 C) with a gas tight syringe. This binding was monitored optically (see below) and shown to be reversible by displacement of the O_2 with CO followed by degassing under strong illumination (Brinigar and Chang, 1974). Preparation of the ferryl oxo hemes, $(NMI)Fe^{IV}=O$, was performed according to the procedure of La Mar et al. (1983) with the exception that the anaerobic steps were all carried out in Schlenk line glassware instead of an anaerobic glove box. Although it was not previously reported, the procedure worked well for FePPIXDME in addition to FeOEP and FeTPP. Use of the non-esterified protoheme was prohibited by its negligible solubility in toluene. Isotopic labeling of both the ferrous oxy and ferryl oxo compounds was achieved by the use of $^{18}O_2$ (98% Cambridge Isotope Laboratories) in the respective synthetic procedures. All optical absorption spectra were obtained with a Perkin-Elmer Lambda 5 UV/Visible spectrophotometer. Low temperature optical absorption spectra were obtained by using a house built optical Dewar mounted in the Lambda 5 (Kean, 1987). The samples were contained in EPR tubes which were cooled to the desired temperature by flowing cold nitrogen gas. Raman spectra were obtained with a Spex 1401 scanning monochromator (with an RCA 31034C PMT detector) by using 15 mW incident power at 406.7 nm (Spectra-Physics model 164 Kr^+ ion) in a backscattering geometry. The samples, contained in EPR tubes, were spun continuously in a dewar while the desired

temperature

sloping back

in the figur

C. RESULTS

The optic

OEP are shown

reported for

1974). The ab

samples (not

(Brinigar and

The peak posi

reported resu

from the abso

oxy species fr

shift of the β

band blue shif

bis-NMI specie

observed for a

spectra of the

DMF are shown

shifts to 547

peak is assigne

shift of 26 cm

simple harmonic

cm^{-1} in the res

5.2d, respectiv

temperature was maintained by flowing cold nitrogen gas. A linear sloping background was subtracted from some Raman spectra, as indicated in the figure legends, but no smoothing was done.

C. RESULTS

The optical absorption spectra of ferrous bis-NMI and ferrous oxy OEP are shown in Figure 5.1. As expected, this is similar to that reported for an iron mesoporphyrin derivative (Brinigar and Chang, 1974). The absorption spectra of the ferrous oxy protoheme and heme a samples (not shown) are in agreement with previously reported spectra (Brinigar and Chang, 1974, and Babcock and Chang, 1979, respectively). The peak positions are listed in Table 5.1 along with some previously reported results for ferrous oxy species of other porphyrins. As seen from the absorption spectra in Figure 5.1, the formation of the ferrous oxy species from the ferrous bis-NMI species is accompanied by a red shift of the β and α bands and a change in their intensities. The Soret band blue shifts to a value close to that of the corresponding ferric bis-NMI species (see Table 5.1). This same characteristic behavior is observed for all of the porphyrins used in these experiments. Raman spectra of the ferrous oxy complexes of FeOEP, FePPIX, and heme a in DMF are shown in Figure 5.2. For ferrous oxy FeOEP the peak at 573 cm^{-1} shifts to 547 cm^{-1} upon substitution of ^{16}O by ^{18}O; consequently this peak is assigned to the Fe^{II}-O_2 stretching vibration. The frequency shift of 26 cm^{-1} is in agreement with the value predicted by using a simple harmonic oscillator model. Peaks observed at 573 cm^{-1} and ~576 cm^{-1} in the respective FePPIX and heme a samples (Figures 5.2c and 5.2d, respectively) also demonstrate a 26 cm^{-1} downshift upon ^{18}O

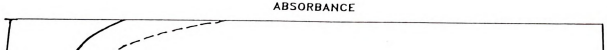

Figure

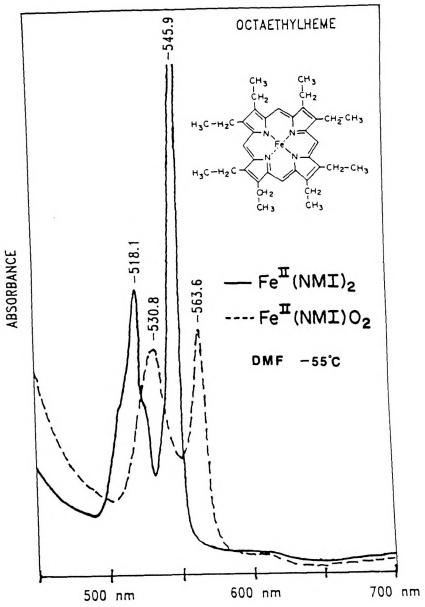

Figure 5.1 Optical absorption spectra of Bis-NMI and "oxy" ferrous octaethylheme.

Table 5.1: O
S

Species	
$Fe^{II}OEP(NMI)_2$	
$Fe^{III}OEP(NMI)$	
$Fe^{II}OEP(NMI)O$	
$Fe^{II}OEP(NMI)O$	
$Fe^{II}PPIX(NMI)$	
Fe^{II}Heme a(NM	
$Fe^{II}TPP(PYR)O_2$	
$Fe^{II}TPivPP(NMI$	
$Fe^{II}TPivPP(THI$	
$Fe^{IV}OEP(NMI)O$	
$Fe^{IV}PPIXDME(NM$	
$Fe^{IV}TPP(NMI)O$	
$Fe^{IV}TmTP(NMI)O$	
$Fe^{IV}TPivPP(THF$	
$Fe^{IV}TPivPP(NMI$	
$Fe^{IV}(ETIO)(NMI$	

Abbreviations:
OEP, octaethyl
TPP, tetrapheny
(O-pivaloylpher
ETIO, etioporp
THF, tetrahydrc
<>, or = sign

Table 5.1: Optical Absoprtion Peaks of Ferrous Oxy and Ferryl Oxo Heme Species.

Species	Soret	β,α	Solvent	Temp	Reference
$Fe^{II}OEP(NMI)_2$	408	517<545	CH_2Cl_2	-80	this work
$Fe^{III}OEP(NMI)_2$	403	524>545	CH_2Cl_2	RT	this work
$Fe^{II}OEP(NMI)O_2$	~404	530=563	CH_2Cl_2	-80	this work
$Fe^{II}OEP(NMI)O_2$	~404	531=564	DMF	-45	this work
$Fe^{II}PPIX(NMI)O_2$	415	540=574	DMF	-45	this work and Brinigar & Chang (1974)
Fe^{II}Heme a(NMI)O_2	426	579<595	DMF	-45	this work and Babcock & Chang (1979)
$Fe^{II}TPP(PYR)O_2$	-	547>583	CH_2Cl_2	-80	Anderson et al. (1973)
$Fe^{II}TPivPP(NMI)O_2$	-	548>>580	BZ	RT	Collman et al. (1973)
$Fe^{II}TPivPP(THF)O_2$	419	538	THF	-70	Schappacher et al. (1985)
$Fe^{IV}OEP(NMI)O$	406	535,546=573	TOL	-90	this work and Kean et al. (1987)
$Fe^{IV}PPIXDME(NMI)O$	416	543,555=584	TOL	-90	this work and Kean et al. (1987)
$Fe^{IV}TPP(NMI)O$	427	555,563>597	TOL	-90	this work
$Fe^{IV}TmTP(NMI)O$	420	~544, ~556>590	TOL	-90	Chin et al. (1980)
$Fe^{IV}TPivPP(THF)O$	419	550	THF	-70	Schappacher et al. (1985)
$Fe^{IV}TPivPP(NMI)O$	426	560>>590	THF	-70	Schappacher et al. (1985)
$Fe^{IV}(ETIO)(NMI)O$	-	~535,550<572	TOL	-80	La Mar et al. (1983)

Abbreviations:
OEP, octaethylporphyrin; PPIX, protoporphyrin IX;
TPP, tetraphenylporphyrin; TPivPP, "picket fence" porphyrin (Tetra-(O-pivaloylphenyl) porphyrin); TmTP, tetramesitylporphyrin;
ETIO, etioporphyrin; NMI, 1-methyl imidazole; PYR, pyridine;
THF, tetrahydrofuran; DMF, dimethylformamide; TOL, toluene; BZ, benzene
<,>, or = sign reflects relative intensities of the absorption bands.

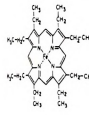

OCTAETHYLHEME

a) [1

b) [1

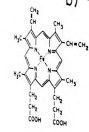

protoheme

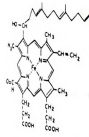

heme a

Figur

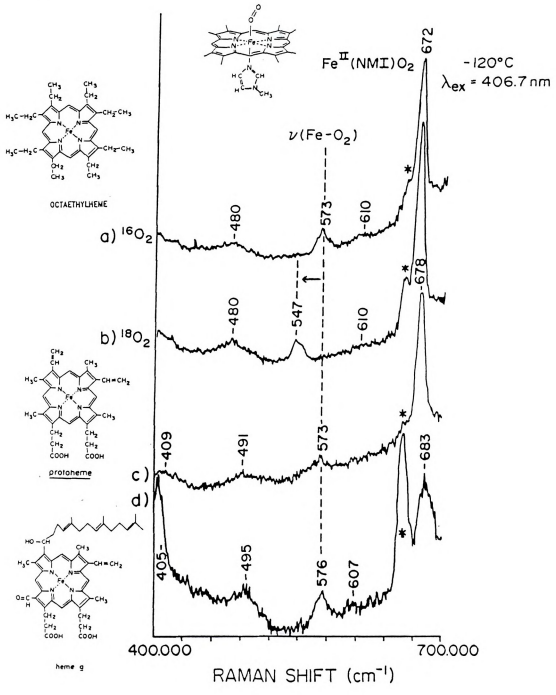

Figure 5.2 Identification of $\nu(Fe^{II}-O_2)$ for ferrous oxy octaethylheme, protoheme, and heme a.

substitution

experiment w

decompositio

low temperatu

spectra. It

region which

and heme a sa

fluorescent p

of these latt

absorption ba

excitation li

done in methy

and we have f

frequency reg

of the corresp

frequency regi

Although the

the peak posit

bis-NMI specie

with those of

The optica

and TPP specie

shift in the sp

the increasing

substituents. T

with those of

substitution (not shown) and are likewise assigned to $\nu(Fe^{II}-O_2)$. This experiment was complicated by the formation of fluorescent heme decomposition products in DMF. The fluorescence is more pronounced at low temperature and obscured the high frequency region of the Raman spectra. It also produced a sloping background in the low frequency region which is subtracted from the data in Figure 5.2. The protoheme and heme a samples were more susceptible to the formation of this fluorescent product. In addition, there is less resonance enhancement of these latter two species owing to the wavelenghts of their Soret absorption bands, which are considerably to the red of the 406.7 nm excitation line. Because of these problems, the remaining oxy work was done in methylene chloride, in which the heme decomposition is minimal, and we have focused on the FeOEP complex. A portion of the low frequency region is displayed in Figure 5.3 along with the same region of the corresponding Fe^{III} bis-NMI species. Figure 5.4 shows the high frequency regions in the -127 C Raman spectra of these two samples. Although the spectrum for the ferrous oxy species is overall weaker, the peak positions are nearly identical with those of the ferric bis-NMI species. The peak positions are summarized in Table 5.2 along with those of a variety of other FeOEP species.

The optical absorption spectra of (NMI)Fe^{IV}=O for the OEP, PPIXDME, and TPP species are displayed in Figure 5.5. There is a progressive red shift in the spectra in going from OEP to PPIXDME to TPP which reflects the increasing electron withdrawing ability of the respective ring substituents. The peak positions are also tabulated in Table 5.1 along with those of other ferryl oxo model species which have been previously

RAMAN INTENSITY

Figu

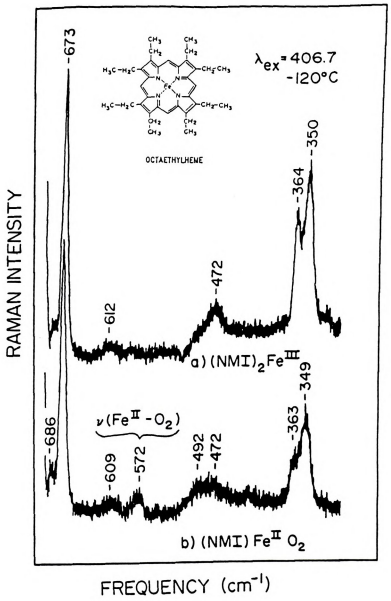

Figure 5.3 Raman spectra of Bis-NMI and "oxy" ferrous octaethylheme (low frequency region).

Figure

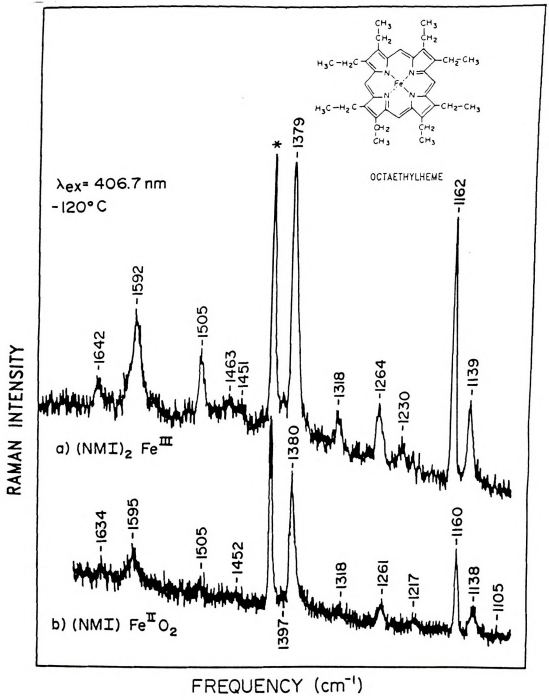

Figure 5.4 Raman spectra of Bis-NMI and "oxy" ferrous octaethylheme (high frequency region).

Table 5.2: R

ASN	Fe^{II} (NMI
ν_{10}	164
ν_2	159
ν_{19}	-
ν_{11}?	-
ν_3	150
?	146
?	145
ν_{29}	-
ν_{20}	139
ν_4	137
?	-
ν_{21}	1318
$\nu_5+\nu_9$	1264
ν_{13}	1230
ν_{30}	1162
$\nu_6+\nu_8$	1139
ν_{22}	-
ν_5	1026
$\nu_{32}+\nu_{35}$	-
?	889
ν(Fe=O)	-
?	-
$\nu_{33}+\nu_{34}$	770
ν_{16}	-
$\nu_{33}+\nu_{35}$	730
ν_7	670
?	612
?	-
ν(Fe-O2)	-
?	550
?	-
?	472
$2\nu_{35}$	364
ν_8	350
?	-
ν_{32}	266
?	187

Assignments ba
nesoheme in Sp
peaks. a From
/ indicates nu
inhomogeneity)

Table 5.2: Raman Peaks of Iron Octaethylporphyrin Species.

ASN	Fe^{III} $(NMI)_2$	Fe^{II} $(NMI)O_2$	Fe^{II} $(NMI)_2$	Fe^{IV} (NMI)O	Fe^{II}	Fe^{IV} O [a]	$(Fe^{III})_2$ O [b]
ν_{10}	1642	1639	1638/ 1623	1643/ 1629	1642/ 1630	1643	1627
ν_2	1592	1595	1598	1603	1600	1598	1583
ν_{19}	-	-	-	1575	1576	1578	1559
ν_{11}?	-	-	1545	-	-	-	-
ν_3	1505	1505	1492	1513/ 1506/ 1499	1515/ 1500	1507	1495
?	1463	1462	1458	1468	-	-	-
?	1451	-	-	1438	-	-	-
ν_{29}	-	-	-	-	-	-	1403
ν_{20}	1393	1397	-	-	-	-	1388
ν_4	1379	1380	1363	1385/ 1370	1380/ 1361	1379	1377
?	-	-	1334	1346	-	-	
ν_{21}	1318	1318	-	1321	-	1315	1315
$\nu_5+\nu_9$	1264	1261	1261	1264/ 1260	1261	~1260	1258
ν_{13}	1230	1217	1218	1222	-	~1218	1211
ν_{30}	1162	1160	1163	-	-	-	1159
$\nu_6+\nu_8$	1139	1138	1138	1141	-	~1140	1136
ν_{22}	-	-	-	-	1123	~1130	1129
ν_5	1026	1024	1022	1025	1025	~1038/ 1010	1023
$\nu_{32}+\nu_{35}$	-	-	-	962	-	-	963
?	889	889	-	-	-	-	-
ν(Fe=O)	-	-	-	820	-	852	-
?	-	-	-	805	-	-	-
$\nu_{33}+\nu_{34}$	770	768	-	770	-	-	-
ν_{16}	-	-	-	749	-	~750	753
$\nu_{33}+\nu_{35}$	730	731	-	737	-	-	733
ν_7	670	673	667	672	674	670	668
?	612	613	614	~613	-	-	-
?	-	-	-	581	-	-	-
ν(Fe-O2)	-	572	-	-	-	-	-
?	550	-	-	-	-	-	-
?	-	-	-	500	493	-	-
?	472	474	477	479/470	-	-	-
$2\nu_{35}$	364	363	-	~366	365	~365	-
ν_8	350	349	348	~350	~348	~350	345
?	-	-	286	~275	-	-	-
ν_{52}	266	263	266	~261	279	-	-
?	187	188	196	-	-	-	-

Assignments based on Abe and Kitagawa (1975); the assignments for mesoheme in Spiro and Burke (1976) were used as a guide to assign some peaks. [a] From Proniewicz et al. (1986) [b] From Hofmann and Bocian (1984) / indicates number below is also the same mode (a result of sample inhomogeneity).

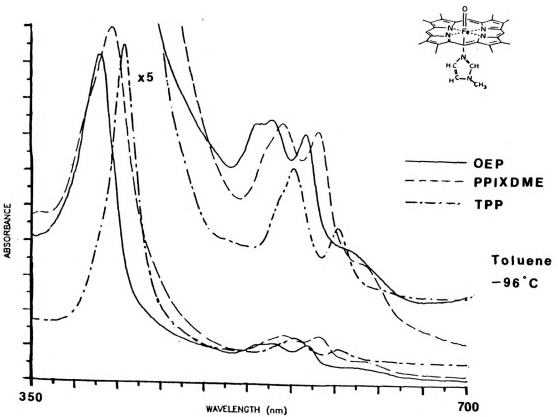

Figure 5.5 Optical absorption spectra of ferryl oxo protoheme, octaethylheme, and tetraphenylheme.

reported in

ferryl PPIX

which is the

species also

the other sa

shifted rela

intermediate

(PPIXDME)].

substitution

vibration. Th

$\nu(Fe^{IV}=O)$ fre

to -190 C, bu

which suggest

temperatures.

$[(NMI)Fe^{IV}=O$

respectively.

cm^{-1} peak upo

$\nu(Fe^{IV}=O)$.

In Figure

for the ferryl

are presented.

the ferryl spe

allows better

species has a

(see Table 5.3

dimer contamin

reported in the literature. The peak at ~619 nm in the spectrum of the ferryl PPIXDME sample is due to a u-oxo dimer impurity $(PPIXDME\ Fe)_2O$ which is the final product of auto-oxidation. The occurrence of this species also accounts for the broadness of the Soret peak relative to the other samples and the observed Soret maximum may be slightly blue shifted relative to a pure sample. In Figure 5.6a we show the intermediate frequency region of the Raman spectrum of $[(NMI)Fe^{IV}=O\ (PPIXDME)]$. The peak at 820 cm^{-1} shifts to 784 cm^{-1} (Figure 5.6b) upon substitution of ^{16}O by ^{18}O, and is assigned to the $Fe^{IV}=O$ stretching vibration. The 36 cm^{-1} shift is expected for a ferryl structure. This $\nu(Fe^{IV}=O)$ frequency was independent of temperature over the range -90 C to -190 C, but the intensity did decrease at the higher temperatures which suggests a greater degree of sample decomposition at the higher temperatures. This vibration is also observed in the spectra of $[(NMI)Fe^{IV}=O\ (OEP)]$ and $[(NMI)Fe^{IV}=O\ (TPP)]$ in Figures 5.6c and 5.6d respectively. These samples likewise exhibit a 36 cm^{-1} shift of the 820 cm^{-1} peak upon ^{18}O substitution (not shown), confirming that this is $\nu(Fe^{IV}=O)$.

In Figure 5.7, the high frequency Raman spectra recorded at -120 C for the ferryl (7a), μ-oxo (7c), and μ-peroxo (7d) species of PPIXDME are presented. For additional clarity, a solvent subtracted spectrum of the ferryl species is presented in Figure 5.7b. The solvent subtraction allows better observation of the 1550 to 1700 cm^{-1} region. The ferryl species has a spectrum which is similar to a low-spin ferric sample (see Table 5.3) and the 1496 cm^{-1} peak is again indicative of a μ-oxo dimer contamination. The spectra of the μ-peroxo and μ-oxo species are

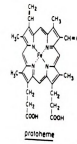

a)

b)

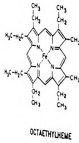

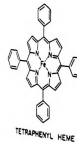

Figur

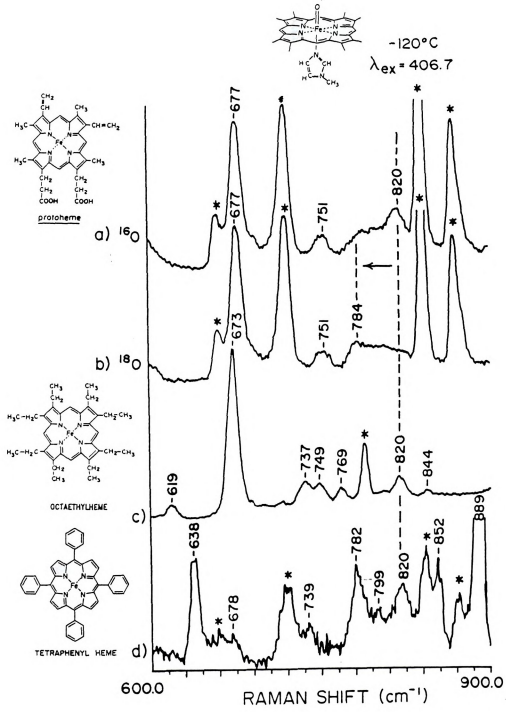

Figure 5.6 Identification of $\nu(Fe^{IV}=O)$ for ferryl oxo protoheme, octaethylheme, and tetraphenylheme.

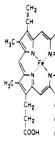

protohem

Fe^{IV}(N
Ferryl

Fe^{IV} (NM
(Solvent Sub

Fe^{III}-O-
μ-oxo d

Fe^{III}-O-O-Fe
μ-peroxo di

Figu

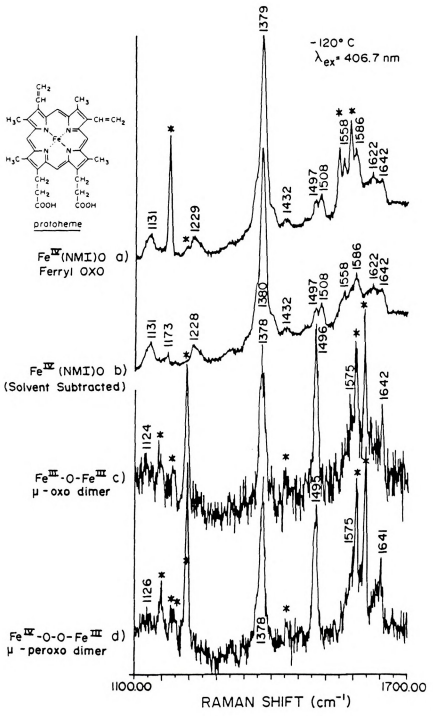

Figure 5.7 Raman spectra of ferryl oxo, μ-oxo dimer and μ-peroxo dimer of protoheme (high frequency region).

Table 5.3:

ASN	Fe (NM
ν_{10}	16
$\nu(C=C)^2$	16
$\nu(C=C)^1$	-
ν_{37}	16
ν_{19}	15
ν_2	15
ν_{11}	15
ν_{38}	15
ν_3	15
ν_{28}	146
$\delta(=CH_2)^1$	143
ν_{29}	140
ν_{20}	139
ν_4	137
$\delta(=CH_2)^2$	134
ν_{21}	130
$\nu_5 + \nu_9$	126
ν_{13}	123
$\nu(C_b\text{-}C_a)$	116
$\nu_6 + \nu_8$	113
ν_{32}	112
$\delta(=CH_2)$	108
$\gamma(CH=)$	100
ν_{45}	997
$\nu_{32}+\nu_{35}$	972
ν_{46}	951
$\gamma(C_m\text{-}H)$	845
$\nu(Fe=O)$	-
ν_6	804
ν_{32}	791
ν_{16}	749
ν_{47}	714
$\gamma(CH=)$	?
ν_7	677
ν_{48}	-
$\nu(Fe\text{-}O_2)$	605
ν_{49}	-
Pyr Fold	561
Pyr Fold	510
Pyr Fold	495
Pyr Fold	425
$\delta(C_bC_aC_\beta)$	419
$2(\nu_{35})$	380

Table 5.3: Raman Peaks of Iron PPIX Protein and Model Species.

	!---------PPIX----------!								
ASN	[a] Fe^{III} $(NMI)_2$	Fe^{III} O^{-2}	Fe^{III} O_2^{-2}	Fe^{IV} NMI,O^{-2}	[b] Mb^{IV} O^{-2}	[c] HRP II	[d] CcP ES	[e] Mb^{II} O_2	[f] HRP^{II} O_2
ν_{10}	1640	1642	1641	1642	1642	1635	1641	1640	1639
$\nu(C=C)^2$	1620	~1630	~1633	1622	1623	1630	1624	1623	1636
$\nu(C=C)^1$	-	1616?	-	-	-	1619	-	-	-
ν_{37}	1602	?	?	?	1606	1603	1605	1606	1601
ν_{19}	1586	?	?	?	?	1585	?	1587	1583
ν_2	1579	1575	1574	1586/ 1575	1589	1582	~1583	1583	1581
ν_{11}	1562	1563?	?	1558	1568	1562	?	~1563	1563
ν_{38}	1554	?	?	?	1550	1563	?	~1548	~1543
ν_3	1502	1496	1495	1508/ 1497	1513	1507	1509	1505	1506
ν_{28}	1469	1474?	1465?	1476?	-	-	-	-	-
$\delta(=CH_2)^1$	1435	1430?	?	1433	-	1432	1431	-	1429
ν_{29}	1402	~1398	?	~1397	1408	1400	?	1401	1401
ν_{20}	1399	~1398?	?	~1406	-	1406	?	-	-
ν_4	1373	~1378	~1377	~1380/ 1365	1381	1378	1378	1375	1377
$\delta(=CH_2)^2$	1346	1339	1337	1344	-	1341	?	1342	?
ν_{21}	1306	1307	?	1307	-	1311	?	1305	?
$\nu_5 + \nu_9$	1260	1241	?	1244	1235?	-	?	-	1246?
ν_{13}	1230	?	?	1228	1225	1239	1228	1225	1234?
$\nu(C_b\text{-}C_\alpha)$	1167	?	~1174	1173	1176?	1176	1177	1173	1179
$\nu_6 + \nu_8$	1130	1132	1132	1134	1139	~1136?	~1128?	-	1133?
ν_{32}	1125	?	?	~1125	1125	~1136?	~1128?	1133	1133?
$\delta(=CH_2)$	1089	?	?	?	-	?	?	1088?	?
$\gamma(CH=)$	1008	?	?	?	-	1008	?	-	?
ν_{45}	997	?	?	?	-	992	?	-	?
$\nu_{32}+\nu_{35}$	972	973	?	?	-	-	?	-	?
ν_{46}	951	?	~937?	?	927	933	?	-	?
$\gamma(C_m\text{-}H)$	845	823?	856?	?	834?	828?	835?	-	?
$\nu(Fe=O)$	-	-	-	820	797	774	767	-	-
ν_6	804	?	810	?	-	810	~803?	-	~805
ν_{32}	791	?	?	791	798	-	~803?	-	?
ν_{16}	749	?	?	752	757	757	~753	755	750
ν_{47}	714	?	?	?	718	717	~718	~713	714
$\gamma(CH=)$	?	?	?	?	690	691	?	-	690
ν_7	677	678	679	677	678	680	679	~677	679
	-	-	-	-	-	-	-	621	631
ν_{48}	605	~610	?	?	-	591	?	591	589
$\nu(Fe\text{-}O_2)$	-	-	-	-	-	-	-	570	562
ν_{49}	561	?	?	?	-	-	?	?	?
Pyr Fold	510	?	?	?	-	-	?	-	-
Pyr Fold	495	494	491	~495	-	-	?	?	?
Pyr Fold	425	428	430	447?	441	432	?	~428	440/422
$\delta(C_bC_\alpha C_\beta)$	419	?	?	422	414	399?	405	411?	408?
$2(\nu_{35})$	380	~374	?	380	381	366?	377	374	383

Table 5.3 (

!--

ASN	Fe (NM
	-
ν_8	3
$\delta(C_bC_\alpha C_\beta)$	3
$\gamma(C_m\text{-}C_\alpha)$	2
ν_9	2
Pyr Tilt	-
	2
	?

a. Choi, S.
b. Stiter et
c. Terner an
(1986a).
d. Hashimoto
e. Van Wart
f. Van Wart
(unpublis
-, peak not
?, peak not
assignmen

Table 5.3 (cont'd.).

	!---------PPIX----------!								
ASN	[a] $Fe^{III}(NMI)_2$	$Fe^{III}O^{-2}$	$Fe^{III}O_2^{-2}$	Fe^{IV} NMI,O^{-2}	[b] $Mb^{IV}O^{-2}$	[c] HRP II	[d] CcP ES	[e] $Mb^{II}O_2$	[f] $HRP^{II}O_2$
	-	-	-	-	362	366?	-	-	-
ν_8	349	~337	?	353	343	323?	341	342	344
$\delta(C_bC_\alpha C_\beta)$	312	?	?	?	?	?	?	309	?
$\gamma(C_m\text{-}C_a)$	296	?	297	?	?	?	?	?	289?
ν_9	276	?	?	271	?	274	287?	276	289?
Pyr Tilt	-	~253	255?	?	255	260	257	256	254
	236	?	?	?	?	?	247?	231	235
	?	?	?	?	?	?	?	218	219

a. Choi, S. and Spiro (1983), Choi et al. (1982).
b. Stiter et al. (1985a).
c. Terner and Reed (1984), Terner et al. (1985), Hashimoto et al. (1986a).
d. Hashimoto et al. (1986b).
e. Van Wart and Zimmer (1985), Spiro and Strekas (1974).
f. Van Wart and Zimmer (1985), R. T. Kean and W. A. Oertling (unpublished results).
-, peak not reported or not identified.
?, peak not reported, impossible to identify with signal to noise, or assignment uncertain.

nearly ide

electronic

species is

the laser

any variati

samples, we

conditions

the correct

the Raman p

species of

ferric proto

Choi and Spi

ferric bis-N

indicated ex

excess of NM

toluene. Othe

previously re

wavenumbers h

In Figure

(8a) and four-

solvent subtra

(Figure 5.8b)

(~1506 cm^{-1}) f

inhomogeneity.

precursor to t

unusually high

nearly identical. It is not clear whether this is reflective of similar electronic structures of the two species or whether the μ-peroxo species is photo unstable and rapidly decomposes to a μ-oxo species in the laser beam (see Hashimoto et al., 1986c). Since we do not observe any variation of the spectrum with time, even in quick scans with fresh samples, we believe that the μ-peroxo heme is stable under the conditions used for data collection and that the former explanation is the correct one. The above results are listed in Table 5.3 along with the Raman peaks of some previously reported ferryl oxo and ferrous oxy species of protoheme containing proteins. Raman data for bis-imidazole ferric protoheme (Callahan and Babcock, 1981; Choi et al., 1982; and Choi and Spiro, 1983) are also listed for comparison. Raman spectra of ferric bis-NMI protoheme samples at -120 C in toluene/NMI (not shown) indicated extensive photoreduction. This may be linked to the large excess of NMI required to induce complete conversion to low-spin in toluene. Otherwise, these spectra exhibited peaks comparable to those previously reported, although some of the peaks were shifted a few wavenumbers higher at the low temperature.

In Figure 5.8, the high frequency Raman spectra of the ferryl oxo (8a) and four-coordinate ferrous (8c) OEP samples are presented. A solvent subtracted spectrum of ferryl oxo FeOEP is also included (Figure 5.8b) for clarity. The splitting of ν_4 ($\tilde{}$1380 cm^{-1}) and ν_3 ($\tilde{}$1506 cm^{-1}) for the ferryl oxo sample are indicative of sample inhomogeneity. The four-coordinate ferrous species is a synthetic precursor to the ferryl oxo species. It is included here because of the unusually high value of ν_3 (1515 cm^{-1}) it displays, which is similar to

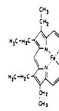

OCTAETH

Fe^{III}(N

Ferryl

Fe^{III}(NM

(Solvent Subs

Fe^{II}

Ferrous 4-coo

Figu

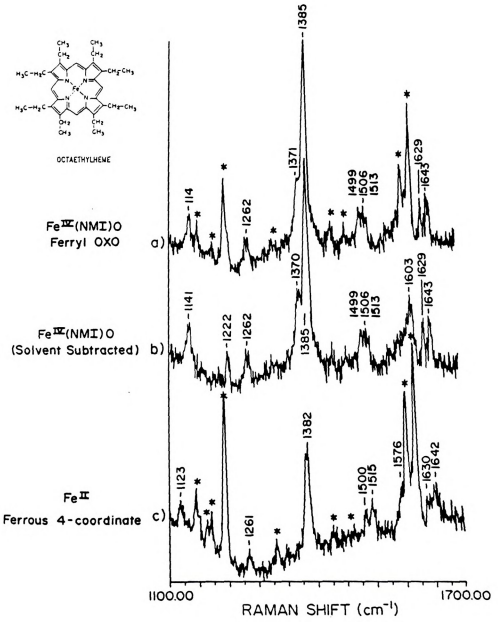

Figure 5.8 Raman spectra of ferryl oxo and four-coordinate ferrous octaethylheme (high frequency region).

a shoulder

possible re

below. Thes

Figure 5.9,

ferryl oxo

cannot be c

contain β s

frequently

TPP results

We have ther

from previou

The Raman pe

of ferryl μ-

which indica

This is in c

5.4), reporte

peak positio

+4.

D. DISCUSSI

In Table

ferrous oxy s

reported in t

ferrous oxy P

other, we see

groups. The fi

between 415 an

a shoulder observed in the ν_3 region of the ferryl oxo spectrum. The possible relationship between these two spectra will be discussed below. These FeOEP Raman results are also included in Table 5.2. In Figure 5.9, the high frequency Raman spectrum (-120 C) is shown for the ferryl oxo FeTPP sample. Although the Raman spectra of TPP species cannot be compared directly with those of protein species (which contain β substituted porphyrins), TPP type porphyrins have been frequently used for the construction of enzyme models and the ferryl TPP results are interesting in relation to these other model species. We have therefore listed our results in Table 5.4 along with results from previously reported Raman studies of some TPP type heme species. The Raman peaks positions for the ferryl oxo model are similar to those of ferryl μ-carbido TPP species reported by Crisanti et al. (1984), which indicates that the iron is essentially in the +4 oxidation state. This is in contrast to the five-coordinate ferryl oxo species (Table 5.4), reported by Proniewicz et al. (1986), which has different Raman peak positions and has been assigned an oxidation state of greater than +4.

D. DISCUSSION

In Table 5.5, we have tabulated the optical absorption peaks of the ferrous oxy species of several heme proteins which have been previously reported in the literature. By comparing these values with that of the ferrous oxy PPIX model (also included in this table) and with each other, we see that they seem to fall naturally into three different groups. The first group resembles the model compound with Soret maxima between 415 and 419 nm, β-bands clustered around 541 nm and α-bands at

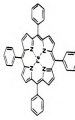

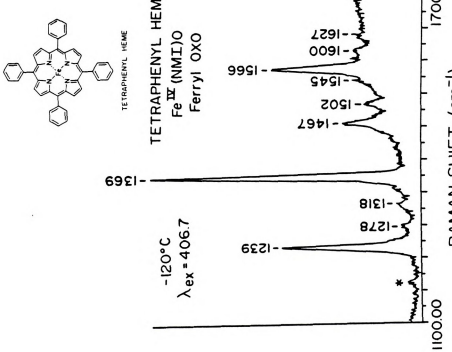

Figure 5.9 Raman spectrum of ferryl oxo tetraphenylheme (high frequency region).

Table 5.4

	a Asn
Phenyl	
$\nu(C_a\text{-}C_m)$	
$\nu(C_b\text{-}C_b)$	
$\nu(C_a\text{-}C_m)$	
$\nu(C_b\text{-}C_b)$	
$\nu(C_a\text{-}C_b)$	
$\nu(C_a\text{-}N)$	
$\nu(C_a\text{-}C_b)$ + $\delta(C_b\text{-}H)$	
$\nu(C_a\text{-}N)$	
$\nu(C_m\text{-}Ph)$	
$\nu(C_m\text{-}Ph)$	
$\nu(O\text{-}O)$	
$\delta(C_b\text{-}H)$	
$\delta(C_{Ph}\text{-}H)$	
$\delta(C_b\text{-}H)$	
$\nu(C_a\text{-}C_b)$	
Phenyl	
Phenyl	
$\nu(Fe\text{=}O)$	
Porp def	
$\nu(Fe\text{-}O_2)$	
Porp def	

a. Burke et al
p = polariz

Table 5.4: Raman Peaks of Various TPP Type Heme Species.

		!----------TPP----------!				!-------TpivPP---------!		
a Asn	a #	Fe^{III} (IM)$_2$[a]	Fe^{III} (NMI)$_2$	Fe^{IV} (NMI)O^{-2}	Fe^{IV} O^{-2}[b]	Fe^{III} (IM)$_2$[a]	Fe^{II} (NMI)O$_2$[a]	Fe^{II} ($C_6HF_4S^-$)O$_2$[c]
		1611	1627p					
Phenyl	1	1605	1601	1600p	~1600	1609	1065	
$\nu(C_a\text{-}C_m)$	2	1582	1584	1585dp				
$\nu(C_b\text{-}C_b)$	3	1568	1561	1566p	1575	1565	1565	1566
$\nu(C_a\text{-}C_m)$	4	1540	1549	1545?				
$\nu(C_b\text{-}C_b)$	5	1505	1501	1502dp		1510	1503	1502
			1476	1479dp				
$\nu(C_a\text{-}C_b)$	6	1456	1454	1467/ 1456		1470		
			1425	1436?				
$\nu(C_a\text{-N})$	7	1370	1367	1369	1374	1366	1366	1366
			1358					
$\nu(C_a\text{-}C_b)$	8	1340		1318?	~1350?	1340		
+ $\delta(C_b\text{-H})$			1304	1302	~1300			
$\nu(C_a\text{-N})$	9	1275	1267	1278			1280	
$\nu(C_m\text{-Ph})$	10	1238	1231	1239	~1230	1258	1257	1253
$\nu(C_m\text{-Ph})$	12					1210p	1208	1208
ν(O-O)								1140
	12a		1120? 1112			1115	1104	
$\delta(C_b\text{-H})$	13	1084	1079	1082	~1090	1085	1078	1073
$\delta(C_{Ph}\text{-H})$	14	1029	1025	1035		1020dp		
$\delta(C_b\text{-H})$	15			1019dp				
$\nu(C_a\text{-}C_b)$	16	1009	994	1007	~1010	1005	1003	
Phenyl	17			995				
			945					
Phenyl	18	890	885	889dp	~890	895	889	
	19		852	852dp				
ν(Fe=O)				820	852			
	20			783				
			734	739p				
			671	673?				
Porp def	21	643	640	640p			642	640
			597	575p	~580			615?
$\nu(Fe\text{-}O_2)$							568	
			494?					
			454?	455?				
	22	398						
Porp def	23	390	392	392p	392	390	384	379
	24							
	25	336	336	340p				
			297					298
	26	232	~230					
	27	204	203	187p?				

a. Burke et al. (1978) b. Proniewicz et al. (1986) c. Chottard (1984)
p = polarized, dp = depolarized

Table 5.5

Species
Ferrous Ox
normal:
Fe^{II}PPIX(N
MbO_2
HbO_2
oxy HRP (M
oxy IN 2,3
LiP cmpII
red-shifte
BPO cmpII
LPO cmpII
IPO cmpII
CPO cmpIII
cyt's P-45C
cyt P-450
cyt P-450
Ferryl Oxo
normal:
Fe^{IV}PPIXDME
Mb^{IV}=0
Hb^{IV}=0
Leg Hb^{IV}=0
HPP II
LiP II
CCP II
red-shifted
BPO II
LPO II
IPO II
CPO II
RMC II

abbreviation
IN 2,3,D, in
Hb, human he
BPO, bromope
CPO, chlorop
Cyt P-450 lm
RMC, bacteri
<, >, or = r

Table 5.5: Optical Absorption Peaks of Protoheme Containing Ferrous Oxy and Ferryl Oxo Species.

Species	Soret	β,α	Reference
Ferrous Oxy series:			
normal:			
$Fe^{II}PPIX(NMI)O_2$	415	540=574	This work and Brinigar and Chang (1974)
MbO_2	418	542<580	Makinen and Churg (1983)
HbO_2	415	541<577	Antonini and Brunori (1971)
oxy HRP (MPIII)	418	541>574	Wittenberg et al. (1967)
oxy IN 2,3,D	415	541<576	Sono (1986)
LiP cmpIII	419	543>578	Renganathan and Gold (1986)
red-shifted:			
BPO cmpIII	424	552>588	Manthey and Hagar (1985)
LPO cmpIII	428	551=590	Kimara and Yamazaki (1979)
IPO cmpIII	430	553>590	Kimara and Yamazaki (1979)
CPO cmpIII	432	555>586	Nakajima et al. (1985)
cyt's P-450:			
cyt P-450 cam	418	555	Peterson et al. (1972)
cyt P-450 lm	418	555	Oprian et al. (1983)
Ferryl Oxo Series:			
normal:			
$Fe^{IV}PPIXDME(NMI)O$	416	542,555=584	This work
$Mb^{IV}=O$	420	550<580	George and Irvine (1952)
$Hb^{IV}=O$	418	545>575	Dalzial and O'Brian (1954)
Leg $Hb^{IV}=O$	418	545>575	Aviram et al. (1978)
HPP II	418	527=553	Blumberg et al. (1968)
LiP II	420	525<556	Renganathan and Gold (1986)
CCP II	419	529<561	Yonetani (1965)
red-shifted:			
BPO II	433	534>564	Manthey and Hager (1985)
LPO II	433	537>568	Kimura and Yamazaki (1979)
IPO II	436	538>565	Kimura and Yamazaki (1979)
CPO II	438	542>571	Nakajima et al. (1975)
BMC II	428	530<568	Theorell and Ehrenberg (1952)

abbreviations:
IN 2,3,D, indoleamine 2,3-dioxygenase; Mb, sperm whale myoglobin; Hb, human hemoglobin; Lip, lignin peroxide; LPO, lacto peroxidase; BPO, bromopenoxidase; IPO, intestine (hog) peroxidase; CPO, chloroperoxidase; Cyt P-450 cam, cytochrome P-450 camphor; Cyt P-450 lm, cytochrome P-450 liver microsomal BMC, bacterial catalase; II, compound II.
<, >, or = reflect relative intensities of the absorption bands.

~577 nm. T

their simi

general re

region fro

and they a

group is t

hemes but

compare the

oxo protein

spectra sim

and to the

more red sh

the globins

5.5) have So

bands are bl

~red-shifted

relative to

(Soret red s

observations

differences b

manifested in

spectra of th

difference fr

(redox state

porphyrin, an

globins and t

the ~red shift

~577 nm. We shall designate these as "normal" heme proteins because of their similarity to the simple model. The next group represents a general red shift relative to the normal hemes, with Soret peaks in the region from 424 to 432 nm, β-bands at ~553 nm and α-bands at ~588 nm and they are therefore designated as "red shifted" hemes. The final group is the cytochromes P-450 which have a Soret band like the normal hemes but exhibit only a single band in the β/α region at 555 nm. If we compare these observations with the data for the corresponding ferryl oxo protein species, we see that only the ferryl globin species have spectra similar to the ferryl oxo PPIXDME model (also in this table) and to the ferrous oxy compounds. The ferryl oxo model, however, has more red shifted β- and α-bands and a blue-shifted Soret relative to the globins. The ferryl oxo species of the "normal" peroxidases (Table 5.5) have Soret bands similar to the ferryl model but the β- and α-bands are blue shifted relative to the model. The ferryl species of the "red-shifted" peroxidases still exhibit a red shifted optical spectrum relative to the "normal" peroxidases but demonstrate mixed behavior (Soret red shift, β/α blue shift) relative to the model. The above observations suggest the following: 1) there are environmental differences between the globins and the peroxidases which are manifested in the ferryl oxo but not the ferrous oxy species, 2) the spectra of the "red shifted" peroxidases display a fairly constant difference from the normal peroxidases (~10 nm) which suggests an iron (redox state and/or axial ligand) independent perturbation to the porphyrin, and 3) the cytochromes P-450 are distinct from both the globins and the peroxidases. Bacterial catalase seems to fall in with the "red shifted" peroxidases but its behavior is also distinct, with a

larger se

than the

of the ir

reference

perturbati

macrocycle

are not st

as other m

nature of

after the

Upon co

Table 5.2 a

six-coordin

most of the

electron de

similar in t

on the iron

the spectrum

oxo species

appears to c

the four coo

impurity comm

any Fe^{II} spec

oxygen even a

is that this

six-coordinat

larger separation of the β- and α-bands and a Soret at lower wavelength than the "red shifted" peroxidases. Due to the interaction and mixing of the iron orbitals and the porphyrin orbitals (Adar, 1978, and references within), the observed optical spectra are sensitive to small perturbations of both the iron environment and to the porphyrin macrocycle. For this reason, interpretation of changes in heme spectra are not straightforward and they do not usually follow the same trends as other metalloporphyrins. Further discussion as to the possible nature of these different heme environments will be reserved until after the discussion of the Raman results.

Upon comparison of the Raman peaks for the various FeOEP species in Table 5.2 a strong homology is seen for the Fe^{III} bis-NMI, ferrous oxy, six-coordinate ferryl oxo, and five-coordinate ferryl oxo species in most of the characteristic marker bands. This implies that the net electron density on the metal, as experienced by the porphyrin, is very similar in these four species even though the formal oxidation states on the iron vary in the range of ~+2 to ~+4. It is also evident in both the spectrum and listed peak positions that the six-coordinate ferryl oxo species is not homogeneous. This is clear in the ν_3 region which appears to contain contributions from both μ-oxo (or peroxo) dimer and the four coordinate Fe^{II} species. The μ-oxo dimer contamination is an impurity common to the synthetic procedure but it is unexpected that any Fe^{II} species should remain, since it reacts very quickly with oxygen even at these low temperatures. The most reasonable explanation is that this is the immediate product of the photoreduction of the six-coordinate ferryl species. Photoreduction has been proposed as the

mechanism
(Stillman
protoheme
strong re
and ν_4 se
Fe^{III} to
species in
negligible
the Raman
demonstrat
oxy and fe
occurrence
place of th
perturbatio
light of th
the differe
porphyrin c

The freq
Table 5.6 fo
protein samp
show only mi
trend in ν(F
myoglobin sa
compounds, we
sensitivity t
$\nu(Fe^{IV}=O)$ for

mechanism for light induced decay of heme protein ferryl species (Stillman et al., 1975). Similar results are demonstrated for the protoheme species (Table 5.3). The ferryl oxo model species bears a strong resemblance to the ferryl oxo protein species. Although ν_2, ν_3, and ν_4 seem to exhibit a general increase in frequency in the series Fe^{III} to ferrous oxy to ferryl oxo, differences between individual species in these latter two groupings are fairly subtle and may be negligible within the variability of sample preparations. Comparison of the Raman data of various FeTPP type model compound (Table 5.4) again demonstrates the spectral similarities of the ferric bis-NMI, ferrous oxy and ferryl oxo species, with the interesting addition that even the occurrence of a trans thiolate ligand (cytochrome P-450 model), in place of the NMI (Chottard et al., 1984), produces only small perturbations in the porphyrin modes. This trend is interesting in light of the large variations of the Fe-ligand (axial) vibrations in the different systems and it indicates only a small perturbation in the porphyrin core size.

The frequencies of these iron-ligand vibrations are summarized in Table 5.6 for various ferrous oxy and ferryl oxo model compound and protein samples. The frequencies for $\nu(Fe^{II}\text{-}O_2)$ in the model systems show only minor variations with porphyrin ring substituents. A similar trend in $\nu(Fe^{II}\text{-}O_2)$ was also observed by Tsubaki et al. (1980) by using myoglobin samples reconstituted with different hemes. With the model compounds, we do observe some sensitivity to solvent and a large sensitivity to axial ligation. The same trend is observed with $\nu(Fe^{IV}\text{=}O)$ for the ferryl oxo model compounds; little variation of

TABLE 5.6: Comparison of Iron-Oxygen Stretching Frequencies for Various Ferrous Oxy and Ferryl Oxo Species.

Species[a]	$\nu(Fe^{II}-O_2)$[b]	Reference
Ferrous Oxy Series:		
HRP III	562	Van Wart and Zimmer (1985)
Hb-O_2	567	Brunner (1974)
Mb-O_2	572	Tsubaki et al. (1980)
(NMI)Fe^{II}-O_2 (OEP)	573[c]	This work
(NMI)Fe^{II}-O_2 (OEP)	572[d]	This work
(NMI)Fe^{II}-O_2 (PPIX)	573[c]	This work
(NMI)Fe^{II}-O_2 (Heme a)	576[c]	This work
(NMI)Fe^{II}-O_2 (TpivPP)	571[e]	Kerr et al. (1983)
(1,2MI)Fe^{II}-O_2 (TpivPP)	562[e]	Kerr et al. (1983)
(NMI)Fe^{II}-O_2 (TpivPP)	567[f]	Walters et al. (1980)
(1,2MI)Fe^{II}-O_2 (TpivPP)	558[f]	Walters et al. (1980)
Ferryl Oxo Series:		
Species[a]	$\nu(Fe^{IV}=O)$[b]	Reference
HRP II pH 6.0	776	Sitter et al. (1985b)
HRP II pH 7.0	775	Hashimoto et al. (1986a)
HRP II pH 10.0	788	Sitter et al. (1985b)
HRP II pH 11.2	787	Hashimoto et al. (1984)
HRP X	788	Sitter et al. (1986)
CcP ES	767	Hashimoto et al. (1986b)
Mb^{IV}=O	797	Sitter et al. (1985a)
Fe^{IV}=O (TMP)	843	Hashimoto et al. (1986c)
Fe^{IV}=O (TPP)	852	Bajdor and Nakamoto (1984)
Fe^{IV}=O (OEP)	852	Bajdor and Nakamoto (1984)
(THF)Fe^{IV}=O (TpivPP)	829	Schappacher et al. (1986)
(NMI)Fe^{IV}=O (TpivPP)	807	Schappacher et al. (1986)
(NMI)Fe^{IV}=O (PPIXDME)	820	This work & Kean et al.(1987)
(NMI)Fe^{IV}=O (TPP)	820	This work & Kean et al.(1987)
(NMI)Fe^{IV}=O (OEP)	820	This work & Kean et al.(1987)

[a] Abbreviations: HRP II, horseradish peroxidase compound II; CcP ES, cytochrome c peroxidase compound ES; Mb, myoglobin; TMP,tetramesitylporphyrin; TPP, tetraphenylporphyrin; OEP,octaethylporphyrin; THF,tetrahydrofuran; NMI, 1-methylimidazole; TpivPP, 'picket fence' porphyrin [tetra(o-pivaloylphenyl)porphyrin]; PPIXDME, protoporphyrin IX dimethyl ester.
1,2MI, 1,2 dimethyl imidazole
[b] Frequency in cm^{-1}.
[c] in dimethylformamide -120 C
[d] in CH_2Cl_2 -120 C
[e] in benzene RT
[f] solid state 25 C

frequency occurs with variation of porphyrin substituents, but this frequency is sensitive to solvent and axial ligation. Extrapolating these model results to those of the protein species, we propose that the frequencies of $\nu(Fe^{II}\text{-}O_2)$ and $\nu(Fe^{IV}\text{=}O)$ are influenced primarily by out-of-plane effects and are fairly insensitive to direct interaction between the protein residues and the porphyrin macrocycle. This is useful in that these oxygen ligands (oxy and oxo) can be considered as sensitive probes of out-of-plane environmental factors. Variations in the iron-ligand stretching frequencies between the various model and protein species should allow us to identify differences in trans ligand strength, trans ligand strain, and hydrogen bonding in the different species. In contrast, the optical absorption spectra are very sensitive to direct perturbations of the macrocycle but relatively insensitive to perturbations of the iron environment except to the extent that these perturbations change the net electron density on the iron center. In addition, the optical spectra are sensitive to changes in the electronic excited states while the Raman spectra reflect only ground state structure. As such, changes in the optical absorption spectra may be sensitive indicators of direct interaction of the protein with the porphyrin macrocycle.

The oxo ligand is both a strong σ-donor and π-donor. It is expected that the binding of electron donating ligands trans to it will compete with it and weaken the bond (Buchler et al., 1978; Kerr et al., 1983; Gersonde et al., 1986). This trans ligand effect is demonstrated by the ferryl oxo model compounds. The five-coordinate models display the highest $\nu(Fe^{IV}\text{=}O)$ frequency, while the strong ligand (NMI),

six-coordinate samples display the lowest frequency. A crystal structure of the (THF)Fe^{IV}=O (TpivPP) structure indicates that the iron is displaced slightly out of plane toward the oxygen (~.13 A) (Schappacher et al., 1985). It is expected that five-coordinate species display a larger displacement and the presence of a strong sixth ligand will hold the iron more in plane. With the iron in plane, greater π-interaction may occur between iron and porphyrin orbitals, along with a weakening of the Fe^{IV}=O π-bond (Sitter et al., 1985a). For the NMI ligated six-coordinate complexes, the difference in the $\nu(Fe^{IV}=O)$ frequency of our models (in toluene) versus the TpivPP species (in THF) (Schappacher et al., 1986) appears to result from solvent effects since temperature and ring substituent effects were ruled out above. This may reflect stronger imidazole binding in the more polar and non-aromatic THF. Higher concentrations of NMI are needed to form the bis-NMI complex in toluene versus most other solvents. This may indicate that the solvation by toluene hinders the NMI binding and perhaps leads to weaker overall binding, which would be consistent with the above data. Results by Sitter et al. (1985a) indicate that, for ferryl myoglobin, hydrogen bonding to the distal histidine is probably not involved (at pH 6 or above). If we rule out hydrogen bonding, the lower $\nu(Fe^{IV}=O)$ frequency of ferryl myoglobin probably indicates stronger imidazole ligation in myoglobin than in the model compounds. Since the imidazole is protein bound in myoglobin it may be fixed in a more strongly ligating configuration than free solution models.

For HRP II samples, hydrogen bonding effects have been clearly demonstrated. An increase in the $\nu(Fe^{IV}=O)$ frequency, from 776 cm^{-1} to

789 cm^{-1} has been associated with the deprotonation of a distal residue (probably histidine) and a loss of catalytic activity (Sitter et al., 1985b). This non-hydrogen bonded frequency is still lower than that for ferryl myoglobin and may reflect some hydrogen bonding to a second residue or more likely, stronger proximal histidine (His) ligation in HRP than for myoglobin. Since the Fe^{IV}-His stretching frequency has not been established in these ferryl oxo species, we estimate the relative ligand strengths by comparison of the reported Fe^{II}-His frequencies for the five-coordinate ferrous species (see Table 5.7). These values are consistently higher in the peroxidase species than in the globin species. It has not been established whether this trend also applies to the relative ferryl oxo species but this assumption is consistent with the observed values of $\nu(Fe^{IV}=O)$ for the various ferryl oxo species. The ferryl oxo species of CcP appears to be hydrogen bonded at all observed values of pH and displays a $\nu(Fe^{IV}=O)$ frequency still lower than that of HRP II (Hashimoto et al., 1986b). Since the non-hydrogen bonded species has not been observed, it is unclear as to whether the lower frequency is due to stronger hydrogen bonding or stronger trans ligation. Since the $\nu(Fe^{II}$-His) of the ferrous CcP protein is very close to that of HRP, and the hydrogen bonded ferryl complex is stable even at pH 11, we suspect that the lower frequency in this case is due to strong hydrogen bonding. Data on the ferryl frequencies of additional peroxidases will be necessary to establish whether our model and assumptions are valid.

Extensive research has been done with the aim of understanding the factors which influence the affinity of O_2 for ferrous heme species and

the strength of the resulting Fe^{II}-O_2 bond. Studies by Chang and Traylor (1975), Traylor et al. (1981) and Collman et al. (1983) indicate that oxygen binding affinity is a function of trans axial ligation, porphyrin ring substituents, hydrogen bonding and solvent/environment polarity owing to the influence of these variables on the oxygen off rate. Steric constraints have only a small affect (Traylor et al., 1985) on the affinity of both CO and O_2. In contrast, the strength of the Fe^{II}-O_2 bond, as determined by $\nu(Fe^{II}\text{-}O_2)$, seems to be independent of porphyrin ring substituents and only weakly dependent on solvent/environment polarity. Steric constraints have been shown to increase the $\nu(Fe^{II}\text{-}CO)$ frequency for CO bound hemes, primarily through a decrease in the effective mass (Yu et al., 1983). Although no similar studies have been reported with bound O_2, the preferred bent binding geometry of O_2 (Loew, 1983, and references within) is likely to minimize any steric effects. Although binding affinity, and binding strength may both be affected by trans axial ligation and hydrogen bonding, it seems evident the binding strength is an independent characteristic which is one component of the overall molecular stability and the remainder of the discussion will focus only on this.

The interpretation of the variations of $\nu(Fe^{II}\text{-}O_2)$ for the ferrous oxy species is more complicated than that of $\nu(Fe^{IV}\text{=}O)$ for the ferryl oxo species. Not only does it exhibit behavior different from that of the ferryl oxo species, but in many cases, it exhibits behavior different from that of the very similar $\nu(Fe^{II}\text{-}CO)$. Increased steric constraint on the trans imidazole ligand (weaker ligation) decreases the frequency of $\nu(Fe^{II}\text{-}O_2)$ in the model compounds, while this same

weakening of the trans ligand causes the $\nu(Fe^{II}\text{-}CO)$ to increase (Kerr et al., 1983). On the other hand, the $\nu(Fe^{II}\text{-}O_2)$ frequency of ferrous oxy HRP (HRP III) is lower than that for ferrous oxy myoglobin (Van Wart and Zimmer, 1985) and the model compounds even though it presumably has stronger ligation and less strain. This is in apparent contradiction to the first trend. Since the binding of O_2 and CO to hemes is of great importance in the study of heme proteins, several researchers have addressed the binding behavior described above. Kitagawa et al. (1975) discussed the relative strengths of π-interactions between iron, porphyrin, and axial ligand orbitals. Kerr et al. (1983) have discussed the different behavior of heme O_2 and CO binding strengths, when trans ligand strain is involved, in terms of a fine balance of σ- and π-bonding interactions. Van Wart and Zimmer (1985) specifically discussed the behavior of oxy HRP (see below), but also noted possible inconsistencies with some of the model compound results.

Although the above mentioned works have been invaluable in the characterization of heme oxygen binding properties, none have been able to account for all the observed behavior. We believe that this behavior can be explained by consideration of the many different factors involved in O_2 binding strength. O_2 is a poor σ-donor due to its high electronegativity and poorer overlap (than CO) with the iron orbitals (Loew, 1983). It appears that the majority of the bonding interaction may occur through the π-overlap and calculations indicate a net delocalization ($\tilde{}0.1\ e^-$) of electron density onto the oxygen from the iron (Loew, 1983, and references within). CO can form stable

five-coordinate low-spin species with ferrous hemes (Kerr et al., 1983) with no apparent structural perturbation relative to their six-coordinate counterparts. In contrast to this, studies with five-coordinate ferrous oxy hemes (Watanabe et al., 1984) indicate a possible intermediate spin species with a distorted and/or side on binding structure. This behavior supports the idea that σ-donation by O_2, along the Z axis, is significantly weaker than that of CO and it is insufficient to induce a full low-spin configuration. With CO bound hemes the presence of σ-donor or π-acceptor trans to the CO will compete with the CO and reduce the bond strength (trans effect). For O_2 bound hemes, a trans σ-donor may actually stabilize the oxy complex by pushing the d_z^2 orbital higher in energy (stabilizing the low-spin configuration) and compensating for the charge delocalized from the Fe to the O_2. The result is partial (Fe^{+III}-O_2^-) ionic character which favors strong trans ligand binding in addition to the strong Fe^{II}-O_2 binding. Note that the reported increase in ν(Fe-His) from 220 cm^{-1} to 271 cm^{-1} for deoxy and oxy myoglobin respectively (Spiro, 1983) is consistent with this picture. This explanation may account for the behavior, mentioned above, that was observed with ferrous oxy and CO model species having sterically constrained trans ligands. For the ferrous CO complexes, the Fe remains close to the heme plane and the $\nu(Fe^{II}$-CO) frequency increases as expected for a weakening of the trans ligand. For ferrous oxy complexes, the iron moves out of plane toward the trans base (Jameson et al., 1980). The resulting Fe^{II}-O_2 bond is weakened (presumably by repulsion from porphyrin orbitals) but overall the complex is more stable due to this unique trans ligand stabilization of O_2 ligated hemes. Myoglobin, like many heme proteins,

binds CO in a bent geometry (Norvell et al., 1975) owing to protein steric constraints on the distal side of the heme. In contrast, CO binds in a linear geometry in the free solution models (Peng and Ibers, 1976). Since the $\nu(Fe^{II}\text{-}O_2)$ frequencies of the corresponding oxy complexes are nearly identical (oxymyoglobin 572 cm^{-1}, oxy models 572 cm^{-1}), we do not expect that steric constraints are a major factor in the determination of the $\nu(Fe^{II}\text{-}O_2)$ frequency in proteins.

Under conditions of no trans ligand strain and strong trans σ-donation, a weakening of the $Fe\text{-}O_2$ bond could presumably occur, similar to the effects observed with ferrous CO and ferryl oxo species. This model has been invoked to explain the lower $\nu(Fe\text{-}O_2)$ for HRP III than for oxy Mb (562 vs 570 cm^{-1}) (Van Wart and Zimmer, 1985) while the $\nu(Fe^{II}\text{-His})$ is higher for HRP in the respective deoxy complexes (244 vs 220 cm^{-1}). Although this may be the correct explanation for the observed result, we offer an alternate possibility. Crystal structures of CcP indicate the presence of an arginine residue within hydrogen bonding range of a heme bound peroxide molecule (Poulos and Kraut, 1980). Even with the shorter bond length of O_2 versus peroxide ($\tilde{}$1.2 A vs. $\tilde{}$1.5 A), this residue should be capable of hydrogen bonding to the terminal oxygen atom of heme bound O_2. Sequence studies confirm that this arginine residue is conserved in HRP and all the other sequenced plant peroxidases indicating that this hydrogen bonding is also possible in HRP. This hydrogen bonding would be expected to increase the amount of electron delocalization from the Fe onto the oxygen which would ordinarily increase the bond strength and the corresponding stretching frequency. However it is also possible that this hydrogen

bonding could distort the binding geometry or increase the effective reduced mass which would lead to lowering of the observed $\nu(Fe^{II}\text{-}O_2)$ frequency. Studies of CO binding to various heme proteins suggest that the terminal oxygen of CO is strongly hydrogen bonded in peroxidases relative to globin species (Smith et al., 1984). The similar size of O_2 to CO and its greater electronegativity make bound O_2 equally or more likely to participate in hydrogen bonding in these peroxidases. More Raman data from different ferrous oxy peroxidase species may be needed to confirm this hypothesis.

Cobalt substituted porphyrins have been popular in oxygen binding studies as models for hemes (see Nakamoto and Oshio, 1985, and references within). However, the additional electron of Cobalt (II), relative to iron (II), represents a serious perturbation relative to the iron system. Calculations indicate that this additional electron is delocalized onto the bound oxygen to produce a formal $(Co^{III}\text{-}O_2^-)$ species (Newton and Hall, 1984), which results in a Raman active $\nu(O\text{-}O)$ vibration (Bajdor et al., 1983). Although these Co porphyrins are poor models for imidazole ligated hemes, they appear to be excellent models for thiolate ligated hemes, such as cyt P-450. The Raman observation of $\nu(O\text{-}O)$ for thiolate ligated hemes (Chottard et al., 1984), and the detection of $\nu(O\text{-}O)$ by Champion et al. (1986) for oxy cyt $P\text{-}450_{cam}$ indicate an extensive delocalization of the thiolate electron onto the trans O_2 like that observed with the Co porphyrins. This represents a substantially different trans ligand effect from that observed with imidazole ligation, but as mentioned above, it also has little affect on the porphyrin modes.

From the Raman results presented above, we suggest that the observed $\nu(Fe^{II}-O_2)$ and $\nu(Fe^{IV}=O)$ frequencies can serve as sensitive indicators of trans ligand strength (proximal ligand) and hydrogen bonding effects (distal side). The connection between these vibrational frequencies and the the optical absorption properties of these oxy and ferryl heme proteins and model compounds, however, is not obvious. There does not seem to be any direct correlation of the optical absorption properties with the nature or strength of the proximal ligand. For LPO and IPO, "red-shifted" peroxidases, imidazole proximal ligands have been identified and the ligand strength does not seem to be significantly different from those of the "normal" peroxidases (see Table 5.7). As shown by EXAFS studies (Dawson et al., 1986), CPO (also "red shifted") appears to contain a thiolate trans ligand identical to that of the cytochromes P-450. Despite the fact that many of its ligand bound complexes have optical properties similar to the cytochrome P-450 analogues (Sono et al., 1986), the ferrous oxy and ferryl oxo species of CPO are distinctly characteristic of a peroxidase (see Table 5.5) and different from cytochrome P-450. These observations suggest that some of the differences in optical absorption spectra of the different heme proteins are due to factors other than axial ligand effects.

Possible sources of these non-ligand effects have already been reported. Choi et al. (1982) have suggested protein induced electrostatic fields near the protoheme vinyl groups to explain differences in the resonance Raman spectra of myoglobin species relative to solution models. Shelnutt (1983) observed that the optical absorption spectra of hemes were red shifted (3-5 nm) by π-π

Table 5.7: Iron-Histidine Stretching Frequencies of Five-Coordinate Ferrous Hemes.

Species	$\nu(Fe^{II}$-His)	Reference
Cyt Ox (Bovine Heart)	214	Salmeen et al. (1978)
Deoxy HbA	216	Nagai et al. (1980)
Deoyx Mb	220	Kitagawa et al. (1979)
CcP (alkaline)	234	Hashimoto et al. (1986b)
HRP-C (alkaline)	241	Teraoka & Kitagawa (1981)
HPR-C (acid)	244	"
HPR-A_2 (alkaline)	246	"
CcP (acid)	247	Hashimoto et al. (1986b)
HRP-A_2 (acid)	252	Teraoka & Kitagawa (1981)
IP	254	Kimura et al. (1981)
LP	258	Hashimoto et al. (1986b)
	$\nu(Fe^{II}$-IM)	
Fe^{II}OEP 2MI	205	Nagai et al. (1980)
Fe^{II}TpivPP 2MI	209	Hori & Kitagawa (1980)
Fe^{II}TpivPP NMI	225	"

Abbreviations: CyT Ox, cytochrome c oxidase; HbA, Hemolgobin a; IP, Hog intestine peroxidase; LP, lactoperoxidase; 2 MI, 2-methylimidazole; His, Histidine imidazole; Im, generic imidazole species.

interaction of the porphyrin with neutral aromatic compounds in solution. The presence of cationic aromatic compounds resulted in a blue shift of the visible bands but a red shift of the Soret. π-π interactions with both types of compounds also resulted in small (less than 3 cm^{-1}) shifts in some of the high frequency Raman peaks which were in opposite directions for the neutral and cationic compounds. Desbois et al. (1984) have used resonance Raman spectroscopy, in conjunction with X-ray crystallographic results, to analyze the orientation and environment of the protoheme vinyl substituents in various globin and "normal" peroxidase species. Their results suggest that the vinyl groups of the peroxidases are more in plane with the heme than in the globins and that they probably undergo strong π-π interaction with aromatic amino acid residues. This allows these vinyl groups to have greater electron withdrawing ability and it provides a means for protein regulation of the π-electron density on the heme. Interaction of the porphyrin ring propionyl substituents with protein residues was also implicated in this study. Studies with CcP (Shelnutt et al., 1983) and HRP (Shelnutt et al., 1986) on the pH dependence of ν_4 indicate that π-charge donation from the protein to the porphyrin ring is maximal at the pH of maximal activity (pH 8) and that this behavior may serve to stabilize the ferryl species of compounds I and II during enzyme turnover. Based on these results, we speculate that some of the observed optical absorption differences between heme enzymes are due to the interaction of the porphyrin macrcycle and/or vinyl substituents with aromatic and/or charged protein amino acid residues. This variable π-charge detected for different states of the "normal" peroxidases may account for the differentiation of the optical

spectra of globins and normal peroxidases, upon going from the ferrous oxy species to the respective ferryl oxo species. Alternately, it could reflect a slight change in heme conformation which affects the interaction of the protein with the heme. Other specific protein-heme interactions may be responsible for the different optical absorption properties of the "red shifted" peroxidases and the cytochromes P-450 and that these same factors may influence the specific catalytic reactivity of these different enzymes. Differences in the high frequency Raman spectra of these different heme proteins (see Table 5.3) are consistent with different protein effects, but owing to the small changes expected, comparison should be made under more carefully controlled conditions before interpretation of these differences is attempted.

In conclusion, we have used resonance Raman and optical absorption spectroscopies for the characterization of ferrous oxy and ferryl oxo heme model compounds. Of particular interest to us was the identification of the axial ligand vibrations, $\nu(Fe^{II}-O_2)$ for the oxy and $\nu(Fe^{IV}=O)$ for the oxo species, in the Raman spectra. These out-of-plane ligand vibrations seem to be little affected by direct perturbations to the porphyrin ring in the model compounds. Comparison of these results with those of several previously observed ferrous oxy and ferryl oxo heme protein species suggests that these vibrational frequencies can serve as indicators of trans ligand strength and hydrogen bonding in the various protein species. Although interaction between the protein and porphyrin ring may have important functions in the regulation of catalytic reactivity and specificity, and appear to

have significant effects on the optical absorption spectra of the heme protein species, these effects do not seem to influence the iron-ligand bonds. This suggests two means of catalytic control in heme proteins: direct perturbation of axial ligation, and π-interaction or other direct protein perturbations of the porphyrin ring. The coupled actions of both these effects may account for the diversity and specificity of heme protein functions.

CHAPTER 6

RESONANCE RAMAN SPECTROSCOPY OF CYTOCHROME OXIDASE "PSEUDO-INTERMEDIATES"

A. INTRODUCTION

To avoid the generation of toxic oxygen radical species through single electron donation to dioxygen, cytochrome oxidase catalyzes dioxygen reduction via a pair of two-electron steps. Resolution of the intermediates present at various levels of dioxygen reduction has been generally accomplished through the application of flow-flask methods developed by Gibson and Greenwood (1965) and of triple-trapping techniques introduced by Chance et al. (1975). The oxidase intermediate, termed Compound C, that is present at the two-electron reduction level of dioxygen is currently characterized as a Cu^{+2}-peroxide- cytochrome a_3 complex with Soret band absorbance maximum at 428 nm and difference spectrum absorbance maximum in the alpha band at 607 nm. Generation of Compound C by the tight reversible binding of hydrogen peroxide to the cytochrome a_3 metal center of resting or pulsed oxidase was subsequently demonstrated by Bicker et al. (1982). These results made possible the characterization of the oxidase species at the half reduced dioxygen stage, and further clarification of the distinctions between pulsed and resting forms of the enzyme.

Closely linked to Compound C formation is a second oxidase intermediate with enhanced optical features in the 580/537 nm range. As

with Compound C this complex has been observed under a variety of conditions including: a) the product of Compound C incubation in excess peroxide (Wrigglesworth, 1984); b) oxidase in high potential poised mitochondrial membranes (Wikstrom, 1981, Ereciska and Chance, 1972); c) addition of mM peroxide concentrations to pulsed or resting enzyme (Chance et al., 1983); and d) single turnover experiments of three-electron reduced oxidase at low and room temperatures (Witt et al., 1986). The formation of the 580/537 nm species has thus been shown under a variety of conditions to result from the decay of Compound C in solubilized oxidase as well as oxidase in whole mitochondria. Recent chemical and magnetic data further show that the 580/537 nm optical properties in oxidase correspond to the presence of a proposed Fe^{+4}=0 Cu^{+2} EPR silent species (Blair et al., 1985, Witt et al., 1986). It is proposed (Witt, et al., 1986) that while Compound C is oxidase at the two-electron reduction stage of dioxygen, the 580/537 nm species represents the intermediate resulting from the one electron reduction of Compound C.

Partial characterizations of the various oxidase reactive intermediates have been accomplished through a wide variety of spectroscopic techniques. Resonance Raman and Magnetic Circular Dichroism spectroscopy have proven extremely useful in investigating the spin and oxidation states of intermediates of even spin (Woodruff et al., 1982). However, application of resonance Raman spectroscopy of cytochrome oxidase is often complicated by photoreduction of oxidase with Soret band excitation (Bocian et al., 1979). In light of the rapid photodecomposition of Compound C (vide infra) uncertainty has arisen

concerning the RR spectra reported for Compound C and various "oxygenated" species of oxidase. I present here the resonance Raman spectra of the 580/537 nm species, Compound C, pulsed enzyme, and three cytochrome oxidase species previously uncharacterized by Raman spectroscopy. Low temperature-spinning cell techniques were used to minimize the decomposition of the various intermediates. These spectra are discussed in terms of the structures which have been proposed for these species.

B. MATERIALS AND METHODS

The samples of cytochrome oxidase were prepared by Stephan Witt (California Institute of Technology) as described elsewhere (Blair et al, 1983; Blair et al., 1985; and Witt et al., 1986) and the procedures are briefly summarized as follows. Resting cytochrome C oxidase was prepared by the method of Hartzell and Beinert (1974). Pulsed enzyme was prepared by the addition of oxygen to stoichiometrically reduced (with ascorbate) cytochrome oxidase. Compound C was produced by two different methods. The first method utilizes the reaction of O_2 with mixed valence (half reduced) CO bound oxidase. The second method involved the addition of one equivalent of H_2O_2 to the pulsed enzyme. Both of these samples should be at the level of peroxide bound fully oxidized enzyme. The 580 nm species is prepared by the addition of excess (~10 fold) H_2O_2 to the pulsed enzyme. CO was added to some of the 580 nm species to produce a CO reacted species. The reoxidized sample was produced by the addition of O_2 and PPD (2,5 diphenyl, 1,3,4 oxadiazole) to the reduced enzyme. All samples were made in a phosphate buffer (pH 7.4) with Tween-20 as a detergent to solubilize he enzyme.

Sample concentrations were ~0.02 mM for optical absorption measurements and Raman spectroscopy of liquid samples. Frozen Raman samples were ~0.15 mM in concentration. Samples of the 580 nm and Compound C are estimated to be ~60% pure. The CO reacted and the reoxidized samples are expected to be less homogeneous than the 580 nm and Compound C samples but the compositions could not be accurately determined.

All optical absorption spectra were recorded with a Perkin-Elmer Lambda 5 UV/Visible spectrophotometer which contained a house built low temperature optical dewar. The samples were contained in EPR tubes which were cooled to the desired temperature (normally 4 C) by flowing cold nitrogen gas. Raman spectra were recorded on a Spex 1401 scanning monochromator with an RCA 31034 C PMT detector by using ~3 mW incident power (unless otherwise noted) at 406.7 nm (Spectra-Physics model 164 Kr ion laser). Spectra were collected for liquid samples in a chilled spinning cuvette (~0 C) which utilized a 90 degree scattering geometry. Spectra were also obtained for frozen samples (contained in EPR tubes), which were spun continuously in a Dewar while the desired temperature (~-120 C) was maintained by flowing cold nitrogen gas. This low temperature system utilizes a backscattering geometry (~170 degrees). Data collection time varied with each sample and is noted individually in the figures. None of the spectra were smoothed but for some a linear sloping background was subtracted as indicated. The distorted baselines in some spectra are the result of subtracting a linear background from spectra which suffered from large non-linear fluorescence backgrounds. Alternate background subtractions (not shown) were also performed to confirm that no artifacts were introduced by this process. The poor

signal-to-noise ratios of the Raman spectra are due to the fluorescence background and the inherently poor Raman scattering from frozen aqueous solutions. Raman experiments attempted with ~600 nm excitation on the frozen samples were not successful owing to the large background fluorescence, poor resonance enhancement at this wavelength, and power instability of the laser. Experiments with liquid samples were only attempted with 406.7 nm excitation. Dr. John Manthey (California Institute of Technology) assisted in the data collection and preliminary analysis of these results. Jose Centeno assisted in the assignment of some of the Raman peaks.

C. RESULTS

Resonance Raman spectra of resting enzyme, in both liquid (~0 C) and frozen (-100 C) states, are shown in Figures 6.1a and 6.1b. The use of 25 mW incident power induced extensive photoreduction in both samples as demomstrated by the dominant peaks at 1610 and 1622 cm^{-1} (Babcock et al., 1981). By varying the laser power, we determined that it was necessary to use incident laser power of ~5 mW or less to avoid photoreduction under our experimental conditions. All subsequent samples were run at these lower powers. The dramatic differences in the Raman spectra of these photoreduced samples can be seen by comparison of Figure 6.1 with spectra of the other species which are described below. The Raman peaks of the frozen photoreduced sample, and the peak assignments, are listed in Table 6.1, along with those of the samples described below. For comparison, peak positions and assignments for the Raman spectra of heme a model compounds are listed in Table 6.2.

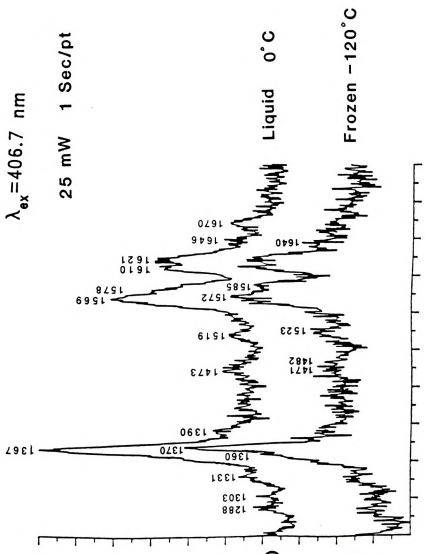

Figure 6.1 High frequency spectra of photoreduced cytochrome oxidase samples (liquid and frozen).

Table 6.1: Distinguishing Characteristics and Raman Peaks of Frozen Cytochrome Oxidase Species.

Distinguishing Characteristics							
	Resting	Photo-reduced	Pulsed	Cmpd C	580 nm	580 nm +CO	Re-oxidized
Optical	424		424	428	428		
(nm)	655		606	607	537,580		
EPR			g=5				rhombic
a_3 site							Cu_B, LS Fe^{II}
Soret Excitation Raman Peaks (cm^{-1}) (frozen samples)							
Assignment	Resting	Photo-reduced	Pulsed	Cmpd C	580 nm	580 nm +CO	Re-oxidized
ν(C=O) a_3	1675	1672	1677	1675	1676	1676	1676
		1661					
ν_{10}(LS) +	1647	1640	1648	1650	1647	1650	1648
ν(C=O..H)			1645	1644		1647	
ν(C=C)a^{II}		1622					
?	1625			1628			1628
ν_{10}(HS) a_3	1612	1610	1616	1613		1613	1613
ν(C=O)a^{II}(LS)		1610					
$+\nu_{10}a_3^{II}$							
ν_2(LS)	1589	1585	1595	1594	1595	1594	1594
ν_2(HS) a_3	1575	1572	1573	1577		?1581	1570
?	1562	1551		1565	1562	1561	
ν_{11}	?1511	1523	?1520	?1519			?1517
ν_3(LS)	1504		1504	1506	1505	1505	1508
ν_3(HS) a_3		1482	1481	1488		1484	1482
ν_{28}	1472	1471	1472	1478	1479	1473	1474
?	1439	1440	1437	1436	1440	1442	1438
?	1395	1394	1397	1395	1395	1400	1399
ν_4	1372	1370	1375	1374	1377	1375	1374
		1360	1364				
?	1335	1327	1338	1338	1337	1335	1335
?	1303	1302	1310	1309	1309	1311	1308
?	1289	1284	1284	1291	1291	1291	1292
?	1246		1250	1249	1253	1253	1252
?	1225		1228	1225	1225	1230	1228

Assignments are based on those of Choi et al. (1983) and Babcock (1986) according to the scheme of Abe et al. (1978).
a = cytochrome a heme, a_3 = cytochrome a_3 heme
Note: Rows without labels are a continuation of the one above and indicate 2 peaks with the same assignment (i.e., a_3 and a or inhomogeneous samples).

Table 6.2: Raman Peaks of Heme a Model Compounds.[a]

	Fe^{II}		Fe^{III}		
ASN	6 Coord Low Spin	5 Coord High Spin	6 Coord Low Spin	6 Coord High Spin	5 Coord High Spin
ν(C=O)	1642	1660	1670	1672	1576
ν(C=O H)	1633	1640	1656	-	1656
ν(C=C)	1622	-	-	-	-
ν_{10}	-	1607	1642	1615	1632
ν_{37}	1605	1565?	-	-	-
ν_2	1587	1578	1590	1572	1581
ν_{19}	1583	-	-	-	-
$\nu_{38}(1)$	1563	-	-	-	1540
$\nu_{38}(2)$	-	-	-	-	1520
ν_{11}	1511	-	-	-	-
ν_3	1493	1473	1506	1482	1492
ν_{28}	1468	1455	1474	-	-
$\nu_{29/20}$	1391	1394	-	-	-
ν_4	1360	1357	1374	1373	1374
$\delta(=CH_2)$	1329	1333	-	-	-
ν_{21}	1307	1314	1312	-	-

[a]From Babcock (1986)

In Figure 6.2, the high frequency Raman spectra of non-photoreduced resting oxidase at 0 C (liquid) (6.2a) and -120 C (frozen) (6.2b) are displayed. The liquid spectrum is consistent with previously reported studies (Babcock et al., 1981; Woodruff et al., 1982; and Copeland et al. 1985). Peaks from both heme centers are observed but several of the peaks from the cytochrome $\underline{a}_3$ center (high-spin) are prominent. This is due to better resonance of the 406.7 nm exiting line with the the absorption band of the high-spin cytochrome $\underline{a}_3$ site than that of the low-spin heme in the cytochrome $\underline{a}$ site. The frozen sample retains many of these features but is overall poorer in quality owing to the higher background fluorescense at the lower temperature and the weaker Raman scattering from frozen aqueous solutions (relative to the analogous liquid samples). There are also some changes evident in the frozen sample. The band centered at 1648 cm^{-1}, which is a composite of several modes (Babcock 1986), is more symmetric and narrower than in the liquid sample, and the 1675 cm^{-1} peak, assigned to νCO of the heme $\underline{a}$ ring formyl group of cytochrome $\underline{a}_3$, is increased in intensity. The increase of intensity at 1589 cm^{-1} indicates increased scattering from a low-spin species. There is also a small increase of intensity at 1610, 1628, and ~1511 cm^{-1}. The nature of these changes will be discussed below. Despite the increased experimental difficulty, most of the details observed in the liquid spectrum are also resolved in the spectrum of the frozen sample and the peak positions are the same in the two spectra (except as noted above). For the frozen sample (2b), the peak positions and assignments are listed in Table 6.1.

In
restin
displa
studie
al. 19
peaks f
due to
absorpt
low-spi
of thes
backgro
scatter
liquid
sample.
modes (
sample,
formyl
of inter
low-spin
1628, an
below. D
details
spectrum
the two
the peak

In Figure 6.2, the high frequency Raman spectra of non-photoreduced resting oxidase at 0 C (liquid) (6.2a) and -120 C (frozen) (6.2b) are displayed. The liquid spectrum is consistent with previously reported studies (Babcock et al., 1981; Woodruff et al., 1982; and Copeland et al. 1985). Peaks from both heme centers are observed but several of the peaks from the cytochrome $\underline{a}_3$ center (high-spin) are prominent. This is due to better resonance of the 406.7 nm exiting line with the the absorption band of the high-spin cytochrome $\underline{a}_3$ site than that of the low-spin heme in the cytochrome $\underline{a}$ site. The frozen sample retains many of these features but is overall poorer in quality owing to the higher background fluorescense at the lower temperature and the weaker Raman scattering from frozen aqueous solutions (relative to the analogous liquid samples). There are also some changes evident in the frozen sample. The band centered at 1648 cm^{-1}, which is a composite of several modes (Babcock 1986), is more symmetric and narrower than in the liquid sample, and the 1675 cm^{-1} peak, assigned to νCO of the heme $\underline{a}$ ring formyl group of cytochrome $\underline{a}_3$, is increased in intensity. The increase of intensity at 1589 cm^{-1} indicates increased scattering from a low-spin species. There is also a small increase of intensity at 1610, 1628, and ~1511 cm^{-1}. The nature of these changes will be discussed below. Despite the increased experimental difficulty, most of the details observed in the liquid spectrum are also resolved in the spectrum of the frozen sample and the peak positions are the same in the two spectra (except as noted above). For the frozen sample (2b), the peak positions and assignments are listed in Table 6.1.

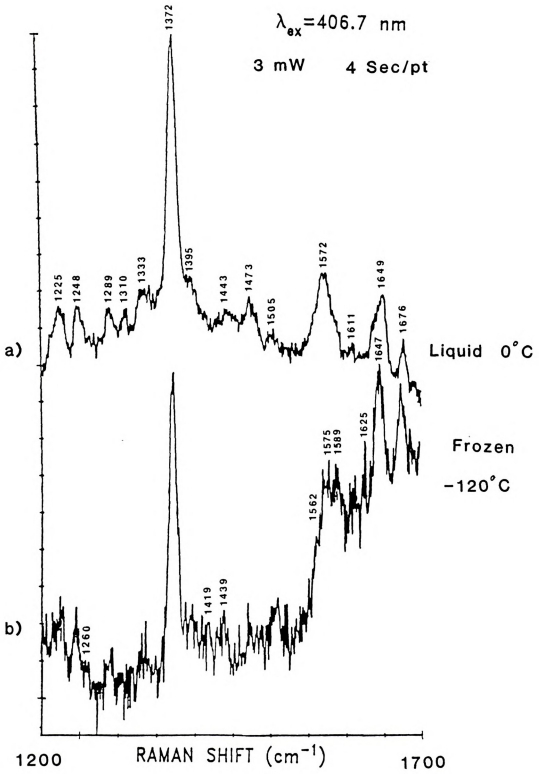

Figure 6.2 High frequency Raman spectra of resting cytochrome oxidase (liquid and frozen).

In Figure 6.3, the high frequency Raman data are shown for the species with 580 and 537 nm peaks in the absorption spectrum (580 nm species). Spectra 3a and 3b were obtained with liquid samples and spectrum 3c with a frozen sample. Spectrum 3a was obtained with a previously unirradiated sample. Spectrum 3b was obtained on the same sample after ~1 1/2 hours of laser irradiation. The initial scan (Figure 6.3a) shows a clear dominance of contributions by low-spin species. This is exemplified by the increased intensity at 1643 and 1589 cm^{-1} and the decreased intensity at ~1572 cm^{-1} which suggests a low spin heme in the cytochrome $\underline{a}_3$ site. The 1505 cm^{-1} peak is more intense than in the resting enzyme and ν_4 (~1374 cm^{-1}) is 2 cm^{-1} higher in frequency than in the resting enzyme. The laser irradiation greatly accelerates the decay of these samples which are ordinarily stable for several hours at 0 C. In addition, there is no evidence of photoreduction. By comparison with spectrum 3b, it is apparent that this sample decays with time into what appears to be the resting enzyme. In spectrum 3c (the frozen sample) there appears to be a complete conversion of the cytochrome $\underline{a}_3$ heme to low spin and the ν_4 frequency is 4 cm^{-1} higher than in the resting enzyme. Again, there is no evidence for photoreduction. In contrast to the liquid sample (3a), the frozen sample can be irradiated for a full day with no detectable change in the Raman spectrum. This indicates a dramatic increase in stability of this sample at the low temperature (-120 C). This observation, along with the more homogeneous appearance of the frozen sample spectrum, suggests that the spectrum observed for the liquid sample (3a) already displays substantial decay of the 580 species.

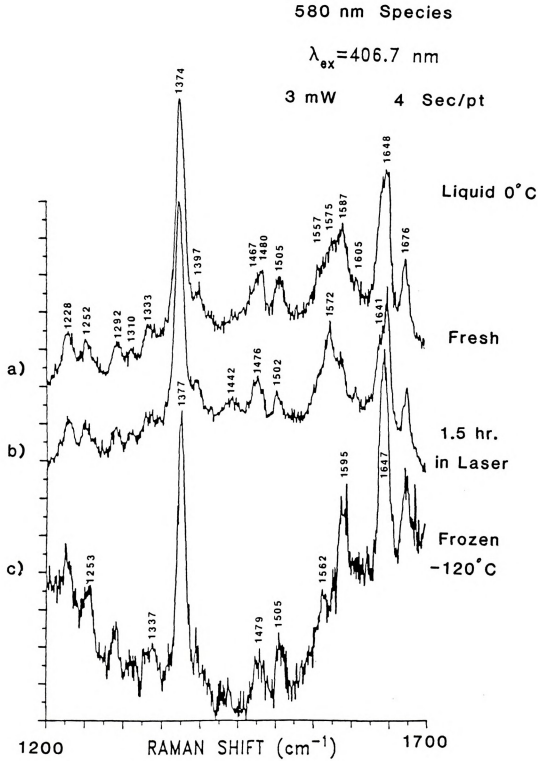

Figure 6.3 High frequency Raman spectra of 580 nm species of cytochrome oxidase (liquid and frozen).

Since the 580 nm species accounts for only about 60 % of the frozen sample, the percentage in the liquid sample must be significantly less.

Our Raman spectra of liquid samples of Compound C (not shown) displayed a strong resemblance to the spectrum of resting oxidase, but optical spectra taken after the scans showed significant sample degradation to a pulsed or resting species. This suggested fairly rapid decay of the liquid compound C samples in the laser beam, such as that which was observed for the 580 nm species. The compound C samples were therefore scanned at low temperature (frozen) to determine if they were more stable under these conditions. These spectra are displayed in Figure 6.4. Figure 6.4a shows the spectrum of compound C produced by the addition of O_2 to the mixed valence CO bound (MVCO) oxidase. The spectrum of compound C, produced by the addition of a stoichiometric amount of peroxide to the pulsed enzyme, is displayed in Figure 6.4b. Both of these samples should be at the level of peroxide bound fully oxidized enzyme. For comparison, the spectrum of pulsed enzyme is shown in Figure 6.4c. The Raman scattering from the pulsed and compound C species was extremely weak overall. In addition, the peaks characteristic of high-spin heme species were reduced in intensity or virtually absent but there were only small increases in the intensity of the peaks which are characteristic of low-spin heme species. Compound C samples produced by two different methods produced similar but not identical results. The pulsed plus peroxide sample (Figure 6.4b) seems to be more homogeneously low-spin (low intensity at 1577 cm^{-1}) and it displays broader features at ~1510 and 1675 cm^{-1} than the MVCO plus O_2 sample (4a). Both of these samples had Raman spectra

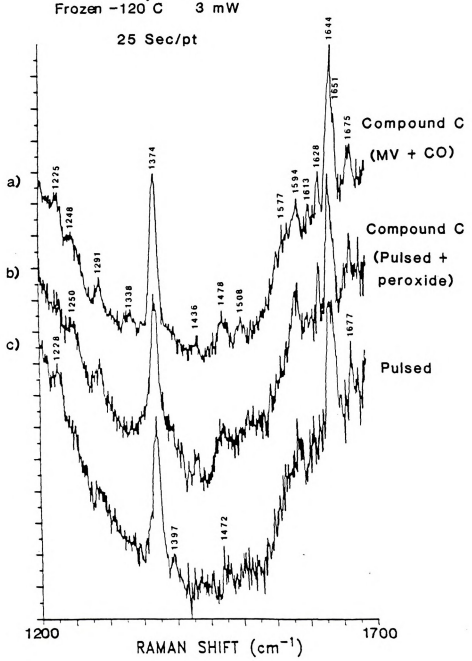

Figure 6.4 High frequency Raman spectra of frozen compound C cytochrome oxidase (MVCO + O_2 and pulsed plus peroxide) and pulsed cytochrome oxidase.

similar to that of the pulsed enzyme. However, the spectrum of the pulsed enzyme was noticeably weaker overall and it is distinguished by a broader band at ~1645 cm^{-1} and the absence of the 1628 cm^{-1} peak. All three of these spectra exhibit ν_4 at ~1374 cm^{-1}. Photoreduction does not appear to be appreciable in any of these three spectra.

Raman spectra of two other species of interest were obtained in the frozen state and these results are shown in Figures 6.5 and 6.6. The first of these is produced by chemical oxidation (PPD) of the enzyme during turnover conditions and it is distinguished by the detectability of Cu_B in the EPR spectrum (Witt et al., 1986). The Raman spectrum of this sample (Figure 6.5) is dominated by contributions from low-spin species (increased intensity at 1508, 1594, and 1648 cm^{-1}) indicating that the cytochrome $\underline{a}_3$ heme is probably low-spin in this sample. Overall it is a more strongly Raman scattering sample than the pulsed and compound C samples but not as strong as the 580 nm sample. The final sample is produced by the reaction of the 580 nm species with CO, which produces CO_2 and a ligated (O_2 or CO) ferrous heme species (Blair et al. 1985, Witt et al. 1986). This Raman spectrum (Figure 6.6) is almost indistinguishable from the spectrum of the starting material (the 580 nm species). However, in Figure 6.6, the spectrum displays increased intensity at ~1473 and ~1484 cm^{-1}, and ν_4 is at 1375 cm^{-1} in contrast to 1377 cm^{-1} for the 580 nm species.

Resonance Raman spectra were attempted for frozen samples (-120 C) of the resting, 580 nm species, compound C and pulsed samples in the low frequency region. The compound C and pulsed samples (not shown)

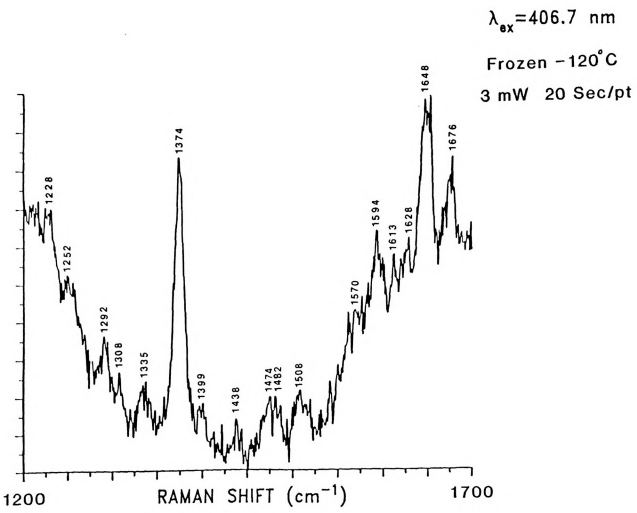

Figure 6.5 High frequency Raman spectrum of frozen "reoxidized" cytochrome oxidase.

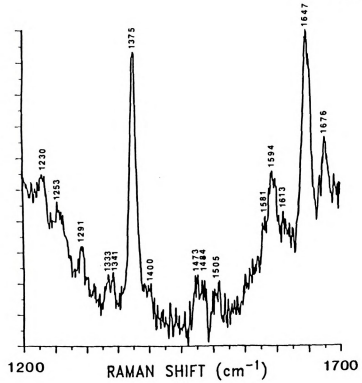

Figure 6.6 High frequency Raman spectrum of CO reacted 580 nm species of cytochrome oxidase.

displayed weak scattering and little detail. Spectra for the resting and 580 nm species exhibited stronger scattering and these results are shown in Figures 6.7, 6.8 and 6.9. Since the 580 nm species has been proposed to be a ferryl oxo species (Fe^{IV}=O), we examined samples made with ^{16}O and ^{18}O in an attempt to identify the (Fe^{IV}=O) stretching frequency via an isotope shift. The spectra of both isotopes obtained over the low and middle frequency ranges are shown in Figures 6.7 and 6.8. In Figure 6.7, we observe that ν_8 for the 580 nm species (347 cm^{-1}) is decreased in intensity and increased in frequency relative to the resting enzyme (341 cm^{-1}). In addition, the peak at 376 cm^{-1} (resting) is esentially absent for the 580 nm species and the 412 cm^{-1} peak is decreased in intensity with a slight increase of intensity at 422 cm^{-1}. The spectrum of the ^{18}O labeled 580 nm species (7c) is not identical to that at the ^{16}O labeled sample (7b) but none of the differences are reproducible. Overall, the spectrum of the ^{16}O sample most clearly displays the spectral characteristics that are reproducible and unique to the 580 nm species. The peak at ~491 cm^{-1} and the broad band centered at ~415 cm^{-1} are mostly due to scattering from the quartz EPR tube. In Figure 6.8, the spectra of ^{16}O and ^{18}O labeled 580 nm species are compared with each other and the spectrum of resting enzyme. Of the small differences observed between the two isotope species, the only one that is reproducible is the slightly higher intensity at 749 cm^{-1}. If this were the $\nu(Fe^{IV}=^{18}O)$ frequency, the corresponding $\nu(Fe^{IV}=^{16}O)$ frequency would be expected at ~785 cm^{-1} (~36 cm^{-1} higher). However the intensity at ~785 cm^{-1}, for the ^{16}O sample is not reproducibly higher and we must concede that we cannot yet assign a $\nu(Fe^{IV}$=O) peak. The most dramatic differences between the

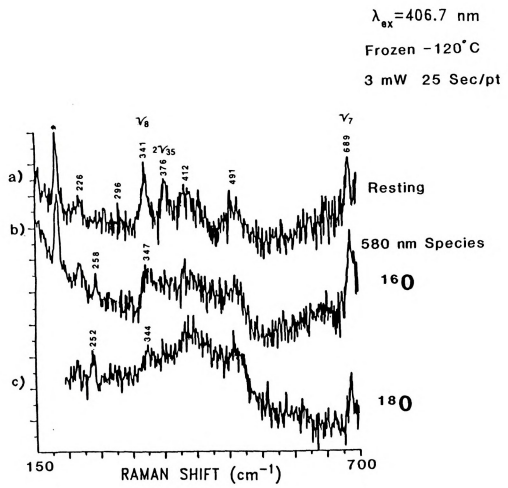

Figure 6.7 Low frequency Raman spectra of frozen resting and 580 nm (^{16}O and ^{18}O) cytochrome oxidase.

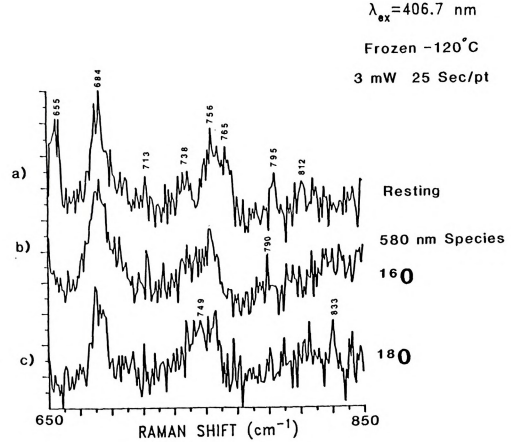

Figure 6.8 Intermediate frequency Raman spectra of frozen resting and 580 nm (^{16}O and ^{18}O) cytochrome oxidase.

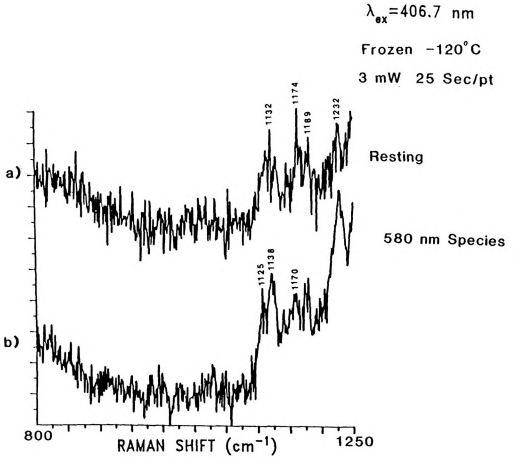

Figure 6.9 Upper-intermediate frequency Raman spectra of frozen resting and 580 nm (^{16}O and ^{18}O) cytochrome oxidase.

spectrum of the resting enzyme (8a) and those of the 580 nm species (8b,c) is a loss of intensity at 765 and 795 cm^{-1} for the 580 nm species and an increase of intensity at ~749 cm^{-1}. In Figure 6.9, we see an increase of intensity at 1138 and 1233 cm^{-1} for the 580 nm species (relative to the resting), as well as a decrease of intensity at ~1170 cm^{-1} and a downshifting of the 1132 cm^{-1} peak to 1125 cm^{-1}. The peaks observed in Figures 6.7 through 6.9 are summarized in Table 6.3.

D. DISCUSSION

The characteristic signs of photoreduction, as demonstrated in Figure 6.1, are the increase of intensity of the peaks at 1360, 1587, ~1520, 1610, and 1621 cm^{-1} and a loss of intensity of the ~1370, and 1676 cm^{-1} peaks and the ~1646 cm^{-1} band. The most dramatic of these changes is the intensity increase at 1610 and 1621 cm^{-1} and the loss of intensity at ~1646 cm^{-1}, and the onset of these characteristics were used as a criterion for the occurrence of photoreduction. Comparison of Figure 6.1a with Figure 6.1b demonstrates extensive photoreduction in both the frozen and liquid samples at high laser power (~25 mW). This is similar to results previously reported by Bocian et al. (1979) under similar conditions. Since the effects of photoreduction on the sample integrity of these various samples is not known, the laser power was lowered on all further samples (~3 mW) to minimize or eliminate this photoreduction. The similarities of the Raman spectra of liquid (0 C) and frozen (-120 C) resting oxidase, Figures 6.2a and 6.2b, assure us that freezing the solution does not cause any major perturbation of the heme environments in resting oxidase. Except for the 1550 to 1660 cm^{-1}

Table 6.3: Assignment of the Mid- and Low-Frequency Raman Peaks of Resting and 580 nm Species of Cytochrome Oxidase.

Assignment	Resting	580 nm Species
$\nu_{13}(a_3)$	1232	1232
?	1189	1188
ν_{30} or ν_{43}	1174	1170
$\nu_6 + \nu_8$	1138	1138
ν_{22}	1132	1125
$\nu_{32}(a_3)$	795	~792
?	765	
$\nu_{16}(a_3)$	756	~755
$\nu_{47}(a_3)$	738	~741
?	713	~716
?	700	~703
$\nu_7(a_3)$	~683	684
?	~650	~648
?(a_3)	420	422
*$\delta(C_b\text{-}C_\alpha\text{-}C_\beta)(a_3)$	412	-
$2(\nu_{35})$ or $\gamma(C_b\text{-}S)$	376	-
$\nu_8(a_3)$	341	347
?	~296	-
?	-	~258
?	226	227

* C_α, C_β are carbons on the vinyl substituent assignment scheme based on that of Abe and Kitagawa (1978).

region, there are no significant changes in peak positions in the frozen sample relative to the liquid sample. The increased intensity at 1589 cm^{-1} for the frozen sample would best be explained by the presence of low-spin heme species in the cytochrome $\underline{a}_3$ site. Since no exogenous strong field ligands are present in solution, these low-spin species would most likely be accounted for by accumulation of low-spin intermediate species during slow photoreductive turnover. Since this additional low-spin component is not detected by low temperature EPR or with magnetic susceptibility (Tweedle et al., 1978), it is unlikely that it represents a low temperature induced protein conformation or a thermal spin state equilibrium.

The spectrum of the 580 species exhibits strong Raman scattering and the peak positions and intensities are consistent only with a low-spin cytochrome $\underline{a}_3$ center. The higher frequency of ν_4 and the stronger ν_3 at 1506 cm^{-1} than low-spin ferric hemes is characteristic of a ferryl oxo species (Fe^{IV}=O) of a physiological type heme (Campbell et al., 1980; Terner & Reed, 1984; Hashimoto et al., 1986; Proniewicz et al., 1986; & Kean et al., 1987). Hydroxide ligation is capable of producing low-spin heme species (Beetlestone & George 1964, Yonetani et al. 1971); however, formation of this species would not be favorable under the experimental conditions used (pH 7.4). In addition, the position and intensity of ν_3 (1506 cm^{-1}) for the Raman spectrum of the 580 nm species are not consistent with that observed for hydroxy metmyoglobin (1479 cm^{-1}, Ozaki et al., 1976) and the EPR properties are not consistent with a Fe^{III}-OH species as discussed by Blair et al. (1985). Simple peroxide ligation cannot be ruled out since its ligation

characteristics are not well known, but it seems unlikely that this would be a strong enough ligand to induce this low spin conformation. The only other reasonable possibility, considering the lack of exogenous ligands in the system, is that the species is a ferrous oxy compound (Fe^{II}-O_2). The observed high frequency modes are consistent with those of other ferrous oxy heme proteins (see Van Wart & Zimmer, 1985 for example). They are also similar to high frequency modes (1374, 1585, and 1650 cm^{-1}) reported by Babcock et al. (1984) for a transient "oxy" species observed during the reaction of oxygen with reduced oxidase. Although an oxy species cannot be positively ruled out on the Raman data alone, the peroxide chemistry of hemes in peroxidase systems (Terner et al., 1985; Hashimoto et al., 1984), globin species (Sitter et al., 1985a), and model compounds (Bruice et al., 1986) are consistent in favoring the formation of a ferryl species when peroxide is present. Our results, like those discussed in Witt et al. (1986), are consistent with the assignment of the 580 nm species as an oxo ferryl heme. This same assignment has been proposed by Wikstrom (1981) as the result of studies with mitochondria poised in a highly oxidized state.

Attempts at conclusive identification of the 580 nm species as a ferryl oxo heme, through observation of the (Fe^{IV}=O) stretching frequency, were not successful since no oxygen isotope sensitive modes could be assigned (see Figure 6.8). This in itself is not significant since several factors could account for the absence of the this peak or the absence of an isotope shift. The mode may be weak like the $\nu(Fe^{IV}=O)$ peak of cytochrome c peroxidase compound ES which was

recently reported by Hashimoto et al. (1986a). Considering the poor signal to noise ratio in Figure 6.8 and the large number of heme modes in this region of the spectrum, the $\nu(Fe^{IV}=O)$ could easily be obscured. Oertling and Babcock (1987) have determined the excitation profile for the $\nu(Fe^{IV}=O)$ peak in horseradish peroxidase compound II with Soret region excitation and have established that the intensity of the $\nu(Fe^{IV}=O)$ exhibits a strong dependence on the excitation wavelength. If 406.7 nm is not near the maximum of the excitation profile for ferryl heme a, then the $\nu(Fe^{IV}=O)$ intensity may be weak and easily obscured. Excitation at wavelengths closer to the Soret maximum (428 nm) than 406.7 nm may be needed to observe this mode. It is possible that the ^{18}O labeled ferryl sample (580 nm species) undergoes a hydrogen bond mediated exchange with the predominantly ^{16}O of water. This behavior has been demonstrated with horseradish peroxidase compound II at neutral pH by Hashimoto et al. (1986b). It is also noted that the intensity of the $\nu(Fe^{IV}=O)$ peak decreases in intensity upon hydrogen bonding.

The 580 nm species is unstable at liquid temperatures and appears to revert to a resting or pulsed species under laser illumination at 0 C (Figure 6.3a,b). This is in contrast to the the results for the frozen sample which indicate that at a temperature of -120 C and with low laser power, no significant decomposition occurs in the course of a full day of laser irradiation. Like the spectrum in Figure 6.3a, previously reported spectra of species that may be the same as the 580 nm species (Woodruff et al., 1982, resting + H_2O_2; and Copeland et al., 1985, "420 nm" + H_2O_2) may also demonstrate significant decomposition

before it is identifiable by optical absorption measurements on the bulk sample. We believe that the use of low temperature (-120 C) frozen samples may allow more reliable Raman characterization of unstable species than previously used liquid samples techniques. In the discussion below, we will also compare our Raman spectra of frozen samples of pulsed and compound C species with those reported for liquid samples by the above mentioned authors. It is hoped that this will help bring a consensus to the field as to the identities of these different species and whether any of the previously reported samples suffer from any major decomposition or heterogeneity.

The pulsed form of oxidase (Soret 420 nm, 424 in our samples) was reported as distinct from resting oxidase and peroxide bound species by Kumar et al. (1984). The Raman spectrum of pulsed cytochrome oxidase has been previously shown, for liquid samples, (Copeland et al. 1985) to resemble that of resting oxidase. These results are contrasted by results from Woodruff et al. (1982) in which the spectrum of pulsed oxidase was quite different from the spectrum of the resting species. This difference was primarily manifested in an overall weakness of the spectrum and a distinct loss of intensity at ~1573 nm (high-spin a_3). Our Raman spectrum of the frozen pulsed enzyme (Figure 6.4c) displays the same trends observed in the results of Woodruff et al. (1982) There is evidence for only a small high-spin contribution (weak 1575 cm^{-1} peak) and the overall Raman scattering intensity is weak for this spectrum in comparison with those of the resting and 580 nm species. Since resonance Raman scattering is strongly dependent on the optical absorption spectrum, we examine the differences in optical absorption

properties between resting and pulsed. Three types of Soret optical absorption changes could account for this reduced scattering intensity: 1) broadening; 2) a decrease of the absorption intensity; or 3) red shifting (further off resonance). The Soret band is not any broader for the pulsed enzyme than the resting enzyme so the first possibility can be excluded. Although the Soret maximum is at approximately the same wavelength as that of the resting enzyme (~424 nm), the Soret band of pulsed enzyme is decreased in intensity and slightly skewed to the red relative to the resting enzyme. This decrease in the intensity of the Soret absorption and slight red shift could account for a decreased Raman scattering intensity and may explain the observed behavior although other factors may be involved too. Since changes in absorption properties often accompany changes in axial ligation (with oxidation state unchanged), the difference in Raman scattering (at low temperature) between the pulsed and resting forms of the enzyme is probably indicative of a difference in heme axial ligation (in the cytochrome $\underline{a}_3$ center) for the respective enzyme samples. A difference in ligation could account for the difference in reactivity and ligand binding rate observed by Brunori et al. (1979) for the pulsed enzyme relative to the resting enzyme. This idea is further supported by EXAFS studies of both the resting and pulsed (Chance et al. 1983) enzyme species. Woodruff et al. (1982) have interpreted the results of their Raman and magnetic circular dichroism (MCD) studies for the pulsed enzyme as indicative of magnetic coupling between an intermediate spin ferric heme, in the cytochrome $\underline{a}_3$ site, and the $Cu_{\underline{B}}$ center. Intermediate spin ferric heme models have been observed (Scheidt & Gouterman, 1983) in both five- and six-coordinated species with weak

axial ligation. The unusually weak iron-imidazole (proximal) bond in cytochrome *a*$_3$ ($\nu(Fe^{II}\text{-His})$, 214 cm^{-1}), as determined by Raman spectroscopy in the five-coordinate ferrous state (Van Steelandt-Frentrup et al., 1981; & Ogura et al., 1983), may be conducive to the formation of an intermediate spin species in the ferric state.

Compound C is postulated to be a species with peroxide bound to the heme of cytochrome *a*$_3$, possibly bridging to Cu_B (Chance & Leigh 1977). This species has been produced by two different methods, addition of O_2 to the half reduced (mixed valence) enzyme and direct binding of peroxide to the fully oxidized enzyme, which produce samples with nearly identical optical absorption spectra. In our Raman studies, however, we observed slight differences in the Raman spectra (~1510 and ~1570 cm^{-1} regions) of the compounds C produced by different different methods, MVCO + O_2 (Figure 6.4a) and pulsed + peroxide (Figure 6.4b). This suggests that they are two distinct species or that both samples contain the same compound C species but that they are heterogeneous and contain different impurities. We favor the latter explanation since the differences between these two samples are small and is not necessarily significant. Since these two samples are made by different methods, it would not be surprising for them to contain different contaminant species. Scattering is so weak from the compound C samples that small amounts of other species could readily alter the observed Raman spectra. The similarity of the spectra of the compound C species (4a,b) with that of the pulsed enzyme samples (4c) was also a source of concern. The two most likely interpretations of this similarity are: 1)

one of the samples rapidly photo-reacts into the other one on a time scale that is short in comparison to the data collection time, or 2) the two species share very similar heme structures. Because of the limited region of laser exposure on these frozen samples, it has not been possible to check the samples effectively by optical absorption spectroscopy after Raman data collection for a transition from one to another. The first possibility does not seem likely since the spectra of these frozen samples do not change significantly over a full day of scanning. This indicates a lack of significant turnover in these samples, which would suggest that they are distinct species. In addition, if the compound C sample is simply a peroxy bridged species as postulated, a one electron reduction of compound C should produce the ferryl species (580 nm), which seems resistant to photoreduction and exhibits a very strong Raman spectrum. It seems unlikely that compound C would photoreduce to the pulsed form without accumulation of detectable amounts of the ferryl species. This conclusion is consistent with the results of both Woodruff et al. (1982) and Copeland et al. (1985), who reported similarities between the Raman spectra of their pulsed and compound C (oxygenated) samples, yet identified them as different species (note that oxygenated oxidase should be the same species as our compound C which was produced by the addition of stoichiometric amounts of peroxide to the pulsed enzyme). The spectrum of oxygenated oxidase, reported by Babcock et al. (1981), also resembles the spectra of the compound C species reported by these other researchers, but it seems to exhibit a greater contribution from low spin hemes.

If we accept that compound C is distinct from the pulsed enzyme, the similarity of the low temperature Raman spectra of the compound C samples to those of the pulsed enzyme is surprising considering the difference in optical absorption spectra. The red shifted Soret band of the compound C samples (428 nm) relative to the resting and pulsed samples (424 nm) indicates a greater contribution from low-spin species. This would be expected to produce a Raman spectrum with stronger low-spin characteristics. This does occur to a limited extent but the effect is small in comparison to that observed for the 580 nm species which also has a Soret maximum at 428 nm. This observed behavior may indicate a mixture of high- and low-spin species or intermediate- and low-spin species in the cytochrome a_3 site of the compound C with both species only weakly scattering. Babcock et al. (1981) discuss the Raman, MCD, and EPR results of the oxygenated oxidase (compound C in our studies) as possibly due to the magnetic coupling of a low-spin heme to the Cu_B^{+2} in cytochrome a_3. Woodruff et al. (1982) conclude that compound C is also an intermediate-spin species (like the pulsed enzyme). The discussion of Copeland et al. (1985) asserts that the spectra of pulsed enzyme and compound C (oxygenated?) are similar and may reflect inhomogeneity or the presence of intermediate-spin ferric heme. They emphasize however that increased photoreduction of the pulsed sample indicates a protein conformation different from that of the compound C. Our final conclusion is that the pulsed and compound C species are different. It is likely that none of the spectra published to date for pulsed enzyme or compound C (including our own) represent scattering from a homogeneous sample and that sample-to-sample variations represent Raman signal from more

strongly scattering heme impurity species. If pulsed cytochrome oxidase is a non-ligand bound species, and compound C is the corresponding peroxide bound species, the peroxide apparently has little effect on the Raman properties of the heme and may reflect weak or disordered binding.

The Raman spectrum of the reoxidized enzyme (Figure 6.5) is dominated by contributions from low-spin species. This spectrum is similar to the spectrum of the 580 nm species, but it is not as strongly scattering and ν_4 is lower (1374 cm^{-1}). The sample is also distinguished from the 580 nm species, by its EPR properties, as noted above, and it has been postulated to be a ferrous oxy species (Fe^{II}-O_2) based on the EPR studies (Blair et al., 1985). The Raman results are consistent with a ferrous oxy species although the ferryl oxo or ferric hydroxy species should not be ruled out from the Raman data alone. Due to the method of preparation, the reoxidized cytochrome oxidase sample is not likely to be homogeneous and it may contain a variety of intermediate species. Fortunately, it is unlikely that any pulsed or compound C type species would be distinguished due to their weak Raman scattering. The observed Raman spectrum would therefore reflect the presence of at least moderate amounts of ferrous oxy or ferryl oxo species in this sample. Further identification cannot be made with the data available.

The reaction of the 580 nm species with CO is expected to yield an O_2 or CO ligated ferrous heme species (Witt et al., 1986). The observed Raman spectrum of this sample (Figure 6.6) demonstrates that the heme

of the cytochrome $\underline{a}_3$ site is predominantly low-spin which would seem to be consistent with either ligated species (O_2 or CO). However, experiments with a mixed valence CO bound sample (not shown) demonstrated that the CO undergoes extensive photolysis even when the laser power is lowered to ~2 mW. This was evident in the Raman spectrum by an overall weaker scattering and a shift of ν_2 to 1578 cm^{-1}, which is characteristic of ferrous five-coordinate high-spin heme $\underline{a}$. By analogy to the mixed valence CO bound species, a ferrous CO species would most likely photolyze and it would not account for the observed spectrum. We therefore conclude that the Raman spectrum of the CO reacted 580 nm species is most likely due to scattering from residual unreacted 580 nm species and/or scattering from an oxy ferrous species.

In conclusion, the study of cytochrome oxidase intermediates and related species has been hindered by a lack of common nomenclature and by confusion over the ligation and redox states of the metal centers in these different species. In an attempt to help clarify this situation, we have obtained low temperature resonance Raman spectra of what we believe to be six distinct cytochrome oxidase species: resting, pulsed, compound C, 580 nm, reoxidized, and 580 nm plus CO. These results suggest that the structures of the cytochrome $\underline{a}_3$ sites of pulsed oxidase and resting oxidase are different and that the spectral differences are best observed at low temperature. The low temperature Raman spectrum of compound C strongly resembles that of the pulsed sample. This may reflect a coincidental similarity in heme geometry and spin state in the two different species. The latter three species exhibit spectra characteristic of a low-spin heme in the cytochrome $\underline{a}_3$

site. The 580 nm form is assigned to a ferryl oxo species owing to the conditions of its formation and its reactivity with CO. The latter two samples are probably not homogeneous and the spectra may be dominated by contributions from ferrous oxy and ferryl oxo species.

CHAPTER 7

CONCLUSIONS AND FUTURE WORK

A. CONCLUSIONS

The goals of my research, as outlined in my second year research proposal, centered on the use of resonance Raman spectroscopy to elucidate the catalytic pathway and intermediate structures in the reduction of oxygen by cytochrome oxidase. The initial technical phase of this research has been completed in full. This included: 1) building hardware and writing software for the interfacing of our computer to our Raman spectrometer; 2) construction of optical Dewars and additional equipment to enable collection of low temperature optical absorption and Raman spectra; and 3) development of specific anaerobic procedures and equipment. Attempts to produce the low temperature trapped intermediates and collect Raman spectra (work in collaboration with Dr. Patricia Moroney) were not successful owing to the difficulty of sample preparation, inherent sample inhomogeneity, sample fluorescence and inexperience with the handling of and data collection from low temperature samples. At this point we realized that much more preliminary experimental work would be necessary before we could hope to do the experiments with these trapped intermediates. The direction of my project shifted from the strict enzyme work to one involving the use of model compounds. Synthetic procedures were available in the literature for a number of heme species which had structural characteristics similar to those proposed for the oxidase

intermediates. Only a few of these had been characterized by Raman spectoscopy. The Raman spectral studies of ferryl and oxy heme species (Chapter 5) was conducted to fill gaps in the existing literature. Our goal was to improve our understanding of the chemistry and biochemistry of these species and to be able to predict the spectroscopic properties that these species would demonstrate if they occurred in cytochrome oxidase. In parallel with this, W. Anthony Oertling was characterizing reaction intermediates of a variety of other heme enzymes which may have analogies with the chemistry of oxidase. The studies of cyanide binding to hemes in solution (Chapter 3) were initiated to try to understand the unusual Raman results from cyanide bound samples of one of these proteins.

Other studies were initiated even more closely related to oxidase. We entered into a collaboration with Dr. C. K. Chang which involved the characterization of a synthetic porphyrin species designed to model the oxygen reduction site of cytochrome oxidase (Chapter 4). My studies using resonance Raman, optical absorption, and EPR spectroscopies were complemented by the magnetic susceptibility and IR studies of M. S. Koo, the student who synthesized these compounds. These studies provided insights into the interactions of copper and iron (heme) atoms in close proximity and the effects of axial ligand variation on the spectroscopic properties. A final series of experiments, in collaboration with the research group of S. I. Chan (California Institute of Technology), utilized low temperature Raman spectroscopy to investigate a number of chemically induced "pseudo" intermediates of cytochrome oxidase (Chapter 6). These experiments provided experience

with data collection from low temperature samples, yet they were more stable, more homogeneous, and simpler to prepare than the cold trapped species. In this study, we characterized what appear to be a ferryl oxo, ferrous oxy and several ferric species of cytochrome oxidase. These experiments have reaffirmed that the chemistry of oxidase is complicated and that Raman spectroscopy will not easily provide unambiguous information about the structures of the cold trapped intermediates without good low frequency data. However, we have demonstrated that we can obtain meaningful results even under these extreme experimental limitations and with fairly inhomogeneous samples. With the technology and expertise we developed while doing these experiments, and the results we obtained, additional work with trapped intermediated shoud be possible and informative.

In the course of the above research, we have learned a great deal about the structure and chemistry of hemes. We have determined that the peripheral porphyrin substituents have little or no affect on the bond strengths of the axial ligands as monitored by their Fe-ligand vibrational frequencies. The chemistry of species such as the ferrous oxy (Fe^{II}-O_2), ferryl oxo (Fe^{IV}=O) and ferric cyanide (Fe^{III}-CN^-) seem to be controlled by out-of-plane effects such as trans ligand strength, steric constraints, and hydrogen bonding. This raises further questions as to the purpose of the unusual heme a ring substituents for the functioning of cytochrome oxidase and the purpose of different iron porphyrin variations in other proteins. In contrast to the Raman spectra, the optical absorption spectra of hemes are easily perturbed by a variety of effects. These include ligation, oxidation state, and

planarity of the iron relative to the heme ring as well as environmental perturbation to the porphyrin macrocycle. Although optical absorption spectroscopy does not give specific structural information, these results reaffirm its importance in the characterization of heme protein species. It has become obvious, in the course of our research, that the interaction of peroxides with cytochrome oxidase is not well understood and past interpretations may have been oversimplified. Further studies will be required to clarify the situation.

B. FUTURE WORK

Low temperature experiments with trapped intermediates should be pursued further. The results from the pseudo-intermediate studies cast doubt as to whether the trapped intermediate studies will yield unambiguous results. However, if samples can be produced which are of more homogeneous composition than those used in our study, it should be possible to identify the intermediate through the assignment of Fe-ligand vibrations in the low frequency region of the spectrum. The alternative, to the cold trapped intermediate studies, is the use of time resolved resonance Raman techniques which can characterize intermediate species at liquid temperatures. Preliminary work has already been done (Babcock et al., 1984, 1985) and more experiments are planned. One problem, that has been a continual hindrance to the use of Raman spectroscopy for the study of cytochrome oxidase, is sample fluorescence and photoreduction. The fluorescence seems to be caused by residual flavins of other fluorescent biomolecules that are accidentally isolated along with the cytochrome oxidase (Adar and

Yonetani, 1978). The amount of fluorescence varies dramatically with preparation technique and even from one prep to another with the same technique. This fact gives hope that a preparation scheme could be developed that would minimize this fluorescence. An alternate approach to the problem is the use of fluorescence rejection Raman techniques. These are based on the fact that Raman scattering is fast ($\sim 10^{-12}$ sec) compared to fluorescence ($\sim 10^{-9}$ to 10^{-6} sec). By using picosecond pulsed lasers and fast detector gating, data collection can be gated off before significant fluorescence occurs (Van Duyne et al., 1974). Alternately, the intensity of a continuous wave laser can be modulated at a high frequency (~megahertz range) and coupled to the detector through a lock in amplifier. Raman scattered photons will be in phase with the amplitude modulation; photons from fluorescence will fall out of phase and can be rejected (Van Hoek and Visser, 1985). Photoreduction is a problem that may be directly linked to fluorescence in cytochrome oxidase but the exact relationship is not clear. The magnitude of photoreduction has been observed to be dependent on enzyme conformation (Copeland et al., 1985), although it is not known whether the reducing equivalent arises from a protein residue from exogenous impurities. This phenomenon should be studied more thoroughly to establish the source of this reducing equivalent and whether photoreduction can be minimized through modification of the isolation procedure.

Although the interaction of hemes with peroxides is fundamental to the chemistry of peroxidase and catalase enzymes, the characterization of this chemistry in solution studies have relied almost exclusively on

kinetic studies, with little direct structural information about the reaction pathways (see Traylor et al., 1984; and Bruice et al., 1986; and references within). The time resolved Raman techniques utilized by Oertling and Babcock (1985) for the characterization of horseradish peroxidase intermediates, may be ideal for characterization of heme-peroxide solution chemistry. The advantage of these solution studies over the use of only protein species, is that axial ligation, solvent polarity, hydrogen bonding interactions, and steric constraints can be varied independantly to determine their effect on the chemistry. Additional studies with heme a models may be useful in further identification of cytochrome oxidase structure and intermediates. Although the chemistry may not be altered by variation of the porphyrin ring substituents (see above), the unusual substituents of heme a produce unique optical absorption and resonance Raman properties which make it difficult to model oxidase with other hemes. Heme a species that may be useful in cytochrome oxidase model studies include: ferryl oxo, ferric (NMI,H_2O), and ferric (NMI,OH^-) as well as additional studies with the ferrous oxy species. Heme a is difficult to work with because the formyl substituent (ring position 7) is easily reduced by reagents commonly used to reduce the iron. In addition, like all physiological hemes, heme a readily aggregates or forms u-oxo dimers under some solution conditions. Heme reduction, necessary for the synthesis of ferryl oxo and ferrous oxy species, may be done more reliably by using the electrochemical techniques which I have described in Chapter 2. Formation of ferric (NMI,H_2O) and ferric (NMI,OH^-) may require the use of attached imidazole ligands and/or anchoring of the heme to a polymer substrate (to prevent aggregation). A procedure for

the attachment of imidazole ligands to the related protoporphyrin species has been described by Brinigar and Chang (1974), and a procedure for attachment to a polymer suport has been described by Tsuchida et al. (1982). Both procedures utilize the heme propionic acid substituents as a linking point and should work for heme a as well as for protoheme. Additional species that may be of interest are heme a with attached imidazole in one axial position and sulfur ligands (either free in solution or also attached) in the other axial position. A bridging sulfur ligand (between heme a and Cu) has been proposed for cytochrome a_3 in the resting state of the enzyme (see Naqui and Chance, 1986, and references within). Sulfur ligated models may give some insight into the expected properties of such a structure.

The studies we have performed on the meso-diphenylporphyrin model compounds may have only begun to utilize their potential as models of the oxygen reduction site of cytochrome oxidase. In the studies discussed in Chapter 4, we examined the properties of these compounds as models for the resting form of cytochrome oxidase, which contained metal centers in their fully oxidized (Fe^{+3}, Cu^{+2}) forms. What yet remains is the study of these model species with reduced metal centers (Fe^{+2} and/or Cu^{+1}) and reactive ligands (O^{2-} and H_2O_2). Since there are only two metal centers (as opposed to four in oxidase), experiments should be easier to perform and the results should be easier to interpret. Through the use of electrochemistry (in non aqueous solvents), it should be possible to reduce one of the metal centers of the copper chelated models selectively; the iron would probably be more easily reduced. It is expected, based on cofacial mixed metal porphyrin

models, that with only iron reduced, the sample will form a stable oxygen bound species (Ward et al., 1981). With the iron and copper reduced, reduction of the oxygen to the peroxide level may occur. Further reduction steps may be possible, in a controlled fashion, by reductive titration or by electrochemistry at room temperature or low temperature. These processes should be detectable by Raman spectroscopy as well as by other physical techniques. The copper chelating group of the meso-diphenylporphyrin models is likely to mimic cytochrome oxidase better than the copper porphyrin of the cofacial models, and the optical spectra or the meso-diphenylporphyrin models are not complicated by the presence of the copper chelating porpyrin. Facilities are already available in the chemistry department for all these experiments.

As discussed above (Chapter 4), additional work will be necessary in order to assign the remaining vibrational modes of the meso-diphenylporphyrins. These studies should initially include depolarization ratios and excitation profiles which will both aid in peak assignment and help establish the extent of symmetry reduction relative to D_{4h} symmetry. If this is not sufficient to make the assignments, studies with isotope substitution (^{2}H, ^{15}N, and ^{13}C) may be required. Although we are relatively confident of the structures of these model compounds, additional verification would help establish the credibility of our results. Ideally, this could be done with X-ray crystallography, but EXAFS may suffice if crystals cannot be obtained. If these meso-diphenylporphyrin models can be emulsified in aqueous detergents or derivatized to increase their solubility in water,

peroxide binding and reaction studies should be attempted. Soluble hemes have already been demonstrated to exhibit peroxidase and catalase activity when peroxide is added to the aqueous solution (Bruice et al., 1986). It would be informative, in terms of cytochrome oxidase chemistry, to determine if the presence of a nearby chelated copper ion modifies this peroxide chemistry or selectively favors one of the possible processes. Finally, attempts should be made to bind bridging sulfur ligands between the iron and copper of these models, to determine if these species will also demonstrate antiferromagnetic exchange coupling in a six-coordinate high-spin state as was determined for the oxygen bridged species discussed in Chapter 4.

APPENDIX

APPENDIX 1

COMMERCIAL COMPONENTS OF THE RAMAN SPECTROSCOPY SYSTEM

Spectrometer

Scanning double monochrometer w/1200 groove/nm gratings
blazed at 500 nm (Spex Ramalog 1401)
Sample illuminator (Spex 1419A)
Photomultiplier tube (PMT) (RCA 31034C)
High voltage power supply and photometer unit (Spex Ramalog 4)
PMT chiller and associated power supply (Products for Research)
Chart recorder (Linear 1200)

Computer

Enclosure (Netcom HV-1123-11-736)
Diskette drive (Data Systems DSD 480120)
Terminal (Zenith HE-WH19) and graphics retrofit board
(Northwest Digital Systems Graphics-Plus)
Plotter (Houston DMP-2)
Real Time Clock (Data Translation DT2769)
Quad Serial Board (DEC DLV11-J)
LSI 11/2 CPU (DEC KD11-HA)
Floating point and expanded instruction set (DEC KEV11)
64KByte memory (Christlin CI-1103)
Photon counting board (custom made with an AM 9513 counting chip)

Lasers

Krypton ion laser, with high-field magnet (Spectra Physics
Model 164-11) with red (647.1/676.4 nm), U.V. (350.7/356.4
nm), and special blue (406.7/413.1 nm) optics
Argon ion laser (Spectra Physics Model 165) with all
lines optics and tuning prism
Power supply (Spectra Physics Model 265)
Dye laser and dye circulator (Spectra Physics Models
375, 376N, respectively)
Helium-cadmium laser and power supply (Liconix 4240)
Powermeter (Scientech 362)

LIST OF REFERENCES

LIST OF REFERENCES

Abe, M., Kitagawa, T., and Kyogoku, Y. (1978) *J. Chem. Phys.* 69, 4526-4534.

Adar, F. (1978) in "The Porphyrins", Vol. 2, Dolphin, D. (ed.). Academic Press: New York, pp. 167-209.

Adar, F. and Yonetani, T. (1978) *Biochem. Biophys. Acta* 502, 180-86.

Anderson, D. L., Weschler, C. J., and Basdo, F. (1974) *J. Am. Chem. Soc.* 96, 5599-5600.

Andersson, K. K., Lipscomb, J. D., Valentine, M., Munck, E., and Hooper, A. B. (1986) *J. Biol. Chem.* 261, 1126-1138.

Andersson, L. A., Loehr, T. M., Chang, C. K., and Mauk, A. G. (1985) *J. Amer. Chem. Soc.* 107, 182-191.

Antonini, E. and Brunori, M. (1971) in "Hemoglobin and Myoglobin in Their Reaction with Ligands." North Holland Publ., Amsterdam, pp. 17-19.

Asher, S. A. and Schuster, T. M. (1979) *Biochemistry* 18, 5377-5387.

Artzatbanov, V. Y., Konstantinov, A. A., and Skulachev, V. P. (1979) *FEBS Lett.* 87, 180-185.

Aviram, I., Wittenberg, B. A., and Wittenberg, J. B. (1978) *J. Biol. Chem.* 253, 5685-5689.

Babcock, G. T., Vickery, L. E., and Palmer, G. (1976) *J. Biol. Chem.* 251, 7907-7919.

Babcock, G. T. and Chang, C. K. (1978) *FEBS Letters* 97, 358-362.

Babcock, G. T., Callahan, P. M., Ondrias, M. R., and Salmeen, I. (1981) *Biochemistry* 20, 959-966.

Babcock, G. T., Jean, J. M., Johnston, L. N., Palmer, G., and Woodruff, W. H. (1984) *J. Am. Chem. Soc.* 106, 8305-8306.

Babcock, G. T., Ingle, R. T., Oertling, W. A., Davis, J. M., Averill, B., Halse, C. L., Stutkins, D. J., Bolscher, B. G., and Wever, R. (1985) *Biochim. Biophys. Acta* 828, 58-66.

Babcock, G. T. (1986) in "Biological Applications of Raman Spectroscopy", Spiro, T. G. (ed.), Wiley: New York, in press.

Babcock, G. T., Jean, J. M., Johnston, L. N., Woodruff, W. H., and Palmer, G. (1985) *J. Inorg. Biochem.* 23, 243-251.

Bajdor, K., Nakamoto, K., and Kincaid, J. (1983) *J. Am. Chem. Soc.* 105, 678-679.

Bajdor, K. and Nakamoto, K. (1984) *J. Am. Chem. Soc.* 106, 3045-3046.

Beetlestone, J. and George, P. (1964) *Biochemistry* 3, 707.

Behere, D. V., Gonzalez-Vergara, E., and Goff, H. M. (1985) *Biochim. Biophys. Acta* 832, 319-325.

Beinert, H., Hansen, R. E., and Hartzell, C. R. (1976) *Biochem. Biophys. Acta.* 423, 339-355.

Berry, K. J., Clark, P. E., Gunter, M. J., and Murray, K. S. (1980) *Nouv. J. Chim.* 4, 581-585.

Bickar, D., Bonaventura, J., and Bonaventura, C. (1982) *Biochemistry* 21, 2661-2666.

Blair, D. F., Martin, C. T., Gelles, J., Wang, H, Brudvig, G. W., Stevens, T. H., and Chan, S. I. (1983) *Chemica Scripta* 21, 43-53.

Blair, D. F., Witt, S. N., and Chan, S. I. (1985) *J. Am. Chem. Soc.* 107, 7389-7399.

Blom, N., Odo, J., Nakamoto, N., and Strommen, D. P. (1986) *J. Phys. Chem.* 90, 2847-2852.

Blumberg, W. E., Peisach, J., Wittenberg, B. A., and Wittenberg, J. B. (1968) *J. Biol. Chem.* 243, 1854-1862.

Bocian, D. F., Lemley, A.T., Petersen, N. O., Brudvig, G. W., and Chan, S. I. (1979) *Biochemistry* 18, 4396-4402.

Brault, D. and Rougee, M. (1974) *Biochemistry* 22, 1598-4602.

Brinigar, W. S., Chang, C. K., Geibel, T. G., and Traylor, T. G. (1974) *J. Am. Chem. Soc.* 96, 5597-5599.

Brinigar, W. S. and Chang, C. K. (1974) *J. Am. Chem. Soc.* 96, 5595-5597.

Bruice, T. C., Zipplies, M. F., and Lee, W. A. (1986) *Proc. Natl. Acad. Sci. USA* 83, 4646-4649.

Brunner, H. (1974) *Naturwiss.* 61, 129.

Brunori, M., Colosimo, A., Rainoni, G., Wilson, M. T., and Antonini, E. (1979) *J. Biol. Chem.* 254, 10769-10775.

Buchler, J. W., Kokisch, W., and Smith, D. (1978) *Structure and Bonding* 34, 79-134.

Burke, J. M., Kincaid, J. R., Peters, S., Gagne, R. R., Collman, J. P., and Spiro, T. G. (1978) *J. Am. Chem. Soc.* 100, 6083-6088.

Burke, J. M., Kincaid, J. R., and Spiro, T. G. (1978) *J. Am. Chem. Soc.* 100, 6077-6083.

Callahan, P. M. and Babcock, G. T. (1981) *Biochemistry* 20, 952-958.

Callahan, P. M. (1983) Doctoral Dissertation, Michigan State University: East Lansing, MI.

Campbell, J. R., Clark, R. J., Clore, G. M., and Lane, A. N. (1980) *Inorg. Chim. Acta* 46, 77-84.

Caughey, W. S., Smythe, G. A., O'Keeffe, D. F., Maskasky, J. E., and Smith, M. L. (1975) *J. Biol. Chem.* 250, 7602-7622.

Centeno, J. (1987) Doctoral Dissertation, Michigan State University E. Lansing, MI, in preparation.

Champion, P. M., Bangcharoenpaurpong, O., Rizos, A. K., Jollie, D., and Sligar, S. G. (1986) "Proc. of Tenth International Conference on Raman Spectroscopy"; Petiolas, W. L. and Hudson, B. (ed.); Univ. of Oregon: Eugene, 1-23.

Chance, B. and Leigh, J. S. (1977) *Proc. Natl. Acad. Sci. USA* 74, 4777-4780.

Chance, B., Saronio, C., and Leigh, J. S. (1975) *J. Biol. Chem.* 250, 9226-9237.

Chance, B., Kumar, C., Powers, L., and Ching, Y. T. (1983) *Biophys. J.* 44, 353-363.

Chang, C. K. and Traylor, T. G. (1975) *Proc. Nat. Acad. Sci. USA* 72, 1166-1170.

Chin, D. H., Balch, A. L., and LaMar, G. N. (1980) *J. Am. Chem. Soc.* 102, 1446-1448 (values from plot).

Chin, D., La Mar, G. N., and Balch, A. L. (1980) *J. Am. Chem. Soc.* 102, 4344-4350.

Choi, S., Spiro, T. G., Langry, K. C., Smith, K. M., Budd, D. L., and La Mar, G. N. (1982) *J. Am. Chem. Soc.* 104, 4345-4351.

Choi, S., Lee, J. J., Wei, Y. H., and Spiro, T. G. (1983) *J. Am,Chem, Soc.* 105, 3692-3707.

Brunori, M., Colosimo, A., Rainoni, G., Wilson, M. T., and Antonini, E. (1979) *J. Biol. Chem.* 254, 10769-10775.

Buchler, J. W., Kokisch, W., and Smith, D. (1978) *Structure and Bonding* 34, 79-134.

Burke, J. M., Kincaid, J. R., Peters, S., Gagne, R. R., Collman, J. P., and Spiro, T. G. (1978) *J. Am. Chem. Soc.* 100, 6083-6088.

Burke, J. M., Kincaid, J. R., and Spiro, T. G. (1978) *J. Am. Chem. Soc.* 100, 6077-6083.

Callahan, P. M. and Babcock, G. T. (1981) *Biochemistry* 20, 952-958.

Callahan, P. M. (1983) Doctoral Dissertation, Michigan State University: East Lansing, MI.

Campbell, J. R., Clark, R. J., Clore, G. M., and Lane, A. N. (1980) *Inorg. Chim. Acta* 46, 77-84.

Caughey, W. S., Smythe, G. A., O'Keeffe, D. F., Maskasky, J. E., and Smith, M. L. (1975) *J. Biol. Chem.* 250, 7602-7622.

Centeno, J. (1987) Doctoral Dissertation, Michigan State University E. Lansing, MI, in preparation.

Champion, P. M., Bangcharoenpaurpong, O., Rizos, A. K., Jollie, D., and Sligar, S. G. (1986) "Proc. of Tenth International Conference on Raman Spectroscopy"; Petiolas, W. L. and Hudson, B. (ed.); Univ. of Oregon: Eugene, 1-23.

Chance, B. and Leigh, J. S. (1977) *Proc. Natl. Acad. Sci. USA* 74, 4777-4780.

Chance, B., Saronio, C., and Leigh, J. S. (1975) *J. Biol. Chem.* 250, 9226-9237.

Chance, B., Kumar, C., Powers, L., and Ching, Y. T. (1983) *Biophys. J.* 44, 353-363.

Chang, C. K. and Traylor, T. G. (1975) *Proc. Nat. Acad. Sci. USA* 72, 1166-1170.

Chin, D. H., Balch, A. L., and LaMar, G. N. (1980) *J. Am. Chem. Soc.* 102, 1446-1448 (values from plot).

Chin, D., La Mar, G. N., and Balch, A. L. (1980) *J. Am. Chem. Soc.* 102, 4344-4350.

Choi, S., Spiro, T. G., Langry, K. C., Smith, K. M., Budd, D. L., and La Mar, G. N. (1982) *J. Am. Chem. Soc.* 104, 4345-4351.

Choi, S., Lee, J. J., Wei, Y. H., and Spiro, T. G. (1983) *J. Am,Chem, Soc.* 105, 3692-3707.

Cho

Cho
(19

Cho
Che

Cla

Col
C.

Col
R.

Co
Le

Cr
Su

Da

Da
Br
10

De
Bi

Eh
1-

En

Fe

F
1

F

F
B

G
C

G
T

G

Choi, S. and Spiro, T. G. (1983) *J. Am. Chem. Soc.* 105, 3683-3692.

Chottard, G., Battioni, P., Battioni, J., Lange, M., and Mansuy, D. (1981) *Inorg. Chem.* 20, 1718-1722.

Chottard, G., Schappacher, M., Ricard, L., and Weiss, R. (1984) *Inorg. Chem.* 23, 4557-4561.

Clark, R. J. H. and Stewart, B. (1979) *Structure and Bonding* 36, 1-80.

Collman, J. P., Gagne, R. R., Halbert, T. R., Marchan, J. K. and Reed, C. A. (1973) *J. Am. Chem. Soc.* 95, 7868-7870.

Collman, J. P., Brauman, J. I., Doxsee, K. M., Sessler, J. L., Morris, R. M., and Gibson, Q. H. (1983) *Inorg. Chem.* 22, 1427-1432.

Copeland, R. A., Naqui, A., Chance, B., and Spiro, T. G. (1985) *FEBS Letters* 182, 375-379.

Crisanti, M. A., Spiro, T. G., English, D. R., Hendrickson, D. N., and Suslick, K. S. (1984) *Inorg. Chem.* 23, 3897-3901.

Dalziel, K. and O'Brien, J. R. P. (1954) *Biochem. J.* 56, 648-659.

Dawson, J. H., Kau, L-S, Penner-Hahn, J. E., Sono, M., Eble, K. S., Bruce, G. S., Hager, L. P., and Hodgson, K. O. (1986) *J. Am. Chem. Soc.* 108, 8114-8116.

Desbois, A., Mazza, G., Stetzkowski, F., and Lutz, M. (1984) *Biochem. Biophys. Acta* 785; 161-176.

Eble, K. S. and Dawson, J. H. (1986) *Adv. Inorg. Bioinorg. Mech.* 4, 1-64.

Erecinska, M. and Chance, B. (1972) *Arch. Biochem. Biophys.* 188, 1-14.

Fermi, G. (1975) *J. Mol. Biol.* 97, 237-246.

Finzel, B. C., Poulos, T. L., and Kraus, J. (1984) *J. Biol. Chem.* 259, 13027-13036.

Frew, J. E. and Jones, P. (1984) *Adv. Inorg. Bioinorg. Mech.* 3, 175.

Frew, J. E. and Jones, P. (1984) "Advances in Inorganic and Bioinorganic Mechanism," V. 3, Academic Press, 175-212.

Gallucci, J. C., Swepston, P. N., and Ibers, J. A. (1982) *Acta Crystallogr., Sect. B*, 38, 2134-2139.

George, P. (1964) In "Oxidases and Related Redox Systems", Vol 1, King, T. E., Mason, H. S., and Morrison, M. (ed.), Wiley: New York.

George, P. and Irvine, D. H. (1952) *Biochem. J.* 52, 511-517.

Gersonde, K., Kerr, E. A., Yu, N-T., Parish, D. W., and Smith, K. M. (1986) *J. Biol. Chem.* 261, 8678-8685.

Gibson, Q.H. and Greenwood, C. (1965) *J. Biol. Chem.* 240, 2694-2698.

Gladkov, L. L. and Solovyov, K. N. (1986) *Spectrochim. Acta* 42a, 1-10.

Goodman, G. and Leigh, J. S. (1985) *Biochemistry* 24, 2310-2317.

Gordon, A. J. and Ford, R. A. (1972) in "The Chemists Companion," Wiley Interscience: New York, p. 439.

Gouterman, M. (1959) *J. Chem. Phys.* 30, 1139-1161.

Gouterman, M. (1961) *J. Mol. Spectrosc.* 6, 138-163.

Gouterman, M. (1978) in "The Porphyrins", Vol III, Dolphin, D. (ed), Academic Press: New York, pp. 1-165,

Griffin, B. W., Peterson, J. A., and Estabrook, R. W. (1979) in "The Porphyrins", Vol VII, Part B, Dolphin, D. (ed.), Academic Press: New York, pp. 333-371.

Groves, J. T. (1985) in "Cytochrome P-450: Structure, Mechanism, and Biochemistry", Ortiz de Montellano, P. (ed), Plenum Press: New York, Chapter I.

Gubelmann, M. H. and Williams, A. F. (1983) *Structure and Bonding* 55, 1-65.

Gunter, M. J., Mander, L. N., Murray, K. S., and Clark, P. E. (1981) *J. Am. Chem. Soc.* 103, 6784-6787.

Hartzell, C.R. and Beinert, H. (1974) *Biochem. Biophys. Acta* 368, 318-338.

Hashimoto, S., Tatsuno, Y., and Kitagawa, T. (1984) *Proc. Japan Acad.* 60, 345-348.

Hashimoto, S., Tatsuno, Y, and Kitagawa, T. (1986a) *Proc. Natl. Acad. Sci. USA* 83, 2417-2421.

Hashimoto, S., Teraoko, J., Inubushi, T., Yonetani, T., and Kitagawa, T. (1986b) *J. Biol. Chem.* 261, 11110-11118.

Hashimoto, S., Tatsuno, Y., and Kitagawa, T. (1986a) *Proc. Natl. Acad. Sci. USA* 83, 2417-2421.

Hashimoto, S., Tatsuno, Y., and Kitagawa, T. (1986c) "Proceedings of the Tenth International Conference on Raman Spectroscopy"; Petiolas, W. L. and Hudson, B. (ed.); Univ. of Oregon: Eugene, pp. 1-28, 1-29.

Henderson, R., Capaldi, R. A., and Leigh, J. S. (1977) *J. Mol. Biol.* 112, 631.

Hewson, W.D. and Hager, L.P. (1979) in "The Porphyrins", Vol VII, part B, Dolphin, D. (ed.). Academic Press: New York pp. 295-332.

Hofmann, J. A., Jr., and Bocian, D. F. (1984) *J. Phys. Chem.* 88, 1472-1479.

Hori, H. and Kitagawa, T. (1980) *J. Am. Chem. Soc.* 102, 3608-3613.

Huong, P. V. and Pommier, J. C. (1977) *C. R. Acad. Sc. Paris* 285, 519-522.

Jameson, G. B., Molinaro, F. S., Ibers, J. A., Collman, J. P., Brauman, J. I., Rose, E., and Suslick, K. S. (1980) *J. Am. Chem. Soc.* 1029, 3224-3237.

Jones, R. D., Summerville, D. A., and Basolo, F. (1979) *Chem. Rev.* 79, 139-179.

Kadish, K. M. (1983) in "Iron Porphyrins", Part Two, Lever, A. B. P. and Gray, H. B. (eds), Addison-Wesley: Reading, Mass., pp. 161-249.

Kean, R. T. and Babcock, G. T. (1986) in preparation.

Kean, R. T. (1987) Doctoral Dissertation, Michigan State University: East Lansing, MI.

Kean, R. T., Oertling, W. A., and Babcock, G. T. in press (1987) *J. Am. Chem. Soc.*

Keifer, W., Schmid, W. J., and Topp, J. A. (1975) *Applied Spectroscopy* 29, 434-436.

Kerr, E. A., Mackin, H. C., and Yu, N-T. (1983) *Biochemistry* 22, 4373-4379.

Kerr, E. A., Yu, N-T., and Gersonde, K. (1984) *FEBS Letters* 178, 31.

Kimura, S. and Yamazaki, I. (1979) *Ars. Biochem. Biophys.* 198, 580-588.

Kimura, S., Yamazaki, I., and Kitagawa, T. (1981) *Biochemistry* 20, 4632-4638.

King, T. E., Orii, Y., Chance, B., and Okunuki, K. (ed) (1979) "Cytochrome Oxidase", Elsevier/North-Holland Biomedical Press: New York.

Kitagawa, T., Kyogoku, Y., Iizuka, T., and Saito, M. I. (1976) J. Am. *Chem. Soc.* 98, 5169-5173.

Kitagawa, T., Abe, M., and Ogoshi, H. (1978) *J. Chem. Phys.* 69, 4516-4525.

Kitagawa, T., Nagai, K., and Tsubaki, M. (1979) *FEBS Lett.* 104, 376-378.

Koo, M. S. (1986) Doctoral Dissertation, Michigan State University: East Lansing, MI.

Koo, M. S. and Chang, C. K. (1987) in preparation.

Kumar, C., Naqui, A., and Chance, B. (1984) *J. Biol. Chem.* 259, 2073-2076.

LaMar, G. N., de Ropp, J. S., Latos-Grazynski, L., Balch, A. L., Johnson, R. S., Smith, K. B., Parish, D. W., and Cheng, R. J. (1983) *J. Am. Chem. Soc.* 105, 782-787 (values from plot).

Lehninger, A. L. (1975) "Biochemistry", Worth: New York.

Lever, A. B. P. and Gray, H. B. (eds) (1983) "Iron Porphyrins", Addison-Wesley: Reading, Mass.

Loew, G. H. (1983) in "Iron Porphyrins", Part One, Lever, A. B. P. and Gray, H. B. (eds), Addison-Wesley: Reading, Mass., pp. 1-87.

Longuet-Higgins, H. C., Rector, C. W., and Platt, J. R. (1950) *J. Chem. Phys.* 18, 1174.

Lukas, B. and Silver, J. (1986) *Inorg. Chim. Acta* 124, 97-100.

Makinen, M. W. and Churg, A. K. (1983) in "Iron Porphyrins", Part One, Lever, A. B. P. and Gray, H. B. (eds), Addison-Wesley: Reading, Mass., pp. 141-235.

Malmstrom, B. G. (1982) *Ann. Rev. Biochem.* 51, 21-59.

Manthey, J. A. and Hager, L. P. (1985) *J. Biol. Chem.* 260, 9654-9659.

McClain, W. M. (1971) *J. Chem. Phys.* 55, 2789-2796.

Mispelter, J., Momenteau, M., Lavalette, D., and Lhoste, J. M. (1983) *J. Am. Chem. Soc.* 105, 5165-5166.

Morgenstern-Badarau, I. and Wickman, H. H. (1985) *Inorg. Chem.* 24, 1889-1892.

Munck, E. (1979) in "The Porphyrins", Vol IV, Dolphin, D. (ed.), Academic Press: New York, pp. 379-423.

Nagai, K., Kitagawa, T., and Morimoto, H. (1980). *J. Mol. Biol.* 136, 271-289.

Nakajima, R., Yamazaki, C., and Griffin, B. W. (1985) *Biochem. Biophys. Res. Commun.* 128, 1-6.

Nakamoto, K. and Oshio, H. (1985) *J. Am. Chem. Soc.* 107, 6518-6521.

Naqui, A. and Chance, B. (1986) *Ann. Rev. Biochem.* 55, 137-166.

Newton, J. E. and Hall, M. B. (1984) *Inorg. Chem.* 23, 4627-4632.

Norvell, J. C., Nunes, A. C., and Schoenborn, B. P. (1975) *Science* 190, 568-569.

Oertling, W. A. and Babcock, G. T. (1985) *J. Am. Chem. Soc.* 107, 6406-6407.

Oertling, W. A., Wever, R., and Babcock, G. T. (1986) in preparation.

Ogura, T., Hon-nami, K., Oshima, T., Yoshikawa, S., and Kitagawa, T. (1983) *J. Am. Chem. Soc.* 105, 7781-7783.

Okawa, H., Kanda, W., and Kida, S. (1980) *Chem. Lett.*, 1281-1284.

Olafson, B. D. and Goddard, W. A. (1977) *Proc. Nat. Acad. Sci.* 74, 1315-1319.

Ondrias, M. R. (1980) Doctoral Dissertation, Michigan State University E. Lansing, MI.

Ozaki, Y., Kitagawa, T., and Kyogoku, Y. (1976) *FEBS Lett.* 63, 369-372.

Oprian, D. D., Gorsky, L. D., and Coon, M. J. (1983) *J. Biol. Chem.* 258, 8684-8691.

Padlan, E. A. and Love, W. E. (1974) *J. Biol. Chem.* 219, 4067-4078.

Palmer, G. (1979) in "The Porphyrins", Vol IV, Dolphin, D. (ed.), Academic Press: New York, pp. 313-353.

Palmer, G. (1985) *Biochem. Soc. Trans.* 13, 548-560.

Peisach, J. and Mims, W. B. (1977) *Biochemistry* 16, 2795.

Peng, S.-M. and Ibers, J. A. (1976) *J. Am. Chem. Soc.* 98, 8032-8036.

Peterson, J. A., Ishimura, Y., and Griffin, B. W. (1972) *Arch. Biochem. Biophys.* 149, 197-208.

Poulos, T. L., Freer, S. T., Alden, R. A., Edwards, S. L., Skogland, U., Takio, K., Eriksson, B., Xuong, N., Yonetani, T., and Kraut, J. (1980) *J. Biol. Chem.* 255, 575-580.

Poulos, T. L. and Kraut, J. (1980) *J. Biol. Chem.* 255, 8199-8205.

Powers, L., Chance, B., Ching, Y., and Angiolillo, P. (1981) *Biophys. J.* 34, 465-498.

Powers, L., Chance, B., Ching, Y., Muhoberac, B., Weintraub, S., and Wharton, D. (1982) *FEBS Lett.* 138, 245-248.

Proniewicz, J. M., Bajdor, K., and Nakamoto, K. (1986) *J. Phys. Chem.* 90, 1760-1766.

Reed, C. A. (1978) in "Metal Ions in Biological Systems", Vol 7, Sigel, H. (ed.), Marcel Dekker: New York, pp. 277-310.

Renganathan, V. and Gold, M. H. (1986) *Biochemistry* 25, 1626-1631.

Sakurai, H. and Yoshimura, T. (1985) *J. Inorg. Biochem.* 24, 75-96.

Salmeen, I, Rimai, L., and Babcock, G. T. (1978) *Biochemistry* 17, 800.

Sawyer, D. T. and Nanni, E. J. (1981) in "Oxygen and Oxy-Radicals in Chemistry and Biology", Rodgers, M. J. and Powers, E. L. (ed.), Academic Press: New York, pp. 15-44.

Schaeffer, C., Momenteau, M., Mispelter, J., Loock, B., Huel, H., and Lhoste, J. (1986) *Inorg. Chem.* 25, 4577-4583.

Schappacher, M., Weiss, R., Montiec-Montoya, R., Trautwein, A., and Tabard, A. (1985) *J. Am. Chem. Soc.* 107, 3736-3738.

Schappacher, M., Chottard, G., and Weiss, R. (1986) *J. Chem. Soc., Chem. Commun.* 2, 93-94.

Scheidt, W. R., Haller, K. J. and Hatano, K. (1980) *J. Am. Chem. Soc.* 102, 3017-3021.

Scheidt, W. R., Lee, Y. J., Luangdilok, W., Haller, K. J. Anzai, A. and Hatano, K. (1983) *Inorg. Chem.* 22, 1516-1522.

Scheidt, W. R. and Gouterman, M. (1983) in "Iron Porphyrins", Part One, Lever, A. B. P. and Gray, H. B. (eds), Addison-Wesley: Reading, Mass., pp. 89-139.

Shelnutt, J. A. (1983) *Inorg. Chem.* 22, 2535-2544.

Shelnutt, J. A., Satterlee, J. D., and Erman, J. E. (1983) *J. Biol. Chem.* 258, 2168-2173.

Shelnutt, J. A., Alden, R. G., and Ondrias, M. R. (1986) *J. Biol. Chem.* 261, 1720-1723.

Sibbett, S. S. and Hurst, J. K. (1984) *Biochemistry* 23, 3007-3013.

Sitter, A. J., Reczek, C. M., and Terner, J. (1985a) *Biochim. Biophys. Acta* 828, 229-235.

Sitter, A. J., Reczek, C. M., and Terner, J. (1985b) *J. Biol. Chem.* 260, 7515-7522.

Sitter, A. J., Reczek, C. M., and Terner, J. (1986). *J. Biol. Chem.* 261, 8638-8642.

Smith, D. W. and Williams, R. J. (1970) *Structure and Bonding* 17, 1-45.

Smith, A. M., Morrison, W. L., and Milham, P. J. (1983) *Biochemistry* 22, 1645-1650.

Smith, M. L., Paul, J., Ohlsson, P. I., and Paul, K. G. (1984) *Biochemistry* 23, 6776-6785.

Sono, M. (1986) *Biochemistry* 25, 6089-6097.

Sono, M., Dawson, J. H., Hall, K., and Hager, L. P. (1986) *Biochemistry* 25, 347-356.

Spaulding, L. D., Chang, C. C., Yu, N-T., and Felton, R. H. (1975) *J. Am. Chem. Soc.* 97, 2517-2525.

Spiro, T. G. (1983) in "Iron Porphyrins", Part Two, Lever, A. B. P. and Gray, H. B. (eds), Addison-Wesley: Reading, Mass. pp. 91-159.

Spiro, T. G. and Strekas, T. C. (1974) *J. Am. Chem. Soc.* 96, 338-345.

Spiro, T. G. adn Bruce, J. M. (1976) *J. Am. Chem. Soc.* 98, 5482-5488.

Stein, P., Ulman, A., and Spiro, T. G. (1984) *J. Phys. Chem.* 88, 369-374.

Stillman, J. S., Stillman, M. J., and Dunford, H. B. (1975) *Biochemistry* 14, 3183-3188.

Stong, J. D., Spiro, T. G., Kubaska, R. J., and Shupack, S. I. (1980) *J. Raman Spectrosc.* 9, 312-314.

Strauss, S. H., Silver, M. E., and Ibers, J. A. (1983) *J. Amer. Chem. Soc.* 105, 4108-4109.

Strauss, S. H., Silver, M. E., Long, K. M., Thompson, R. G., Hudgens, R. A., Spartalian, K., and Ibers, J. A. (1985) *J. Am. Chem. Soc.* 107, 4207-4215.

Takano, T. (1977) *J. Mol. Biol.* 110, 537-568.

Tanaka, T., Yu, N.-T., and Chang, C. K. (1984) *Biophys. J.* 45, 365a.

Tang, J. and Albrecht, A. C. (1970) in "Raman Spectroscopy", Vol 2 Szimanski, H. A. (ed), Plenum: New York, pp. 33-68.

Teraoko, J.; Kitagawa, T. (1980) *Biochem. Biophys. Res. Comm.* 93, 694-700.

Teraoka, J.; Kitagawa, T. (1982) *J. Biol. Chem.* 256, 3969-3977.

Terner, J. and Reed, D. E. (1984) *Biochim. Biophys. Acta* 789, 80-86.

Terner, J., Sitter, A. J., and Reczek, C. M. (1985) *Biochem. Biophys. Acta* 828, 73-80.

Theorell, H. and Ehrenberg, A. (1952) *Arch. Biochem. Biophys.* 41, 442.

Traylor, T. G., Lee, W. A., and Stynes, D. V. (1984) *J. Am. Chem. Soc.* 106, 755-764.

Traylor, T. G., White, D. K., Campbell, D. H., and Berzinis, A. P. (1981) *J. Am. Chem. Soc.* 103, 4932-4936.

Traylor, T. G., Tsuchiya, S., Campbell, D., Mitchell, M., Stynes, D., and Koga, N. (1985) *J. Am. Chem. Soc.* 107, 604-614.

Tsubaki, M., Nagai, K., and Kitagawa, T. (1980) *Biochemistry* 19, 379-385.

Tsuchida, E., Nishide, N., Sato, Y., and Kaneda, M. (1982) *Bull. Chem. Soc. Soc., Jpn.* 55, 1890.

Tweedle, M. F., Wilson, L. J., Garcia-Iniguez, L., Babcock, G. T., and Palmer, G. (1978) *J. Biol. Chem.* 22, 8065-8071.

Uyeda, M. and Peisach, J. (1981) *Biochemistry* 20, 2028-2035.

Van Duyne, R. P., Jeanmaire, D. L., and Shriver, D. F. (1974) *Anal. Chem.* 46, 213.

Van Hoek, A. and Visser, A. J. W. G. (1985) *Anal. Instrum.* 14, 143-154.

Vanneste, W. H. (1966) *Biochemistry* 5, 838-848.

Van Steelandt-Frentrup, J., Salmeen, I., and Babcock, G. T. (1981) *J. Am. Chem. Soc.* 103, 5981-5982.

Van Wart, H. E. and Zimmer, J.; (1985) *J. Biol. Chem.* 206, 8372-8377.

Walters, M. A., Spiro, T. G., Suslick, K. S., and Collmann, J. P. (1980) *J. Am. Chem. Soc.* 102, 6857-6858.

Wang, J. H., Nakahara, A., and Fleischer, E. B. (1958) *J. Am. Chem. Soc.* 80, 1109.

Ward, B., Wang, C-B., and Chang, C. K. (1981) *J. Am. Chem. Soc.* 103, 5236-5238.

Ward, B. and Chang, C. K. (1982) *Photochem. Photobiol.* 35, 757-759.

Watanabe, T. Ama, T., and Nakamoto, K. (1984) *J. Phys. Chem.* 88, 440-445.

Wikstrom, M. (1981) *Proc. Natl. Acad. Sci. USA* 78, 4051-4054.

Terner, J., Sitter, A. J., and Reczek, C. M. (1985) *Biochem. Biophys. Acta* 828, 73-80.

Theorell, H. and Ehrenberg, A. (1952) *Arch. Biochem. Biophys.* 41, 442.

Traylor, T. G., Lee, W. A., and Stynes, D. V. (1984) *J. Am. Chem. Soc.* 106, 755-764.

Traylor, T. G., White, D. K., Campbell, D. H., and Berzinis, A. P. (1981) *J. Am. Chem. Soc.* 103, 4932-4936.

Traylor, T. G., Tsuchiya, S., Campbell, D., Mitchell, M., Stynes, D., and Koga, N. (1985) *J. Am. Chem. Soc.* 107, 604-614.

Tsubaki, M., Nagai, K., and Kitagawa, T. (1980) *Biochemistry* 19, 379-385.

Tsuchida, E., Nishide, N., Sato, Y., and Kaneda, M. (1982) *Bull. Chem. Soc. Soc., Jpn.* 55, 1890.

Tweedle, M. F., Wilson, L. J., Garcia-Iniguez, L., Babcock, G. T., and Palmer, G. (1978) *J. Biol. Chem.* 22, 8065-8071.

Uyeda, M. and Peisach, J. (1981) *Biochemistry* 20, 2028-2035.

Van Duyne, R. P., Jeanmaire, D. L., and Shriver, D. F. (1974) *Anal. Chem.* 46, 213.

Van Hoek, A. and Visser, A. J. W. G. (1985) *Anal. Instrum.* 14, 143-154.

Vanneste, W. H. (1966) *Biochemistry* 5, 838-848.

Van Steelandt-Frentrup, J., Salmeen, I., and Babcock, G. T. (1981) *J. Am. Chem. Soc.* 103, 5981-5982.

Van Wart, H. E. and Zimmer, J.; (1985) *J. Biol. Chem.* 206, 8372-8377.

Walters, M. A., Spiro, T. G., Suslick, K. S., and Collmann, J. P. (1980) *J. Am. Chem. Soc.* 102, 6857-6858.

Wang, J. H., Nakahara, A., and Fleischer, E. B. (1958) *J. Am. Chem. Soc.* 80, 1109.

Ward, B., Wang, C-B., and Chang, C. K. (1981) *J. Am. Chem. Soc.* 103, 5236-5238.

Ward, B. and Chang, C. K. (1982) *Photochem. Photobiol.* 35, 757-759.

Watanabe, T. Ama, T., and Nakamoto, K. (1984) *J. Phys. Chem.* 88, 440-445.

Wikstrom, M. (1981) *Proc. Natl. Acad. Sci. USA* 78, 4051-4054.

Wikstrom, M., Krab, K., and Saraste, M. (1981) "Cytochrome Oxidase A Synthesis", Academic Press: New York.

Wilson, E. B., Decius, J. C., and Cross, P. C. (1955) "Molecular Vibrations", Dover: New York, p. 336.

Witt, S. N., Blair, D. F., and Chan, S. I. (1986) *J. Biol. Chem.* 261, 8104-8107.

Wittenberg, J. B., Nobel, R. W., Wittenberg, B. A., Antonini, E., Blunoi, M., and Wyman, J. (1967) *J. Biol. Chem.* 242, 626-634.

Woodruff, W. H., Dallinger, R. F., Antalis, T. M. and Palmer, G. (1981) *Biochemistry* 20, 1332-1338.

Woodruff, W. H., Kessler, R. J., Ferris, N., S., Dallinger, R. F., Carter, K. R., Antalis, T. M., and Palmer, G. (1982) *Adv. Chem. Ser.* 201, 625-659.

Wrigglesworth, J. M. (1984) *Biochem. J.* 217, 715-719.

Yamanaka, T. and Okunuki, K. (1974) in "Microbial Iron Metabolism", Neilands, J. B. (ed), Academic Press: New York, p. 349.

Yonetani, T. (1965). *J. Biol. Chem.* 240, 4509-4514.

Yonetani, T., Iizuka, T., and Waterman, M. R. (1971) *J. Biol. Chem.* 246, 7683.

Yoshikawa, S., O'Keeffe, D. H., and Caughey, W. S. (1985) *J. Biol. Chem.* 260, 3518-3528.

Young, R. and Chang, C. K. (1985) *J. Am. Chem. Soc.* 107, 1338.

Yu, N-T., Kerr, E. A., Ward, B., and Chang, C. K. (1983) *Biochemistry* 22, 4534-4540.

Yu, N.-T., Benko, B., Kerr, E. A., and Gersonde, K. (1984) *Proc. Natl. Acad. Sci. USA* 81, 5106-5110.

Zerner, M., Gouterman, M., and Kobayashi, H. (1966) *Theoret. Chim. Acta* (Berlin), 6, 363-400.